

**Fabrication of Tubular Al₂O₃ Membrane Using Agar Al₂O₃
Mixtures and Glass-Tube Molds**

Nantawadee Udomsri

**A Thesis Submitted in Partial Fulfillment of the Requirements
for the Degree of Master of Science in Materials Science**

Prince of Songkla University

2023

Copyright of Prince of Songkla University



**Fabrication of Tubular Al₂O₃ Membrane Using Agar Al₂O₃
Mixtures and Glass-Tube Molds**

Nantawadee Udomsri

**A Thesis Submitted in Partial Fulfillment of the Requirements
for the Degree of Master of Science in Materials Science**

Prince of Songkla University

2023

Copyright of Prince of Songkla University

Thesis Title Fabrication of Tubular Al₂O₃ Membrane Using Agar Al₂O₃ Mixtures and Glass-Tube Molds

Author Miss Nantawadee Udomsri

Major Program Materials Science

Major Advisor**Examining Committee:**

.....
(Asst. Prof. Dr. Kowit Lertwittayanon)

..... Chairperson
(Asst. Prof. Dr. Wichitpan Rongwong)

.....Committee
(Assoc. Prof. Dr. Anukorn Phuruangrat)

.....Committee
(Asst. Prof. Dr. Kowit Lertwittayanon)

.....Committee
(Asst. Prof. Dr. Methee Promsawat)

The Graduate School, Prince of Songkla University, has approved this thesis as fulfillment of the requirements for the Master of Science, Degree in Materials Science.

.....
(Asst. Prof. Dr. Thakerng Wongsirichot)
Acting Dean of Graduate School

This is to certify that the work here submitted is the result of the candidate's own investigations. Due acknowledgement has been made of any assistance received.

.....Signature
(Asst. Prof. Dr. Kowit Lertwittayanon)
Major Advisor

.....Signature
(Miss Nantawadee Udomsri)
Candidate

I hereby certify that this work has not been accepted in substance for any degree,
and is not being currently submitted in candidature for any degree.

.....Signature
(Miss Nantawadee Udomsri)
Candidate

Thesis Title	Fabrication of tubular Al ₂ O ₃ Membrane Using Agar Al ₂ O ₃ Mixtures and Glass-Tube Molds
Author	Miss Nantawadee Udomsri
Major Program	Materials Science
Academic Year	2022

ABSTRACT

In this research, the effect of kaolin addition on the creation of pore size in the ceramic membrane support layer and understanding the mechanism of pore formation was investigated using kaolin particles at the amounts of different kaolin from 0-12 wt% (denoted as K0, K4, K5, and K12) combined with Al₂O₃-agar gelcasting mixture. The alumina slurry, clay, and agar solution were all made separately in the first stage. The mixture was then poured into the glass mold, where it formed into a tubular-shaped gel as the temperature decreased. The gel tube was then taken out of the mold after cooling up for 10 min. It was then submerged in acetone for 50 h. The results of based on the analysis of rheological and viscous behavior, resulting in a confirmed forming change of the state in the temperature range ~42-60 °C. All the membrane support tubes were formed of the mullite phase mainly, which was altered by the inclusion of kaolin particles and contained tiny amounts of quartz and cristobalite. Additionally, to having an impact adding kaolin can result in a larger pore distribution. When consolidated, gab had a pore size distribution that ranged from 0.03-0.2 μm. Moreover, the membrane ducts were under control within the porosity ratio and the bulk density was 34-46% and 2.0 to 2.4 g/cm³, and the resulting flexural green strength was between from 55 to 90 MPa. Furthermore, the flexural strength increased by 2 times with after strength between 629 and 4264 MPa under the specified conditions of sintering at 1350 °C and the water permeability was 40, 73, 1,280, and 12,987 L/m²·h, respectively. Thus, the membranes support K0, K4, K8, and K12 can be later used for the fabrication of asymmetric support membranes. In this, work is underway to deposit ultrafiltration membranes as well as support low-cost and environmentally friendly materials produced from kaolin. Thus, the membranes support K8 membrane supports can be used later for the production of asymmetrical support membranes. It depends on factors such as kaolin content, forming temperature, pore size, mechanical strength and water permeability performance. This work is underway to deposit ultrafiltration membranes as well as support low-cost and environmentally friendly materials produced from kaolin.

Keywords : Al₂O₃ membrane, Kaolin, Agar, Gelcasting, Pore size

ชื่อวิทยานิพนธ์	การขึ้นรูปเมมเบรนอะลูมินาที่ออลวงโดยใช้ของผสมเอการ์อะลูมินาและแม่พิมพ์ ท่อแก้ว
ผู้เขียน	นางสาวนันธวดี อุดมศรี
สาขาวิชา	วัสดุศาสตร์
ปีการศึกษา	2565

บทคัดย่อ

งานวิจัยนี้ศึกษาอิทธิพลของการเติมดินขาว สำหรับประติษฐานท่ออะลูมินาเมมเบรน เพื่อการสร้างขนาดรูพรุนในชั้นรองรับเมมเบรนเซรามิก และสามารถเข้าใจกลไกการเกิดรูพรุนจากการใช้อุณหภูมิดินขาวที่ปริมาณดินขาวตั้งแต่ 0-12 wt% (แสดงเป็น K0, K4, K5, และ K12) ร่วมกับสารผสมเอการ์เจลแคสดีตั้งกระบวนการแรกเตรียมสารละลายอะลูมินา, สารละลายดิน และสารละลายปูน จะถูกเตรียมแยกออกจากกัน ถัดไปนำส่วนผสมเอการ์เจลแคสดีมาเทลงในแม่พิมพ์ท่อแก้วที่ประกอบขึ้น เมื่ออุณหภูมิลดลงสารละลายจะเปลี่ยนสถานะเป็นเจลที่มีรูปร่างเป็นท่อ จากนั้นนำท่อเจลออกจากแม่พิมพ์แล้วทิ้งไว้ที่อุณหภูมิห้องเป็นเวลา 10 นาที ต่อไปนำไปแช่ในอะซิโตนเป็นเวลา 50 ชั่วโมง จากการขึ้นรูปท่ออะลูมินาเมมเบรนปริมาณดินขาวที่เติมมีผลต่อโครงสร้างเมมเบรน สามารถตรวจสอบจากการวิเคราะห์พฤติกรรมการไหลแบบรีโอโลยีและความหนืด ส่งผลให้เกิดการเปลี่ยนแปลงสถานะในช่วงอุณหภูมิ $\sim 42-60$ °C ท่อรองรับเมมเบรนทั้งหมดประกอบด้วย เฟสซิลิกาเป็นหลัก คริสโตบาไลต์ และ ควอร์ต เป็นองค์ประกอบย่อย ซึ่งเกิดจากการเปลี่ยนแปลงเฟสโครงสร้างทางจุลภาคของการเติมดินขาว รวมถึงส่งผลต่อโครงสร้างเมมเบรนสามารถตรวจสอบความขรุขระของพื้นผิว, ขนาดรูพรุน, การกระจายตัวของอนุภาคดินขาวในเมมเบรน, ความแข็งแรงเชิงกล, และประสิทธิภาพการซึมผ่านของน้ำ อาจกล่าวได้ว่าการกระจายรูพรุนที่กว้างขึ้นเมื่อเติมดินขาวเพิ่มขึ้น มีการรวมตัวโพรงที่มีการกระจายขนาดรูพรุนอยู่ระหว่างช่วง $0.03-0.2 \mu\text{m}$ ยิ่งไปกว่านั้นท่อเมมเบรนอยู่ภายใต้การควบคุมภายในอัตราส่วนความพรุน และความหนาแน่นรวมมีค่าเท่ากับ 34-46% และ 2.0 ถึง 2.4 g/cm^3 , ความแข็งแรงดัดที่รับต่อชิ้นงานก่อนเผาผนึกอยู่ระหว่าง 55 ถึง 90 MPa นอกจากนี้ความแข็งแรงดัดยังเพิ่มขึ้นเป็น 2 เท่า เมื่อชิ้นงานหลังเผาผนึกอยู่ระหว่าง 629 ถึง 4264 MPa ภายใต้เงื่อนไขที่กำหนดของการเผาผนึกที่อุณหภูมิ 1350 °C และการซึมผ่านของน้ำมีค่าเท่ากับ 40, 73, 1,280, and 12,987 $\text{L/m}^2\cdot\text{h}$ ตามลำดับ จากผลการทดลองตัวอย่างท่อรองรับเมมเบรน K0, K4, K8, and K12 ดังนั้นท่อรองรับเมมเบรน K8 สามารถนำไปใช้ในภายหลังสำหรับการผลิตเมมเบรนรองรับแบบอสมมาตร ทั้งนี้ขึ้นอยู่กับปัจจัย เช่น ปริมาณดินขาวที่เติม, อุณหภูมิการขึ้นรูป, ขนาดของรูพรุน, ความแข็งแรงเชิงกล และประสิทธิภาพการซึมผ่านของน้ำ อย่างไรก็ตามงานนี้กำลังดำเนินการเพื่อสะสมเมมเบรนอัลตราฟิลเตรชัน รวมทั้งการสนับสนุนต้นทุนต่ำและเป็นมิตรต่อสิ่งแวดล้อมที่ผลิตจากดินขาว

คำสำคัญ : เมมเบรนอะลูมินา, ดินขาว, เอการ์, เจลแคสดี, ขนาดรูพรุน

ACKNOWLEDGMENTS

The thesis on the fabrication of tubular Al₂O₃ membrane using agar Al₂O₃ mixtures and glass-tube molds can be successfully completed. Due to the courtesy, sacrifice, and generosity of many personnel many parties together. The author of the research would like to thank all of you for this opportunity.

I would like to express my gratitude to my advisor, Asst. Prof. Dr. Kowit Lertwittayanon, for providing me with the chance and a positive research experience. He gave me a lot of advice, which was quite helpful. It enables me to carry out my work. Working with him has taught me a lot.

Thank you to everyone of the materials science faculty and personnel. To aid with instruments and facilitate research, Prince of Songkla University Department of Materials Science and Technology Faculty of Science.

I would like to thank all the people and friends in the department. To assist whenever needed in this research.

Moreover, I couldn't have done it without all of you. Thank you to the Center of Excellence in Membrane Science and Technology (CoE-MST), Prince of Songkla University, the research funded by the government expenditures of Prince of Songkla University, and Scholarships to support graduate students from the Faculty of Science Prince of Songkla University All for the procurement of chemicals and various facilities. In addition, we would like to thank all professors for their kindness as a committee for this research.

Finally, I would like to thank my family and my supporter who understand and support me during the thesis make it possible to complete it well.

Nantawadee Udomsri

CONTENTS

	Page
Abstract (English)	v
Abstract (Thai)	vi
Acknowledgements	vii
Contents	viii
List of Tables	xi
List of Figures	xii
List of Abbreviations and Symbols	xv
List of Papers	xvi
Chapter 1 Introduction	1
1.1 Background and Rationale	1
1.2 Objectives	2
1.3 Significance of the Research	2
1.4 Scope of the Research	2
Chapter 2 Review related literatures	3
2.1 Ceramic membranes	3
2.2 Porous ceramic membranes	6
2.3 Ceramic porous materials	6
2.3.1 Pore orientation	7
2.3.2 Components of the pore structure	7
2.3.3 Pore shape	8
2.3.4 Outstanding properties of porous ceramics	8
2.4 Historical overview of kaolin materials	10
2.4.1 Physical properties of kaolin	11
2.4.2 The phase transformation and growth of kaolin	14
2.4.3 The phase transformation of kaolin by XRD	14
2.4.4 Advantages of kaolin	16
2.5 Alumina (Al ₂ O ₃)	17

CONTENTS (Continued)

	Page
2.6 Agar	18
2.6.1 Molecular structure of agar	18
2.6.2 Properties of Agar	20
2.7 Agar gelcasting	20
2.7.1 Gelcasting forming process.	21
2.8 Rheology	22
2.9 Bending strength (test for cylindrical specimen)	24
2.10 Related Research	25
Chapter 3 Research methodology	28
3.1 Materials and Methods	28
3.2 Samples preparation for Al ₂ O ₃ membrane tubes	28
3.2.1 Preparation of gelcasting mixture	29
3.2.2 Preparation of kaolin slip for gelcasting mixture.	29
3.2.3 Agar gelcasting of prepared mixtures	30
3.3 Characterizations	31
3.4 Membrane performance	33
Chapter 4 Results and discussion	35
4.1 Effect of the gelcasting mixture rheological behavior	35
4.2 Dynamic viscosity	37
4.3 Phase analyses of porous ceramic membrane supports	40
4.4 Microstructure of tubular Al ₂ O ₃ membrane	44
4.5 Pore size distribution of tubular Al ₂ O ₃ membrane	46
4.6 Density of Al ₂ O ₃ membrane tubes	49
4.7 Mechanical properties of tubular Al ₂ O ₃ membrane	49
4.8 Permeation test of tubular Al ₂ O ₃ membrane support	51
Chapter 5 Conclusions	53
References	54

CONTENTS (Continued)

	Page
Appendices	62
Vitae	77

LIST OF TABLES

	Page
Table 2.1 Type of membrane separation processes	4
Table 2.2 Advantages and disadvantages of ceramic membrane	5
Table 2.3 The synthesis of porous ceramics frequently includes a substance that disappears during the thermal treatment of sintering	9
Table 2.4 Properties of Kaolin	12
Table 2.5 The research results of the study of chemical composition by X-ray fluorescence technique of Kaolin composed of main compounds, K ₂ O, SiO ₂ , Al ₂ O ₃ are similar but found in different amounts	13
Table 2.6 Properties of Alumina	17
Table 2.7 Fabrication of ceramic membrane using kaolin	25
Table 3.1 The Al ₂ O ₃ slurry is all for preparation and use in the process	29
Table 3.2 The preparation of kaolin slip for mixing in the Al ₂ O ₃ slurry	29
Table 3.3 Characterization of membrane samples	31
Table 4.1 Average pore size and porosity from mercury intrusion porosimeter	46
Table 4.2 The average strength of Al ₂ O ₃ tubes membrane both before and after sintering	49
Table 4.3 Porosity, bulk density, pore sizes, flexural strength, pure water of all tubular Al ₂ O ₃ membrane support form gelcasting method of after sintering at 1350 °C	51

LIST OF FIGURES

		Page
Fig. 2.1	Tubular membrane support systems with single and multiple holes	3
Fig. 2.2	Schematic diagram of asymmetrically structured ceramic membrane	5
Fig. 2.3	The general ceramic porous material	6
Fig. 2.4	The Schematic drawing sample image of porous ceramics	7
Fig. 2.5	Sample image of Orbray's pore orientation and pore structure components by SEM	8
Fig. 2.6	Sample image of pore size and pore shape with control porous ceramics	8
Fig. 2.7	Examples of porous ceramics in industry	8
Fig. 2.8	SEM image of kaolinite stacks	10
Fig. 2.9	Scanning electron micrograph of a low defect kaolinite	11
Fig. 2.10	Computer generated model of the kaolinite unit cell	12
Fig. 2.11	XRD analysis for kaolin	14
Fig. 2.12	XRD analysis of kaolin transformation into metakaolin	15
Fig. 2.13	Shows the structure of Al_2O_3	17
Fig. 2.14	The crystal structure of $\alpha\text{-Al}_2\text{O}_3$	18
Fig. 2.15	Structure of agarobios	19
Fig. 2.16	Structure of agarose	19
Fig. 2.17	The structure of agaropectin	19
Fig. 2.18	Mechanism of agar gelation	20
Fig. 2.19	The Stress-strain rates for concentrated suspension flow curves	23
Fig. 2.20	Different shear stress routes may be seen going up and down (shear rate) in a non-thixotropic (1) and a thixotropic (2) solution...	23
Fig. 2.21	Three-point bending strength	24
Fig. 3.1	Schematic drawing of glass molds and Al_2O_3 tubes after sintering	28

LIST OF FIGURES (Continued)

		Page
Fig. 3.2	Flow chart of forming the tubular Al ₂ O ₃ membrane by agar gelcasting	30
Fig. 3.3	Sample of K0, K4, K8 and K12 (a)-(b) Before and after sandpaper polishing	32
Fig. 3.4	3-point bending test	32
Fig. 3.5	System schematic for measuring membrane performance	34
Fig. 4.1	G', G'', and Phase angle (δ) of gelcasting mixtures with respect to temperature for K0(a), K4(b), K8(c), and K12(d)	35
Fig. 4.2	The viscosity of all the gelcasting mixtures with respect to temperature ramp at a range 80 to 20 °C	37
Fig. 4.3	The viscosity of an Al ₂ O ₃ slurry at various kaolin contents varied with temperature in the range of 20 to 80 °C: Kaolin is added in at 0, 4, 8, and 12 wt% in the figures (a)–(d)	38
Fig. 4.4	X-ray diffraction of raw kaolin after sintering at 1350 °C for 1 h; (M: mullite), (Q: quartz), and (C: Cristobalite)	41
Fig. 4.5	XRD patterns of the raw kaolin and the gelcasting samples after sintering	41
Fig. 4.6	The schematic diagrams showing the mechanism of pore formation from using the kaolin particles together with Al ₂ O ₃ -agar gelcasting mixtures after sintering at 1350 °C at 10000x magnification.....	43
Fig. 4.7	SEM images of tubular Al ₂ O ₃ membrane adding kaolin at 0, 4, 8, and 12 wt% for K0, K4, K8, and K12, respectively after sintering at 1350 °C at different magnification	45
Fig. 4.8	Pore size distribution of all the tubular Al ₂ O ₃ membrane support ...	46

LIST OF FIGURES (Continued)

	Page
Fig. 4.9 Average pore size of all tubular Al ₂ O ₃ membrane by different adding kaolin at 0 to 12 wt% for K0, K4, K8, and K12, (a-d) after sintering at 1350 °C.....	47
Fig. 4.10 Porosity and bulk density of all the tubular Al ₂ O ₃ membrane.....	49
Fig. 4.11 Three-point bending test of tubular Al ₂ O ₃ membrane: (a) before and (b) after sintering at 1350 °C for adding the kaolin particles from 0 to 12 wt%.	50
Fig. 4.12 Pure water flux with applied pressure (0-2 bar) for all sintered Al ₂ O ₃ membrane support tubes	51

LIST OF ABBREVIATION AND SYMBOLS

Abbreviations and symbols	Full word and definition
Al ₂ O ₃	Alumina
Al ₂ Si ₂ O ₅ (OH) ₄	Kaolin
Al ₂ O ₃ ·2SiO ₂ ·2H ₂ O	Kaolinite
3Al ₂ O ₃ ·2SiO ₂	Mullite
HDPE	High density polyethylene
MF	Microfiltration
UF	Ultrafiltration
NF	Nanofiltration
RO	Reverse osmosis
ICDD	International centre for diffraction data
DHR	Discovery Hybrid Rheometer
SEM	Scanning electron microscopy
UTM	Universal testing Machine
MIP	Mercury intrusion porosimetry
XRD	X-ray Diffractometer
HIP	Hot isostatic pressing
nm	Nanometer
μm	Micrometer
mm	Millimeter
Pa	Pascal
MPa	Megapascal
GPa	Gigapascal
g	Grams
g/cm ³	Grams per cubic centimeter
L	Liter
L/ m ² ·h	Liter per hour square centimeter
wt%	Percent of weight
rpm	Revolutions per minute
kV	Kilovolt
N	Newton
bar	bar
psi	Pound per square inch
mA	Milliampere
sec	Second
min	Minute
h.	Hour
°C	Celsius
°C/min	Celsius per minute
°	Armstrong
%	Percentage

LIST OF PAPERS

Reprints were made with permission from the publishers



Nantawadee Udomsri <nantawadeeudomsri858@gmail.com>

Fw: Editor Decision - Accept on your article MATPR-D-22-02304R1

1 message

kowit lertwittayanonh <kowitpakky@yahoo.com>
To: Nantawadee Udomsri <nantawadeeudomsri858@gmail.com>

3 June 2022 at 13:20

FYI

Sent from Yahoo Mail for iPhone

Begin forwarded message:

On Friday, June 3, 2565, 12:46 PM, Rattikorn Yimnirun <em@editorialmanager.com> wrote:

Ms. Ref. No.: MATPR-D-22-02304R1
Title: Effect of clay addition to Al₂O₃-agar mixture on pore size and distribution of tubular Al₂O₃ membrane support fabricated by agar gelcasting
Materials Today: Proceedings

Dear Asst. Prof. Dr. Kowit Lertwittayanon,

I am pleased to inform you that your paper "Effect of clay addition to Al₂O₃-agar mixture on pore size and distribution of tubular Al₂O₃ membrane support fabricated by agar gelcasting" has been accepted for publication in Materials Today: Proceedings.

Below are comments from the editor and reviewers.

Thank you for submitting your work to Materials Today: Proceedings.

Yours sincerely,

Rattikorn Yimnirun
Managing Guest Editor
Materials Today: Proceedings

Comments from the editors and reviewers:

More information and support:

You will find information relevant for you as an author on Elsevier's Author Hub:
<https://www.elsevier.com/authors>

FAQ: How can I reset a forgotten password?
https://service.elsevier.com/app/answers/detail/a_id/28452/supporthub/publishing/kw/editorial+manager/

For further assistance, please visit our customer service site: <https://service.elsevier.com/app/home/supporthub/publishing/>. Here you can search for solutions on a range of topics, find answers to frequently asked questions, and learn more about Editorial Manager via interactive tutorials. You can also talk 24/7 to our customer support team by phone and 24/7 by live chat and email.
#AU_MATPR#

To ensure this email reaches the intended recipient, please do not delete the above code

In compliance with data protection regulations, you may request that we remove your personal registration details at any time. (Use the following URL: <https://www.editorialmanager.com/matpr/login.asp?a=r>). Please contact the publication office if you have any questions.

CHAPTER 1

1. INTRODUCTION

1.1 Background and Rationale

Ceramic membranes, over the past several decades, have been developed for water and oil treatment [1-2], gas separation [3-4], biopharmaceutical [5], and food and beverage processing [6] etc. Most commercial ceramic membranes are produced from alumina due to the stability of the chemical structure and good heat resistance [7]. However, Al₂O₃ based ceramic membranes exhibit disadvantages of high sintering temperatures (up to 1500 °C). In addition, there is a need for a compromise between mechanical strength and porosity when forming a membrane from micron-sized alumina powder [8] at this high sintering temperature.

The ideal aspects of ceramic membranes should be an asymmetrical structural architecture comprising a flawless, very thin isolation topmost layer with small porosity and large pore support layer. Ceramic membrane support is generally a layer that needs high mechanical strength. Optimal porosity dimensions are required, i.e., small pore sizes, size distribution. Therefore, the membrane supports are quite important. We therefore offer a new alternative methods to the production of ceramic membrane supports.

At the same time, this research focuses on the fabrication of Al₂O₃ tubular membrane supports from kaolin addition because kaolin helps to create porosity. It also reduces production costs [9] by means of a phase change mechanism. It is a method that can be implemented with simple equipment, inexpensive, and solves the problem of narrowing the pore size range of ~1-5 μm of the Al₂O₃ ceramic membrane tube support layer. By studying the amount of kaolin at 0, 4, 8, and 12 wt%, the porosity formed between the kaolin particles and the agar molecules might result in the optimal pore structure and size for the preparation of membrane supports based on interaction of kaolin particles [10] and functional groups of agar molecules [11-12]. There is a tendency to produce a repulsive interaction between the surface negative charge at the edge of kaolin and the negative ions of SO⁻³ and OH⁻ in the agar molecules. The repulsive result leads to the separation between the agar and kaolin, creating voids or pores due to shrinkage and decomposition during drying and sintering, respectively. It is assumed that the addition of kaolin at different amounts leads to kaolin phase transition. Therefore, in this work, an alternative pore-interconnection is suitable for use as the desired asymmetric microfiltration membrane support. In combination with gelcasting technique, the production of low-cost Al₂O₃ membranes can be successfully developed in the ceramic industry.

1.2 Objectives

1. To create pore size in ceramic membrane support using kaolin particles together with Al_2O_3 -agar gelcasting mixtures.
2. To understand the mechanism of pore formation from using the kaolin particles together with Al_2O_3 -agar gelcasting mixtures.

1.3 Significance of the Research

1. The alternative of creating pore size in ceramic membrane support can be found.
2. The ceramic membrane support can be sintered at lower temperature leading to lower cost price.

1.4 Scope of the Research

1. Al_2O_3 membrane support is fabricated by agar gelcasting using kaolin particles at different amounts from 0 to 12 wt%.
2. Rheological behavior of agar gelcasting mixtures is studied.
3. Green body of Al_2O_3 membrane support is characterized in terms of bending strength and shrinkage.
4. Sintered body of Al_2O_3 membrane support is characterized in terms of bending strength, pore size distribution and water flux.

CHAPTER 2

2. REVIEW RELATED LITERATURES

Theories and guiding ideas, this research was conducted by looking for information in books or research, as well as relevant studies for a study to succeed in its goals. You can categorize the content as follows:

2.1 Ceramic membranes

Ceramic membranes have undergone much development over the past decades in water and oil treatment, gas separation, biopharmaceuticals, food and beverage processing and fuel cells, because of their good thermal stability and corrosion resistance, high mechanical strength and separation efficiency, and low environmental impact. [13-18] Ceramic membranes, on the other hand, are asymmetric layered structures made up of a separation layer that performs the real membrane function and a ceramic support structure made up of 1 to 5 layers. The support structure acts as a substrate and must have wider pores than the separation layer for general mechanical stability. The support structure is typically made up of a single or multiple-hole support tube (Fig. 2.1)

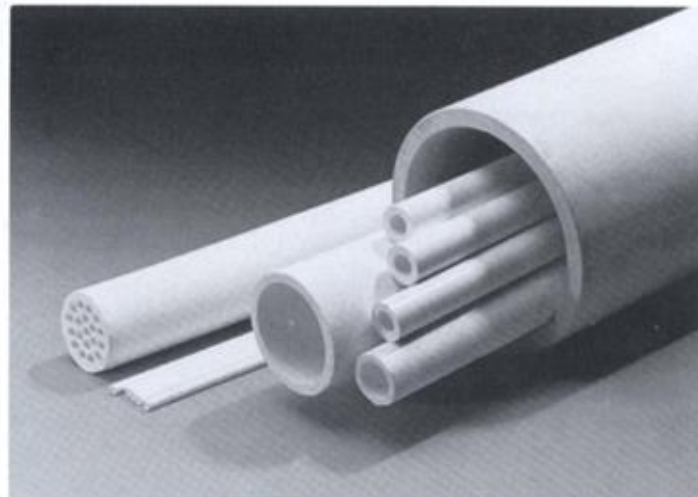


Fig. 2.1 Tubular membrane support systems with single and multiple holes. [19]

A macroporous support is used to create an asymmetric porous ceramic that is then covered in successively thin layers to create an inorganic membrane. The medium encounters mechanical resistance from the support. Depending on their pore sizes, the succeeding layers are active in reverse osmosis (RO), ultrafiltration (UF), nanofiltration (NF), and microfiltration (MF). Table 2.1 lists the main categories for ceramic membranes.

Table 2.1 Type of membrane separation processes.

Membrane type	Structure	Typical average pore size diameter	Separation layer	Constituents passing
MF	1-3 layer	10-0.1 μm (100 nm)	macroporous	Water, high molecular weight, low molecular weight, & ionic species
UF	4 layers	0.1-0.01 μm (10 nm)	mesoporous	Water, low molecular weight, & ionic species
NF	4 layers	10-1 nm	mesoporous	Water & ionic species
RO	5 layers	< 1 nm	microporous	Water

Typically, the support thickness is about 1-2 mm, the MF layer is 10-30 μm thick, UF membranes are a few microns thick and NF membranes are less than 1 μm thick. The support and the MF layer are elaborated by classical ceramic techniques; the top layers (UF or NF) are formed using the sol-gel process (Fig. 2.2).

A ceramic support is formed by shaping a powder and then consolidation of the green body by sintering. The fabrication process consists of four main stages: the choice of inorganic material, paste preparation, shaping, and firing.

The following are the various steps involved in the preparation of ceramic supports:

- selection of inorganic powder (nature and particle size), followed by selection of organic ingredients, then mixing
- pugging to make a paste and aging the paste
- extrusion for shaping, drying, and sintering

There are two primary ways for producing ceramic supports:

- extrusion
- tape casting (or doctor blade)

The shaping procedure chosen must be appropriate for the geometry of the end product, namely extrusion for tubular configurations (mono or multichannel) and tape casting for flat supports.

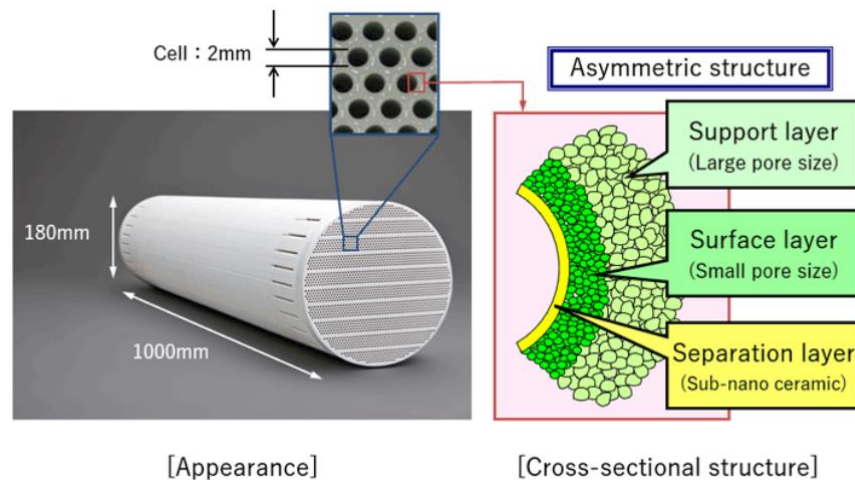


Fig. 2.2 Schematic diagram of asymmetrically structured ceramic membrane. [20]

The following characteristics of ceramic membranes are available:

1. The ability to separate molecules.
2. Consistent pore size for superior separation efficiency.
3. Develop separation technologies that are more energy-efficient and compact.
4. High durability, pressure resistance, and resistance to heat.
5. High permeability and reduced pressure loss.
6. A big membrane surface area provides a lot of processing power.

One of the key advantages of ceramic membranes, which are gaining popularity, is their capacity to withstand extremely harsh conditions, such as strongly acidic solutions. Table 2.2 demonstrates the benefits and drawbacks of the ceramic membrane. [21]

Table 2.2 Advantages and disadvantages of ceramic membrane.

Advantages	Disadvantages
Able to resist high temperatures up to 280 °C. A special development onto modules and system could reach up to 700 °C.	Brittle. Need a very careful handling.
Excellent corrosion resistance (towards organic solvents and a wide pH range).	Most ceramic membranes are in disc or tubular shape; possess low surface area/volume ratio.
Suitable for cleaning and steam sterilization High mechanical strength.	The investment cost of ceramic membrane is very high.
Possess long lifetime.	
High membrane flux for porous membrane.	

Most ceramic membranes are made from oxide powders. ZrO_2 and Al_2O_3 are the most common compounds for microfiltration membrane materials. Mesoporous UF membranes usually also consist of oxides. Al_2O_3 , ZrO_2 , TiO_2 , CeO_2 are most commonly used. Membranes from non-oxide compounds such as C, are also noted in literature. [22]

The next section will demonstrate how support requirements may be both general and particular. The chemical make-up of the membrane material has a direct impact on the individual elements.

2.2 Porous ceramic membranes

Porous ceramic membranes are employed in several industrial processes and have gained a lot of interest during the past 10 years. because it has great qualities such a strong mechanical construction, chemical resistance, and thermal stability. Nevertheless, when it is utilized in strong alkaline media separation and some cost-effective environmental applications, several shortcomings of porous alumina membrane, such as its expensive raw material price and low alkaline resistance, might be exacerbated. [23]

Hence, the scientific community has begun to pay greater attention to the creation of the affordable ceramic membrane resistant to thermal stress and corrosion. [24]

2.3 Ceramic porous materials

Porous ceramics, as their name indicates, are ceramics with a lot of tiny holes (pores) throughout their structure because they have unfilled holes, porous ceramics are light and have low heat capacities. One other option is unidirectional pores. While allowing air to pass through, the ceramic materials long unidirectional pores preserve the material's high rigidity and stiffness. (Fig. 2.3)

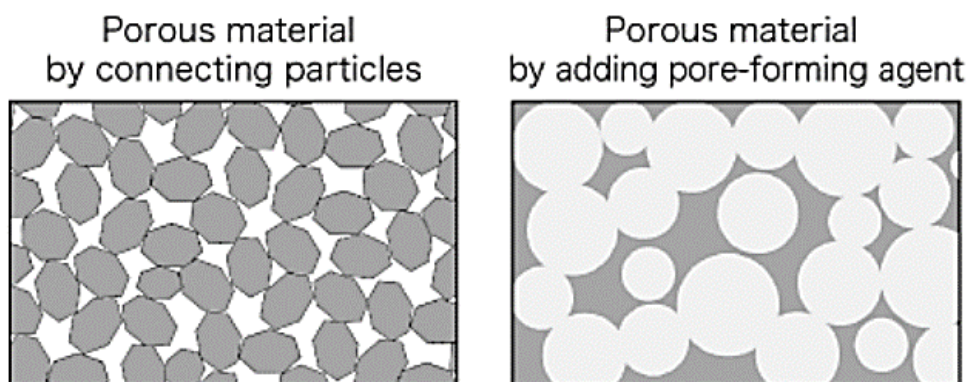


Fig. 2.3 The general ceramic porous material [25].

In general, the term "ceramics" refers to a type of inorganic materials that are made by heating particles to a high point and hardening them. For porous ceramics, the powder is baked at a temperature that prevents complete densification or by using ingredients that add porosity to the structure as it bakes. The procedure, however, gets increasingly challenging as pore diameters decrease. Smaller holes frequently seal, and form separate closed cells, reducing the porosity of the ceramic. With the aid of our proprietary technology, Orbray's porous ceramics maintain excellent porosity even at pore sizes as tiny as a few dozen micrometers. [25]

In order to develop a variety of filtering options for water treatment, exhaust mufflers, jigs and containers for high temperature operations, Orbray uses porous ceramics, which benefit from the great chemical stability and heat tolerance of ceramics. Also, utilizing this high-performance material for environmental causes has gained attention recently. (Fig. 2.4)

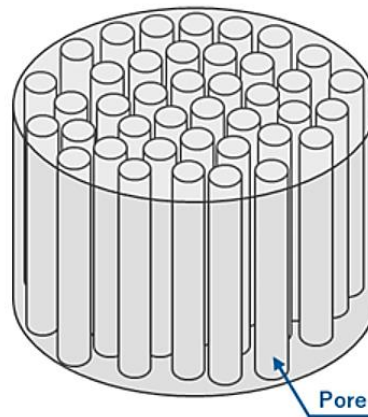


Fig. 2.4 The Schematic drawing sample image of porous ceramics [25].

2.3.1 Pore orientation

Orbray's porous ceramics' pores may be orientated in any way. Unlike most other porous ceramics on the market, our pores are interconnected, resulting in an open cell structure with excellent stiffness and rigidity.

2.3.2 Components of the pore structure

On the outside of our ceramics, it is possible to create a densified layer. Unidirectional pores can potentially have stronger walls. This allows for the controlled formation of nano-porous structures. (Fig. 2.5)

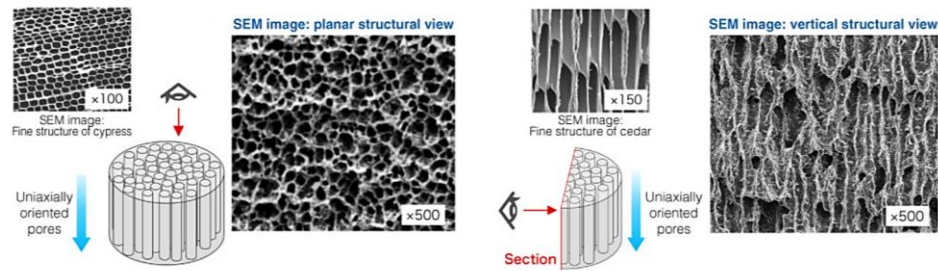


Fig. 2.5 Sample image of Orbray's pore orientation and pore structure components by SEM [25].

2.3.3 Pore shape

Pore size regulation You may create porous ceramics in a range of sizes. As a result, it is possible to adjust the form and arrangement of the pores as needed and exert tight control over their structure. (Fig. 2.6) However, the porosity and strength of the ceramic are also impacted by the pore size.

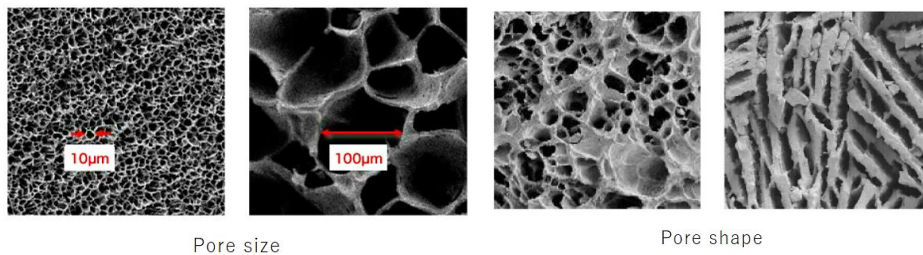


Fig. 2.6 Sample image of pore size and pore shape with control porous ceramics [25].

2.3.4 Outstanding properties of porous ceramics

Porous ceramics have many outstanding properties: light weight, low density. High surface area low thermal conductivity It is a good heat insulator. Has high flow properties good mechanical strength resistant to abrasion and chemical corrosion at high temperatures and resistant to sudden temperature changes.

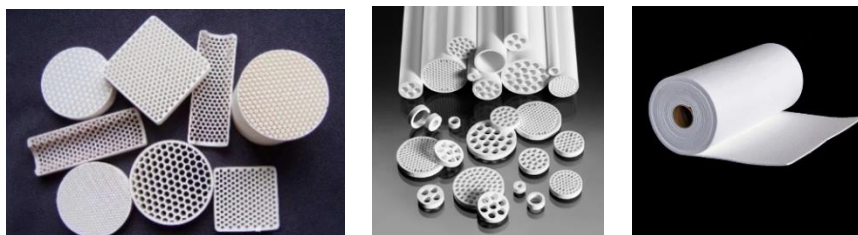
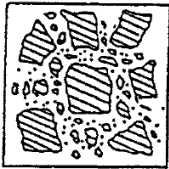
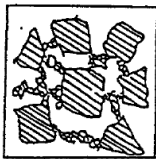
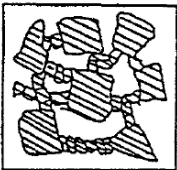
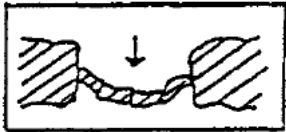



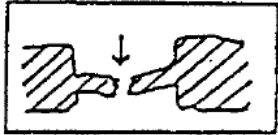
Fig. 2.7 Examples of porous ceramics in industry [26-28].

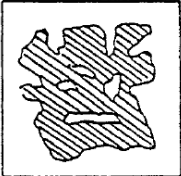
In addition, the research team has developed porous ceramics are used in a wide range of industries including refractory, food, beverage, pharmaceutical, biomedical, chemical, petrochemical, textile, water treatment and water purification using ceramic forming process technologies such as extrusion and slip casting, including laboratory-developed porous ceramic prototypes, including honeycomb ceramic, membrane tube, ceramic sheet. porous substrate, porous alumina board and ceramic water filter. (Fig. 2.7)

In 2008 Chevalier et al. [29] Reviews on the topic revealed that the creation of porous ceramics frequently entails the use of a material that disintegrates during the thermal treatment of sintering (Table 2.3), either through decomposition, evaporation, melting, or burning. This results in the creation of an additional network of pores that alters the membrane pore size distribution that would otherwise be obtained using the ceramic composition alone. For example, Zeng et al., [30] description of the melting and evaporation of polymethyl methacrylate (PMMA). Vijayan et al., description of the decomposition of urea, or Slosarczyk et al., [31-32] description of the burning of flour in ceramics a wide range of materials are employed to create porosity.

Table 2.3 The synthesis of porous ceramics frequently includes a substance that disappears during the thermal treatment of sintering. [33]

Sintering temperature (°C)	Textural evolution	Mechanical resistance
1220	 <p>No sintering</p>	No sintering
1260	 <p>Formation of grain boundaries</p>	Slight mechanical resistance
1300	 <p>Growth of grain boundaries</p>	 <p>Increase of mechanical resistance relative deformation</p>

1340		
	Monolythic ceramic	Decrease of elasticity

1380		Increase of resistance
------	---	------------------------

2.4 Historical overview of kaolin materials

Kaolin or (China Clay) (interchangeably referred to as kaolin) can be easily defined that it is a type of clay that occurs naturally in the earth. It has a white, soft, earthy powder and is formed by the decomposition of silicate minerals by chemical weathering, such as feldspar. [34]

Over the centuries, the historical name of kaolin, it comes from the Chinese word for "Kao-ling", named after a hill near Jauchau Fu, China. [35] by Johnson and Blake used the name "kaolin" for the first time in 1867 [36]. Most of them consist mainly of Kaolinite clay minerals when viewed with an electron microscope. (Fig. 2.8) They are found to consist of hexagonal platy crystals about $0.1\ \mu\text{m}$ to $10\ \mu\text{m}$ or larger in size. [37-39] (Fig. 2.9) These crystals may take vermicular and booklike, and sometimes large macroscopic patterns near the millimeter. Thus, natural kaolin frequently other minerals, such as muscovite, quartz, feldspar, and anatase, are frequently present in variable proportions in kaolin. [40]

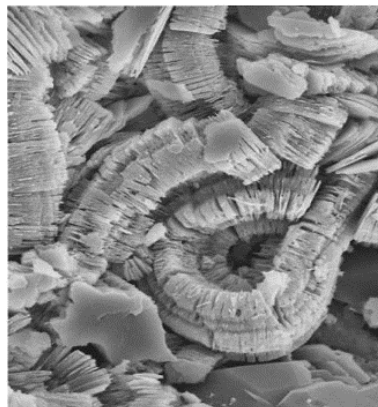


Fig. 2.8 SEM image of kaolinite stacks [41].

Furthermore, clay minerals comprise 80-90% or more of the total mineral composition, with quartz and fine mica making up most of the impurities. [36] Evaporation or a filter press are two methods for removing water from clay. Larger than average particle size compared to kaolin silt, China clay has lower plasticity and green strength, and its narrow particle size distribution also plays a role in these characteristics (not sintered). contains smaller clay mineral particles than clay. little shrinkage occurs because of drying.

Nevertheless, iron hydroxide pigments are frequently used to color raw kaolin yellow. In order to get rid of the iron pigment and other minerals, it is frequently required to bleach the clay using chemicals. To make kaolin ready for additional industrial usage. [42]

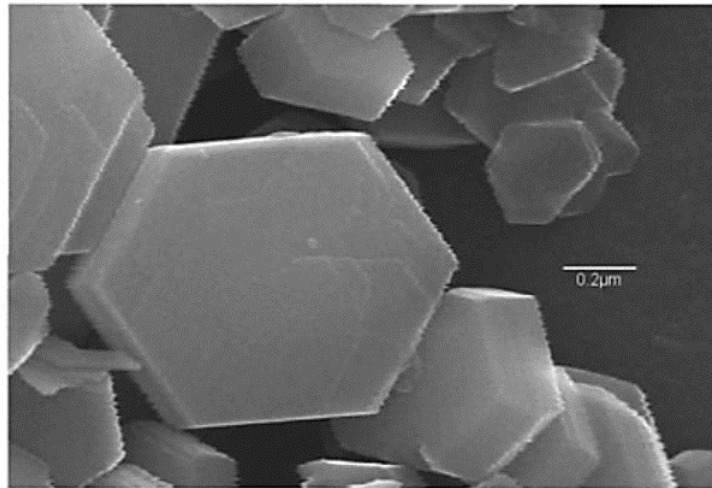


Fig. 2.9 Scanning electron micrograph of a low defect kaolinite [43].

2.4.1 Physical properties of kaolin

Physical properties of kaolin, kaolin has low shrinkage, low cation exchange, chemical resistance, low electrical and thermal conductivity. [44-45] In chemical composition, kaolin approaches the mineral kaolinite ($\text{Al}_2\text{O}_3 \cdot 2\text{SiO}_2 \cdot 2\text{H}_2\text{O}$) formula. Show additional properties in that table. 2.4

Kaolin consists of a structure. $\text{Al}_2\text{Si}_2\text{O}_5(\text{OH})_4$ of clay minerals in the ratio of 1:1 to alumina-silicate This results in a large compaction of SiO_4 tetrahedral sheets and $\text{AlO}_2(\text{OH})_4$ octahedral sheets [46]. The hydrogen bonds of AlOHOSi are attached to two undissociated layers because the kaolinite layer is neutral. An asymmetrical environment of the tetrahedral lamellae with hydroxyl groups is formed on the interlayer surface. However, the tetrahedral lamellae have an oxide surface. These layers are less tightly bonded by Vander Waal forces through the 'c-axis' direction. Classified as a non-expandable mineral [47]. (Fig. 2.10)

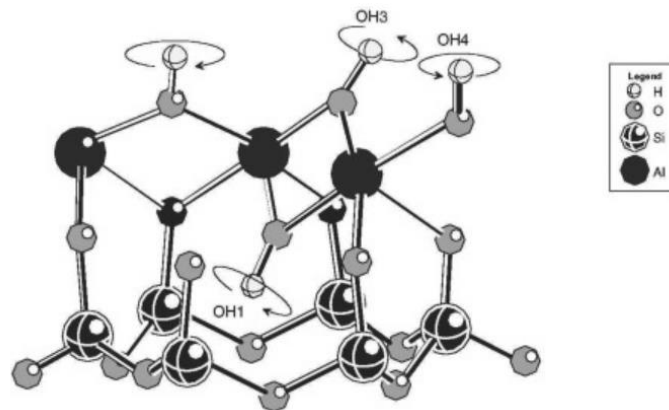


Fig. 2.10 Computer generated model of the kaolinite unit cell [48].

Table 2.4 Properties of Kaolin

Properties	
Chemical formular	$(Al_2Si_2O_5(OH)_4)$ or $(Al_2O_3 \cdot 2SiO_2 \cdot 2H_2O)$
General	It is white, soft, tough, and strong.
Particle size	0.1-10 μm
Particle shape	Hexagonal platy crystals
Melting point	More than 1800 °C
Drying Shrinkage	High shrinkage 6-17% at 1300 °C

Matsushima et al., 1967 [49] The melting point of the extremely refractory clay kaolin is about 1800 °C. As a result of kaolin itself being difficult to mold, kaolin itself is challenging to form. To mature by firing at a hard, thick object is challenging. Kaolin is consequently rarely used by itself in practice; additional materials are typically added to it to make it more workable and to decrease the kiln temperature required to create a hard, thick product. Kaolin does not shrink as much as one might anticipate, given its relatively coarse grain structure and poor dry strength. The essential kaolin ingredients, K_2O , SiO_2 , and Al_2O_3 , are the same yet present in different amounts, making up the pertinent results shown in table 2.5.

Table 2.5 The research results of the study of chemical composition by X-ray fluorescence technique of Kaolin composed of main compounds, K₂O, SiO₂, Al₂O₃ are similar but found in different amounts.

No.	Chemical compositions (wt.%)									Ref.
	SiO ₂	Al ₂ O ₃	Fe ₂ O ₃	TiO ₂	MgO	Na ₂ O	K ₂ O	CaO	LOI	
										[50-55]
1	54.0	32.0	0.98	0.45	0.31	0.25	1.65	0.06	13.1	Chen et al.,2004 (950-1300 °C)
2	50.56	34.15	1.15	0.28	0.31	-	7.18	0.02	6.35	Harabi et al.,2004 (1000-1250 °C)
3	44.76	36.18	0.83	0.84	0.11	3.12	1.15	0.13	12.89	Nuntiya et al.,2006 Narathiwat kaolin
4	51.52	36.9	0.96	-	0.08	-	-	0.58	13.0	Hubadillah et al.,2016 (1200-1500 °C)
5	57.63	37.76	0.86	0.60	0.59	-	1.80	0.34	-	Shehu Yahaya et al.,2017
6	47.85	37.60	0.83	0.74	0.17	-	0.97	0.57	11.27	Rekik et al.,2017 (1000 °C)

LOI: Loss on ignition

2.4.2 The phase transformation and growth of kaolin

There are many different types of kaolin. According to the sources on the surface of the earth, most of them are soils that occur in the original rock decay (Residual Clay), often found in mountains or plains. The sources of kaolin production in the world come from many countries such as the People's Republic of China, South Africa, India, the United States, Pakistan, Czech Republic, Brazil, South Korea, Bulgaria, Bangladesh, Germany, Australia, etc. In Thailand, it can be found in many provinces such as Narathiwat, Uttaradit, Nakhon Si Thammarat, Chumphon, Lampang, Ranong, Surat Thani. Chumphon, Ranong, Prachinburi, Chiang Rai, etc.

In 1921, Chakraborty [56] kaolin was first used in research to study its heating and cooling behavior. In this study kaolin was heated for 4 h in an electric furnace at temperatures ranging from 110 to 1400 °C. It was found that the structure of kaolin was changed due to heat application, i.e., kaolin shifted to an isotropic structure at temperatures above 900 °C and to kaolin is more granular and refractive at 1200 and 1300 °C. At present, there is a large amount of data on the thermal transformation of kaolin. A detailed review of the phase transition of kaolinite clays. These studies are very important as they provide information on structural changes during the sintering process.

2.4.3 The phase transformation of kaolin by XRD

Siti Khadijah Hubadillah et al, 2017. [53] studied how kaolin changes from kaolin to metakaolin, spinel, and mullite through its crystal structure. By comparing the peaks produced by the diffraction patterns with charts developed using JCPDF software registered in the ICDD, the crystalline phase was identified (International Centre for Diffraction Data). The XRD pattern of the kaolin powder as received is shown in Figure 6 [57]. Its crystal structure is converted into amorphous metakaolin when heated at the range of 500 to 925 °C as illustrated in Fig. 2.11. When the sintering temperature exceeds 925 °C, the amorphous structure will transform back into the crystal structure.

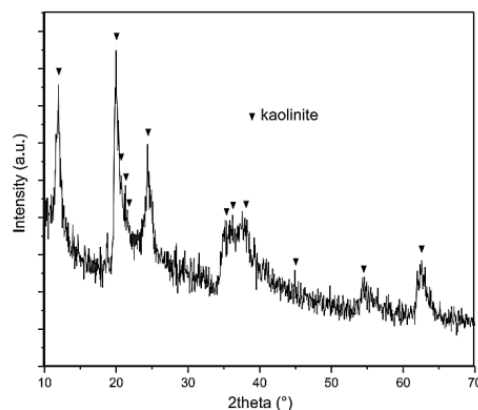


Fig. 2.11 XRD analysis for kaolin [58].

Brindley and Nakahira [53,58] provided a well-integrated description of the sequence of events from the initial layer structure of kaolinite, through a residual layer structure in metakaolin, to a cubic spinel type phase, and finally to a chain type structure in mullite in 1959. They said as follows:

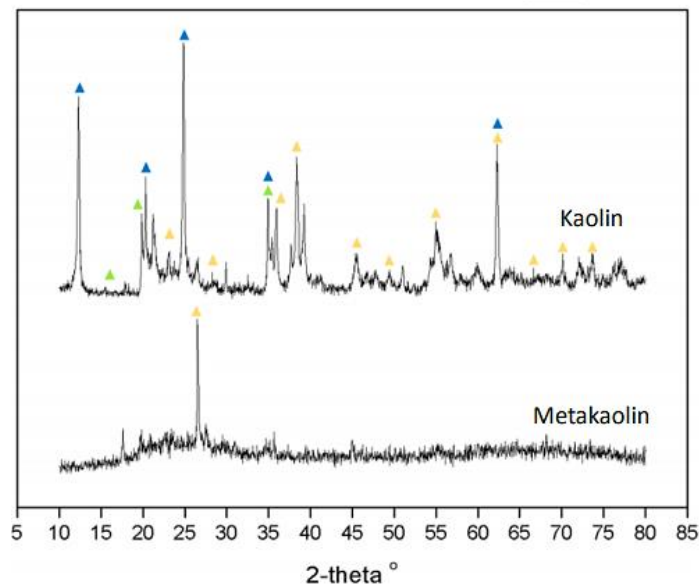
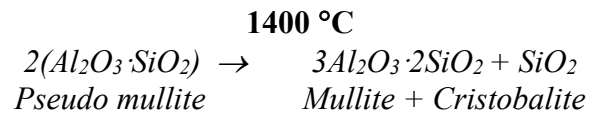
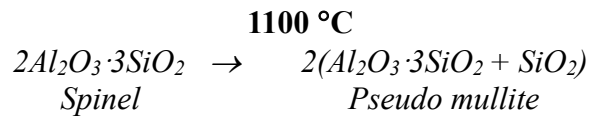
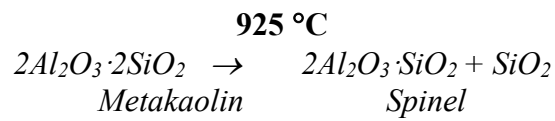
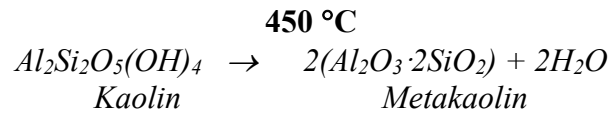


Fig. 2.12 XRD analysis of kaolin transformation into metakaolin [59].

The ceramic membrane is also created by transforming kaolinite into spinel and mullite. Due to its exceptional high temperature stability, mechanical qualities, low creep rate, low thermal expansion coefficient, and low thermal conductivity, mullite is one of the most significant potential materials for porous ceramic membranes [60]. Kaolin is an important raw material and is widely used in various industries. These include water treatment, porcelain production, cement, and ceramics and are equally used as fillers for polymers, paints, and rubbers [61-63]. It is especially important to potters. It's fun to produce clean white porcelain. It contains a primary mineral called kaolinite.

Kaolin frequently contains other minerals such as quartz, feldspar, anatase, and muscovite [64]. Additionally, iron hydroxide pigments can leave a yellow stain on raw kaolin. It is often necessary to chemically decolor the clay to remove the iron pigment and rinse it with water to extract other minerals or separate layers to create kaolin for use in various industries [65-67]

Lee et al and Brindley et al, 1999. [68-69] research study of sintered kaolinite phase changes with great success, this group of researchers set out to settle the argument. At least for clay minerals in their opinion the distinguishing feature of the entire kaolinite-mullite series is their structural continuity and retaining a dense oxygen layer primarily as meta kaolinite ($\text{Al}_2\text{O}_3 \cdot 2\text{SiO}_2 \cdot 2\text{H}_2\text{O}$) sintered at 900-1000 °C and then the Al-Si spinel they claim to be. $\gamma\text{-Al}_2\text{O}_3$ with SiO_2 in $\text{Si}_3\text{Al}_4\text{O}_{12}$ containing solid solution. The metakaolin phase and Al-Si spinel both show a short sequence in the crystal structure. When mullite starts to crystallize at temperatures over 1000 °C and adopts the required orientation with the c-axis parallel to the Al-Si spinel phase.

2.4.4 Advantages of kaolin

Advantages of kaolin it aids in the creation of porosity during the wastewater treatment process and is used in the manufacturing of animal feed, cement, and concrete. Moreover, related research exists and several more advantages shown in table 2.5.

Franco et al.,2007 and Li et al.,2015, [70-71] kaolin can be used as an economical additive that can form a uniform distribution to improve product properties. Important characteristics of kaolin that are important for industrial applications are particle size distribution, structure order, particle shape, irregularity and crystallinity, specific surface area, and whiteness. Many properties of kaolin are controlled by its surface properties mostly in the industry, bulk loads and viscosity are required. These also include the development of adsorbed surface types that alter their characteristics [72]. In addition, many industrial methods take particle size as an important factor [73-74]. Chemical, mechanical, and optical properties, mixing behavior, and the biological distribution of many resources and final products is influenced by particle size and shape.

2.5 Alumina (Al₂O₃)

Alumina has a chemical name that Aluminum oxide (Al₂O₃) is a natural name that is corundum, which is an impurity mineral. Well known for its abrasive material. Corundum includes Andalusite, Sillimanite, and Kayanite, where Andalusite is an aluminosilicate mineral with stability at different pressures and temperatures, in contrast to sillimanite minerals, which are stable at high temperatures, alumina is usually colored. White or colorless, but if there is a small amount of impurities in the structure of alumina. Resulting in different colors, which will be more beautiful, becoming a valuable mineral such as the red color of rubies caused by the presence of chromium in the alumina, etc. and show additional properties in the table. 2.6

Table 2.6 Properties of Alumina [75]

Properties	
Chemical formular	Al ₂ O ₃ : Aluminum dioxide, alumina
Density (g/cm ³)	3.5-3.96
Melting temperature (°C)	2054
Boiling point (°C)	2977
Elastic modulus (GPa)	520
Indentation hardness (GPa)	20

The structure of alumina contains very strong aluminum-oxygen bonds. requires high energy. This makes alumina very hard. The material is stronger than alumina, only diamond. In addition, alumina has many outstanding properties such as a high melting point. High hardness and high chemical stability. Alumina is also extremely resistant to heat and corrosion from many chemicals. and has good insulating properties as well. (Fig. 2.13)

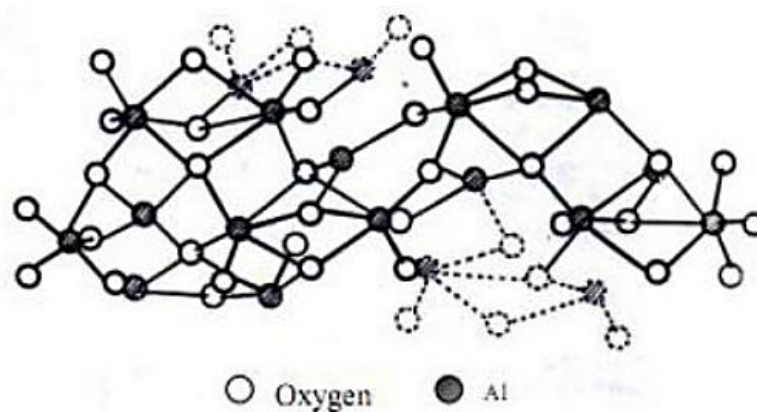


Fig. 2.13 Shows the structure of Al₂O₃ [75].

For the crystal structure of alumina, there are 2 forms: alumina in the form of single crystal (Single crystal), which is a very high value alumina. Because it is used as an ornament and alumina in complex crystal structure form (Polycrystalline) will be cheaper. But it is a raw material that plays a huge role in various industries, especially those that require high temperature applications. Alumina is used in a wide variety of industries such as alumina products used to make grinding balls and wall panels material trimming tools used in fire work, automotive materials, flame retardants, ammunition hazard reducers. as well as parts of medical replacement organs such as joints, artificial bones, etc.

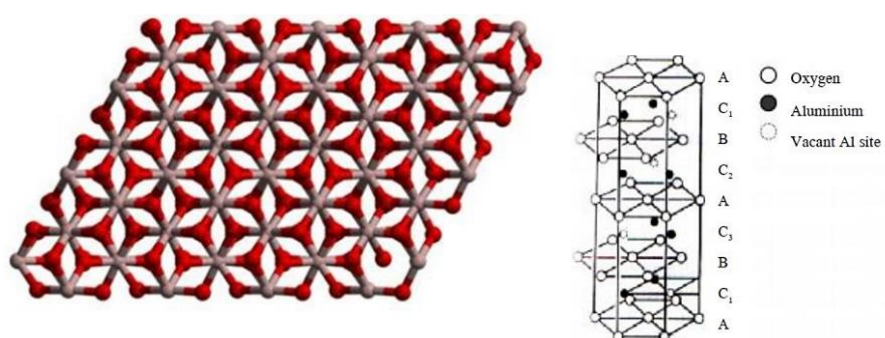


Fig. 2.14 The crystal structure of α - Al_2O_3 [76].

The most stable alumina is in the form Alpha-alumina (α - Al_2O_3) (Fig. 2.14), which has a hexagonal structure, is a unit cell of the structure consisting of six parallel ion layers, each containing aluminum ions and oxygen ions. Only 2/3 of all positions (Dioctahedral) to balance the planar charge of the aluminum ions and there are 3 arrangements according to the position of the gap from the structure. The coordinate number of the positive ion was 6 and the negative ion was 4. The radii of aluminum and oxygen ions were 0.053 and 0.138 nm, respectively.

2.6 Agar

Agar is a hydrocolloid extracted from red seaweed in the phylum Rhodophyta. Most of the red seaweeds used for agar extraction are *Gracilaria* spp. seacoast of Japan, Mexico, Portugal, Denmark, and Morocco. Red seaweed found in Thailand is *Gracilaria fisheri* found in Pattani Bay and Songkhla Lake.

2.6.1 Molecular structure of agar [77]

Agar molecules are composed of polysaccharides 2 important types are Agarose and Agaropectin. Agarose is a long chain polymer of the sugar galactose. Its molecular structure consists of subunits of double sugar molecules is Agarobiose (Fig. 2.15), which contains β -D-Galactose. 3,6-Anhydro- α -L-Galactose are connected at positions 1-4, where each molecule is alternately connected by a glycosidic linkage, agarose. It is electrically neutral or has a very small charge,

therefore it is called a non-ionic polysaccharide. Agarose Structure shown in Fig. 2.16

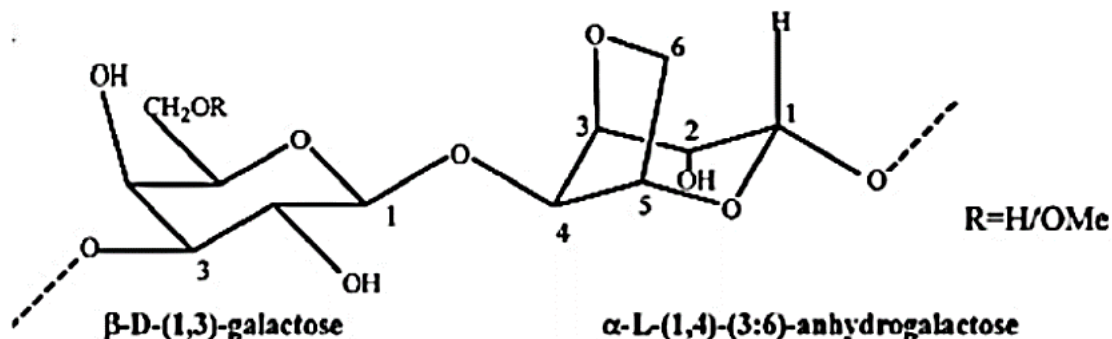


Fig. 2.15 Structure of agarobios.

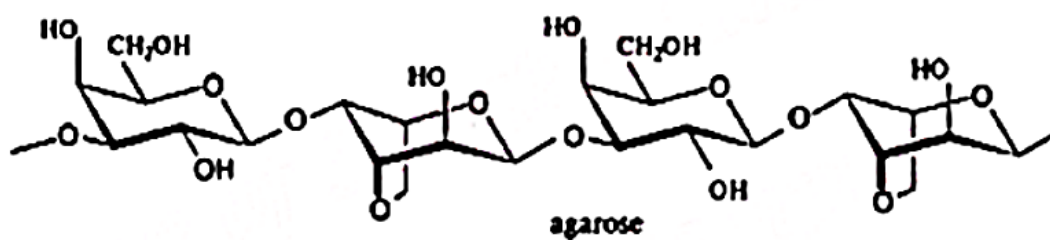


Fig. 2.16 Structure of agarose.

Agaropectin (Fig. 2.17) is similar in structure to agarose but is more complex. This is because some molecules of 3,6-Anhydro α -L- Galactose have a sulfate radical which is replaced by L-Galactose sulfate, and some molecules of D-Galactose have been replaced by D-Galactose sulfate or have a pyruvate group attached. is (4,6-0-(1-Carboxy ethylidene) D-Galactopyranose), which causes these polymers to have a charge. It is sometimes called charged agarose.

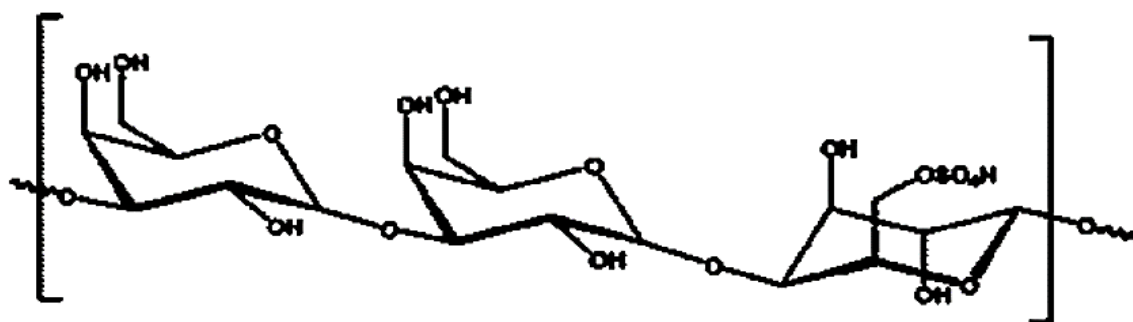


Fig. 2.17 The structure of agaropectin.

2.6.2 Properties of Agar

Solubility properties, agar is normally insoluble in water at 25 °C but is very soluble in water. Heat at a temperature of 85 °C or more. If using agar solution at a concentration of 5%, it must be heated at a temperature of 95-100 °C together with stirring the solution while heating until it dissolves completely. If using a concentration higher than 5 percent, an autoclave must be used to help dissolve.

Gelation of agar the mechanism of gelation of agar (Fig. 2.18) occurs when agar powder is dissolved at a high temperature of 95-100 °C. The agarose molecules in the solution form a random coil. The structure of the molecules is disordered. When the temperature of the solution decreases individual polymer cables double helices are formed when the temperature is lowered. The ends of each double helices are joined together and joined together by hydrogen bonds. This junction is called the Junction zone, which, when combined more, will cause more gel to solidify. cause to be strong 3D lattice structure If the agar gel is heated again, the polymer that binds together in a spiral will gradually loosen from each other. When the temperature is higher than 95 °C, the structure of the gel is formed, relaxes to become a solution in the form of a random coil again, so the agar gel has properties thermoreversible gel because the structure of the gel changes with changing temperature. [78]

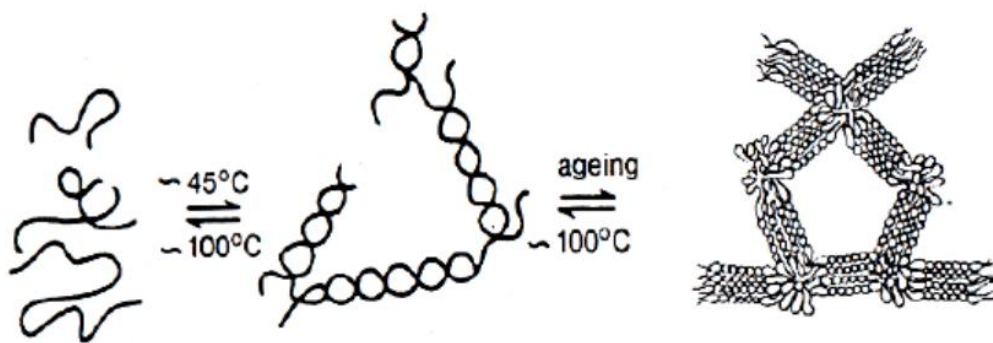


Fig. 2.18 Mechanism of agar gelation.

2.7 Agar gelcasting

Modern ceramics are not primarily made from clay like in the past but are made from synthetic raw materials of high purity. Then be formed by various methods such as hot isostatic pressing (HIP) and injection molding (Injection molding), etc. The resulting ceramic products have good properties such as blades of turbochargers. rotor and rocket launcher.

Around 2000, ceramic researcher Mark Janney et al. [79] at Oak Ridge National Lab, USA, developed a gelcasting method, a new kind of molding that made a ceramicist's dream come true. Gel casting is a molding that is like slip casting, which is well known among ceramicists, with some differences, including the ingredients in the slurry to pour the slurry of gel-casting consists of monomers that will harden into a gel to hold the ceramic powder to adhere to the molded form. Therefore, molds used in the gel casting technique do not need to be made of water-absorbing materials. As good as plaster in pouring patterns.

2.7.1 Gelcasting forming process.

Step 1 Stir and mix the slurry. In this step, the ceramic powder is stirred and mixed with monomer solution with dispersants. Generally, slurry in gelcasting technique is powdered more than 50% ceramic by volume.

Step 2 Put the mixture in step 1 into a vacuum system to separate air bubbles in the slurry, otherwise air bubbles in the slurry will cause pore in the workpiece, resulting in a reduction in the strength of the workpiece to go down.

Step 3 Add initiator and catalyst to activate the reaction. polymerization.

Step 4 Take the slurry into molds made of metal, glass, plastic or wax and bake the mold containing the slurry at about 40-80°C to accelerate the polymerization to complete. This slurry is transformed into a gel with a strong 3D structure.

Step 5 Remove the model and bake the gel from step 4 by starting with controlling the relative humidity in the oven to a relatively high value until the workpiece stops shrinking, then gradually increasing the temperature, and reducing the relative humidity in the oven. Then continue to bake until the workpiece is dry. At this point, the workpiece that has not been burned (Green body) will be strong and can be used for machining is cutting, polishing, or drilling holes without having to be sintered. This point is the advantage of forming gelcasting, finishing the workpiece while it is not sintered is very easy. It is also possible to use a variety of cutting tools such as cutting stones, abrasive stones and drill bits made of plain carbon steel. They are cheaper than diamond trimming tools.

Step 6 In this step, the finished workpiece will be burned to remove binder (Binder burnout) and sintering because the remaining polymer in the dried gel is only 2- 4 wt%, so we may burn the binder and sintering at the same time, which greatly reduces the time and cost compared to having to burn the binder and sinter separately, for example in the case of molding. by injection.

Because the tubular membrane design is the most prevalent configuration, it may be concluded that the gelcasting process is the most significant means of manufacturing ceramic supports. There are more and more articles on the gelcasting technology in the literature, and this practical approach will be used in the future to prepare. To create repeatable ceramic supports using these procedures, several tests and in-depth study of each preparation stage are required. [80]

2.8 Rheology

The well-known Einstein equation predicts the viscosity of an extremely diluted dispersion of non-interacting particles as follows:

$$\eta = \eta_0(1 + 2.5\phi) \dots\dots\dots (2.1)$$

where η_0 is the viscosity of the dispersing medium and η is the suspension viscosity. The so-called inherent viscosity (η) for spheres has a value of 2.5. When applied to anisotropic particles, their value rises.

Low molecular mass liquids with diluted particle dispersions nonetheless exhibit Newtonian behavior. This indicates that there is a linear relationship between the shear rate $\dot{\gamma}$ and the shear stress τ :

$$\tau = \eta\dot{\gamma} \dots\dots\dots (2.2)$$

For greater volume fractions of practical consequence, semi-empirical models like Dougherty-Krieger's are helpful: according to Van Houten's research [81], the greatest packing fraction that can be predicted from the rheology of concentrated alumina suspensions is the maximum wet packing fraction that can be attained during the processing of colloidal ceramics. The relative viscosity of suspension typically decreases with increased shear. In colloidally stable suspensions, which may behave practically Newtonian up to large volume fractions, this shear thinning effect is fairly mild.

However, it is highly potent in agglomerated suspensions, where the viscosity drops due to shear-induced disruption of the agglomerates. The difference in behavior between colloidally stable and unstable solutions may be determined.

The height of the repulsive maximum, if present, and the depth of the (primary) minimum, where the particles are imprisoned in the absence of a shear force, have a significant impact on the rheological behavior of agglomerated suspensions. In some circumstances, it appears that flow must be triggered by a minimum shear stress. The period, however, can also have an impact on this behavior (De number). The yield value of the suspension is the (apparent) minimal stress necessary. Fig. 2.19 provides an illustration of this tendency. Concentrated suspensions may undergo shear thickening at high shear rates (a kind of crowding effect). It can be difficult to pump or mix the solution due to this tendency, however low shear dip-coating processes do not have this problem.

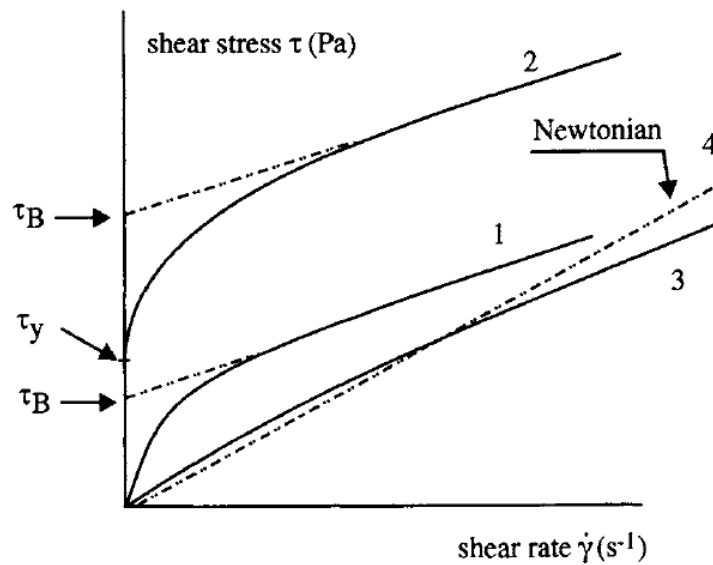


Fig. 2.19 The Stress-strain rates for concentrated suspension flow curves [81].

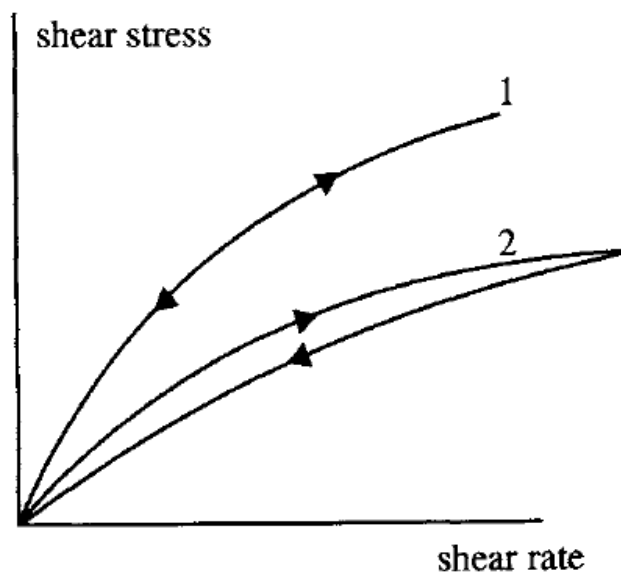


Fig. 2.20 Different shear stress routes may be seen going up and down (shear rate) in a non-thixotropic (1) and a thixotropic (2) solution. [81].

When diffusional relaxation of a suspension brought out of equilibrium by shearing is slow with respect to the timescale of the process, the suspension is said to be thixotropic. This behavior is illustrated in Fig. 2.20. Thixotropy is usually unwanted in ceramic membrane support coatings but does occur for some suspension formulations. For film coating using the same suspension but a variable shear history, the layer thickness might then vary.

Many semi-empirical relationships have been proposed to describe non-Newtonian suspension behavior. For more information the reader is referred to other textbooks on suspension rheology.

2.9 Bending strength (test for cylindrical specimen)

Typically, the three-point bending strength test is performed to check a material's quality. Due to the association between the mechanical resistance and the sintering temperature, which is directly related to the material's porosity properties, this test is not truly intended to characterize the membrane but rather simply the sintered material.

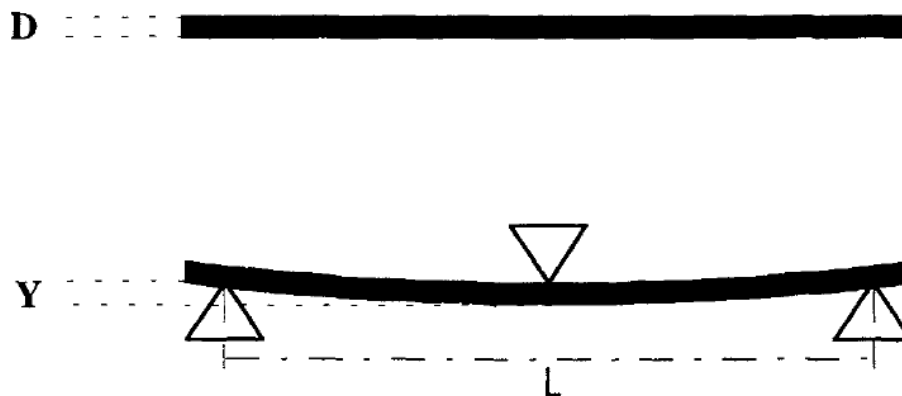


Fig. 2.21 Three-point bending strength [82].

The basic idea is to place the sample on two supports and exert pressure on it until it cracks, as illustrated in Fig. 2.21

By measuring the stress and strain, it is possible to calculate the material's mechanical resistance as a function of the firing temperature. Cylindrical samples are simpler to prepare via extrusion. It is usually assumed that the length to diameter ratio is more than 10. This defines the fracture stress by the equation:

$$\sigma_F = \frac{8LD}{\pi \cdot (D^4 - d_i^4)} \dots\dots\dots (2.3)$$

Where F (Flexural strength) is the action force, L is the distance length between the samples at both ends (span length) in mm, D and d_i are the outer and inner samples diameter in mm of the Al_2O_3 tubular membrane. Each condition was tested on 5 samples to obtain the average strength.

2.10 Related Research

Table 2.7 Fabrication of ceramic membrane using kaolin.

Year	Kaolin contents (wt%)	Fabrication methods	Particle sizes (μm)	Porosity (%)	Flexural strength (MPa)	Applications	Ref. [83]
2012	-	Extrusion	6.8	49-50	28-56	Wastewater filtration	Sarkar et al.,2016
2013	10-28	Extrusion	-	45-52	87	Water filtration	Harabi et al.,2013
2014	4.2, 8.4, and 12.6	Pressing	-	20	180	Water filtration	Done et al.,2014 (1450-1525 °C)
2014	-	Pressing	-	50	20	Water filtration	Liao et al.,2014 (1200-1300 °C)
2015	-	Pressing	-	36-50	-	Water filtration	Chen et al.,2015 (1300-1550 °C)
2016	14-39	Phase inversion	0.04-0.6 and 10-15	27.7	98.9	Support for gas separation	Hubadillah et al.,2016
2016	-	In-situ reaction	-	31.6	100.2(ρ_F)	-	Zhu et al.,2016

Ramnaree et al., [84] conducted research on fabrication of low cost alumina tube through agar gelcasting for membrane microfiltration. In this work, a tubular alumina membrane was formed by combining gel casting technique and acetone drying technique, in the first step Al_2O_3 slurry and agar solution were prepared separately. The mixture was then poured into the mold at a constant temperature of 70 °C. As the temperature decreased, the solution transformed into a tubular and then the gel tubing removed from the mold was immersed in acetone for 50 h. The gel dries quickly after being removed from the acetone by leaving it under atmosphere at room temperature as a result of the research, tubular alumina membranes were prepared from alumina powders with significantly different particle sizes, $\sim 5 \mu\text{m}$ and $0.167 \mu\text{m}$, with different proportions ranging from 5 to 20 wt%. After sintering at 1350 °C, the tubular alumina membrane had an average pore size of between 0.1 and 10 μm , showing great potential as a membrane. which is suitable for MF and UF applications.

Abdallah et al., [85] research the production of ceramic membranes from high alumina roller kiln waste powder with a nano-rosette structure waste powder for desalination application by reusing as a raw material to produce membranes for use in water filtration. The membranes were prepared in disc form using organic binder (PVA) with concentrations ranging from 2% to 8%, sintered at temperatures ranging from 1100-1300 °C for 1,2 and 3 h soaking time. The best properties were examined at 1250 °C sintering due to reduced porosity. Increased small open pores It was shown that the pore size values for the as-prepared membrane ranged from (0.1-0.005 μm), indicating a possible application in NF and UF filtration. 1250 °C, it has high desalination efficiency, high flux value, and shows suitable mechanical strength to withstand water pressure.

Sheikhi et al., [86] research the evaluation of coagulant addition in the study on a kaolinitic clay-based ceramic microfiltration membrane for oily wastewater treatment. Based on the research on the efficiency of inline coagulation-microfiltration (IMF) system for oily wastewater treatment using mem. Kaolinitic clay-based bran ceramics were used as the microfiltration ceramic membrane as the substrate and PVA as the binder. From the results, it can be seen that the IMF process plays an important role in oil wastewater treatment. The membrane minimizes fouling and maximizes filtration efficiency. It can be considered a promising system.

Omatete et al., [87] study was done on gelcasting, from laboratory development to commercial manufacturing. They studied how the gelcasting ceramic molding process was developed to be more successful than other complex shape molding techniques such as molding. Injection molding and gelcasting based on research, an organic monomer solution is poured into the mold and polymerized to create in the form of a mold. Therefore, it is a mixture of polymer chemistry that is processed and according to ceramic standards. The simplicity of this process has

attracted more industry partners and cooperation among them. The process is progressing from the laboratory to industrial production.

Wang et al., [88] conducted research based on gelcasting with 2-hydroxyethyl methacrylate and tert-butyl alcohol to study porous alumina ceramic. Through a new gel casting system used in this work, tert-butyl alcohol (TBA) was used as solvent, acrylamide (AM) as monomer and methylene-bis-acrylamide (MBAM) as a mesh linker. This system has the advantage of allowing low shrinkage of the workpiece. The polymerization of the HEMA-TBA gelcasting system was analyzed by the thermal behavior of the target. Microstructure mechanical properties of sintered workpieces and bending resistance test the results showed that (1) 10 mg/ml of benzoyl peroxide was the most suitable amount for the polymerization of this gelcasting system at 25 °C; The HEMA-TBA gelling system exhibited a shear-thinning behavior. The shear force was low enough for the gelation process. (3) The decomposition temperature. and the combustion of HEMA-MBAM polymerization was about 420 °C. (4) The flexural strength of porous alumina ceramic samples with porosity from 42. % to 56% from (8±0.5) to (91±4.5) MPa was achieved.

Guo et al., [89] studied the pore differences of Al₂O₃ formed by gel formation utilizing polystyrene spherical templates to conduct research on the impact of the forming process on the integrity of pore gradient Al₂O₃ ceramic foams. This approach allows the design of porous ceramics with pore interface degree and gradation layer height through optimum selection of the size and number of spheres. Production process for open cell porous ceramics limited by polymer sponge templates edge cracks and closed porosity can be fixed. In this way, to achieve the best production conditions to maintain structural integrity was studied. The effect of the solid loading of the solution the results showed that at 55 vol.% Al₂O₃ solution containing 0.5 wt.% ammonium polyacrylate maintained good fluidity for casting and avoided excessive internal shrinkage. The different shrinkage behaviors of the top and bottom of the sample were minimized effectively due to approximately the same vapor diffusion area at the top and bottom Thus, the integrity of the dendritic coagulation structure is completely maintained through mold versus direct heating.

CHAPTER 3

3. RESEARCH METHODOLOGY

3.1 Materials and Methods

The utilization of kaolin particles was the main focus of this study. The kaolin from Narathiwat province that was deposited in southern Thailand was employed as the primary raw material to create the pores in the samples. The Al_2O_3 membrane tube was fabricated using Al_2O_3 powder with a mean particle size of $0.2\ \mu\text{m}$ (TM-5D, Taimei Chemicals Co., LTD.) and a purity of 99.99%, Agar powder was employed as a gelling agent. Dispersant, Dispex[®] AA 4040 (water-based, O-BASF) and magnesium oxide (MgO) nanopowder, 99+%purity (Alfa Aesar, metal base) were used for preventing the agglomeration of Al_2O_3 particles and functioning as sintering aid, respectively. Acetone (active ingredient: CH_3COCH_3 99.8%) was utilized as a liquid drying agent. All the preparation was performed with reverse osmosis (RO) water.

3.2 Samples preparation for Al_2O_3 membrane tubes

Al_2O_3 tubes were fabricated by the agar gelcasting in the glass molds. The molds used in the fabrication have outer and inner diameters of 14 mm and 10 mm respectively, as shown in Fig. 3.1.

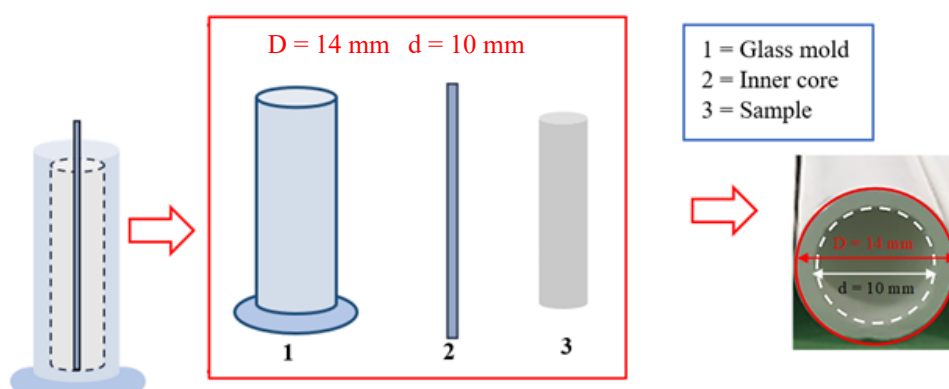


Fig. 3.1 Schematic drawing of glass molds and Al_2O_3 tubes after sintering.

3.2.1 Preparation of gelcasting mixture

Al₂O₃ slurry was prepared by ball milling for 2 h in a 250 ml HDPE bottle using zirconia beads for dispersing the Al₂O₃ particles thoroughly. All the compositions were shown in table 3.1. After ball milling, the Al₂O₃ slurry was filtered using a metal sieve and heated in an ultrasonic (Model: GT SONIC-D6) at a temperature of 60 °C. Subsequently, the warmed Al₂O₃ slurry was mixed with the kaolin slip at 0, 4, 8, and 12 wt% on dry basis.

Table 3.1 The Al₂O₃ slurry is all for preparation and use in the process.

Samples	K0	K4	K8	K12
Alumina (TM-5D)	75	71	67	63
R/O Water	25	25	25	25
Agar powder	0.6 wt% of alumina solid loading			
MgO powder	0.03 wt% of alumina solid loading			
Additive (Dispersant)	1.0 wt% of alumina solid loading			

3.2.2 Preparation of kaolin slip for gelcasting mixture.

The kaolin powder was added into the Al₂O₃ slurry at 0, 4, 8, and 12 wt.% and finally mixed with the agar solution. The kaolin powder was ball milled in HDPE bottle with large zirconia balls. The kaolin powder of 290 g was weighed for ball milling for 45 min in order to avoid the formation of kaolin clusters and agglomeration. After that the mixture of kaolin slip and Al₂O₃ slurry was continuously stirred at 700 rpm for 30 min. A magnetic bar for stirring was used to avoid the settle of the particles in the prepared mixture shown in table 3.2

Table. 3.2 The preparation of kaolin slip for mixing in the Al₂O₃ slurry.

Samples	K0	K4	K8	K12
Kaolin content (wt%)	0	4	8	12
R/O Water	100	96	92	88
Additive (Dispersant)	2.0 wt% of kaolin slip loading			

Agar solution of 2 wt% concentration was prepared. It was added to the warmed Al₂O₃ slurry to provide the final agar content of 0.6 wt%. The mixture of Al₂O₃ slurry and agar solution was stirred and kept at 60 °C.

3.2.3 Agar gelcasting of prepared mixtures

The gelcasting mixtures were molded by pouring into the glass tubes. After the mixtures transformed into the gel state and shaped into tube, the gelling tube was demolded and then soaked in acetone for 50 h. The gelling tube was removed from acetone and left dried at room temperature to become green tube. Finally, the green body will be the Al₂O₃ membrane tube after sintering at 1350 °C for 1 h by Muffle Furnace (Brand: LENTON, Model: UAF-CG). Fig. 3.2 displayed the flow chart of forming by agar gelcasting.

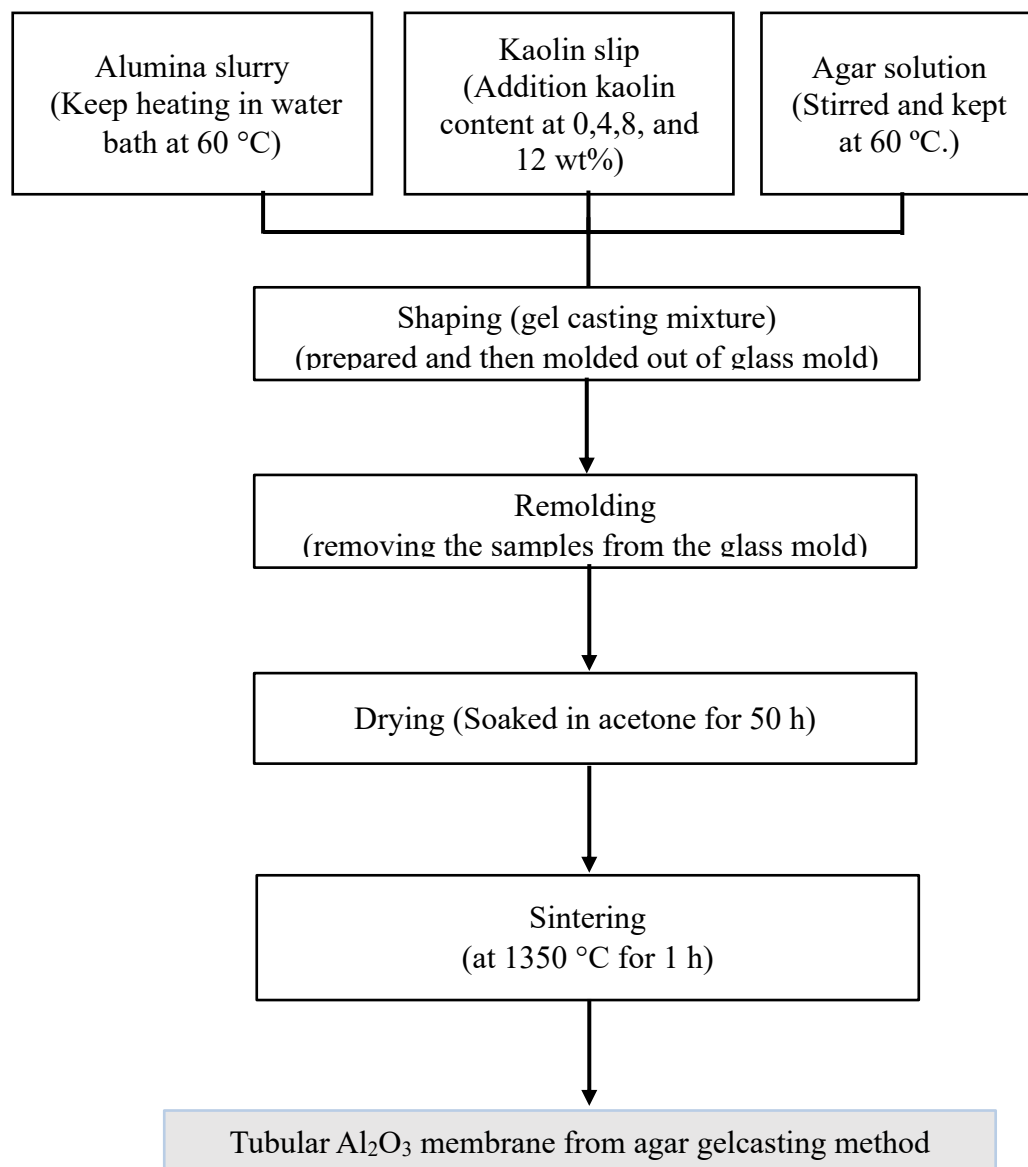


Fig. 3.2 Flow chart of forming the tubular Al₂O₃ membrane by agar gelcasting.

3.3 Characterizations

The characterization of tubular Al₂O₃ membrane was shown in table 3.3.

Table 3.3 Characterization of membrane samples.

Equipments	Models	Conditions
Discovery Hybrid Rheometer (DHR)	Discovery HR 10: TA Instruments; USA	Temperature Ramp (80-20 °C), Ramp rate 20 °C/min, Time step 1 C, Strain 10%, Frequency 10 Hz. And the used cup diameter of with 15 mm.
Scanning electron microscopy (SEM)	(SEM-JSM5800LV,JEOL) : Japan	Operated at voltage of 20 kV and 10 ⁻⁵ Pa.
Universal testing Machine 50 kN (UTM)	Model 5569 Instance under three-point force technique.	Used load cell 500 N with rate 0.5m/min and maintaining a support span of 85 mm.
Mercury intrusion porosimetry (MIP)	(Poremaster, Quantachrome Intruments)	Using instruments capable of measurements at pressures between 0.2 and 60,000 psi.
X-ray Diffractometer (XRD)	Empyrean, DANalytical, Netherlands	X-ray tube: Cu tube, Cu-K _α radiation at 40 kV & 30 mA, wavelength 0.154 nm (Cu-K _α), Scan rage (2θ): 5-90°, Step size: 0.026°, time/step: 70.125 sec.

The rheological behavior was a study of deformation shape to material flow by applying force to the slurry example K0, K4, K8, and K12 to measure the viscosity and elasticity of the samples from a solution of fluid to a solid.

The procedure for preparing samples before testing is followed by the samples K0, K4, K8 and K12 which are sintered at 1350 °C into cold mounting with epoxy resin mixed with the hardener designer 2:1 to support the sample, and then dried the product in the Oven (Brand: BINDER GMBH Model: ED240-E2) at 45-50 °C, as shown in the figure 3.3. 600 and 1200 numbered sandpaper, respectively, were machined and cleaned with the ultrasonic cleaner machine (Model: GT SNIC-D6). Then let it dry at normal room temperature for 24 h. To observe the structure, a sample must be coated with gold before being inserted into an SEM. Various magnifications are used to compare the surface and shape of an Al₂O₃ tubular membrane.



Fig. 3.3 Sample of K0, K4, K8 and K12 (a)-(b) Before and after sandpaper polishing.

The bending test using under three-point force technique, as shown in figure 3.4. All tests were based on ASTM C1866-08 [90] The test specimen is cylindrical in shape, its cross-section is circular, used to calculate the bending strength before and after sintering at 1350 °C section is shown as an equation (3.1):

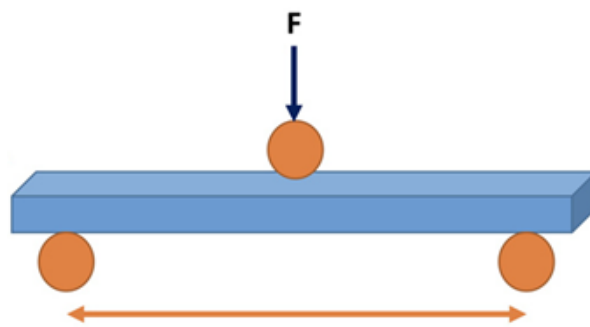


Fig. 3.4 3-point bending test.

The bending strength was obtained from the equation (3.1):

$$\sigma_F = \frac{8LD}{\pi \cdot (D^4 - d_i^4)} \dots\dots\dots (3.1)$$

Where F (Flexural strength) is the action force, L is the distance length between the samples at both ends (span length) in mm, D and d_i are the outer and inner samples diameter in mm of the Al_2O_3 tubular membrane. Each condition was tested on 5 samples to obtain the average strength.

Physical properties in terms of density were examined by Archimedes' method according to ASTM C373-88 [91]. When sintered at 1350 °C, it then boiled Al_2O_3 membrane samples (K0, K4, K8, and K12) in water for 5 h, And lets it cool down at room temperature for 24 h to the density according to the equation.

Where assigned W_1 is the after-sintering weight (g), W_2 is the in water weight (g) and W_3 is the saturated weight in water (g).

ρ are the samples density

$$\rho = \frac{W_3}{W_2 - W_1} \dots\dots\dots (3.2)$$

ρ_A is the apparent density

$$\rho_A = \frac{W_1}{W_1 - W_2} \dots\dots\dots (3.3)$$

$\%A_w$ is the water absorption (%)

$$\%A_w = \frac{W_3 - W_1}{W_1} \times 100 \dots\dots\dots (3.4)$$

$\%\rho_A$ is the apparent porosity (%)

$$\%\rho_A = \frac{W_3 - W_1}{W_3 - W_2} \times 100 \dots\dots\dots (3.5)$$

Finally, the bulk density (ρ_B) is the density of the substance in the sample (g/cm^3).

$$\rho_B = \frac{W_1}{W_3 - W_2} \dots\dots\dots (3.6)$$

3.4 Membrane performance

A membrane permeation test was conducted using a crossflow filtration system. The pure RO water is entered into the sample using the N_2 gas applied pressures from 0-2 bar. Therefore, the water flux value can be calculated per unit area of the tubular Al_2O_3 membrane per time unit by equation (3.7):

$$J = \frac{V}{A \times t} \dots\dots\dots (3.7)$$

Where, J is the permeate water flux ($L/m^2.h$), V is a permeate volume (L), A is the area of samples in m^2 , T is the filtration time (h).

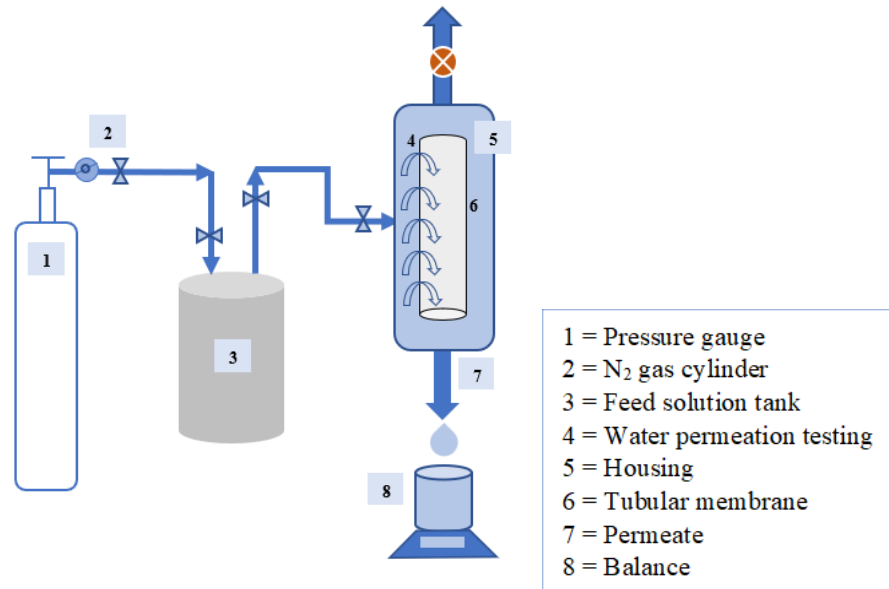


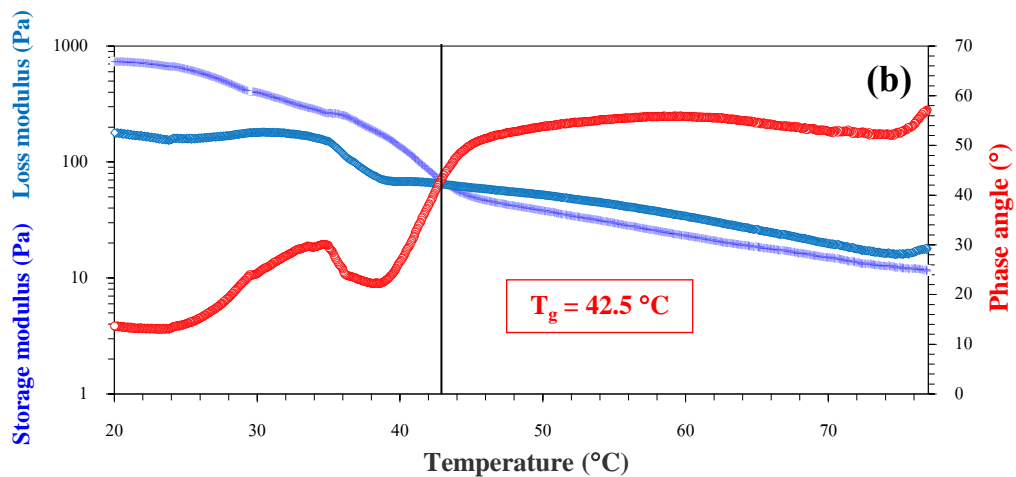
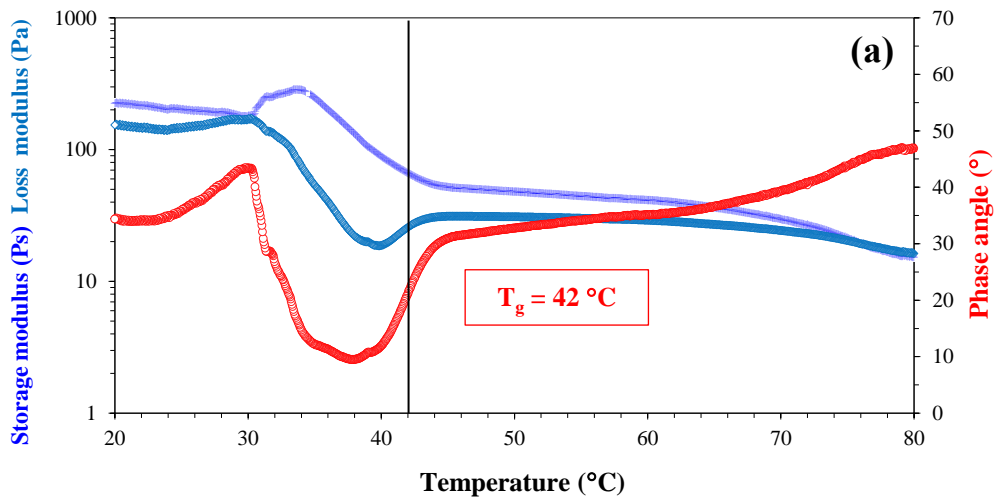
Fig. 3.5 System schematic for measuring membrane performance.

CHAPTER 4

4. RESULTS AND DISCUSSION

4.1 Effect of the gelcasting mixture rheological behavior

Rheological behavior was examined with an HR-2 rheometer (TA Instruments), with a cylindrical aluminum cup with a diameter of 15 mm and using a rotary measuring principle (indenter) to apply force to the mixture. It described the rheological behavior in terms of storage modulus (G') loss modulus (G''), phase angle (δ), gelling temperature, (T_g) and viscosity as shown in Fig. 4.1 and 4.2.



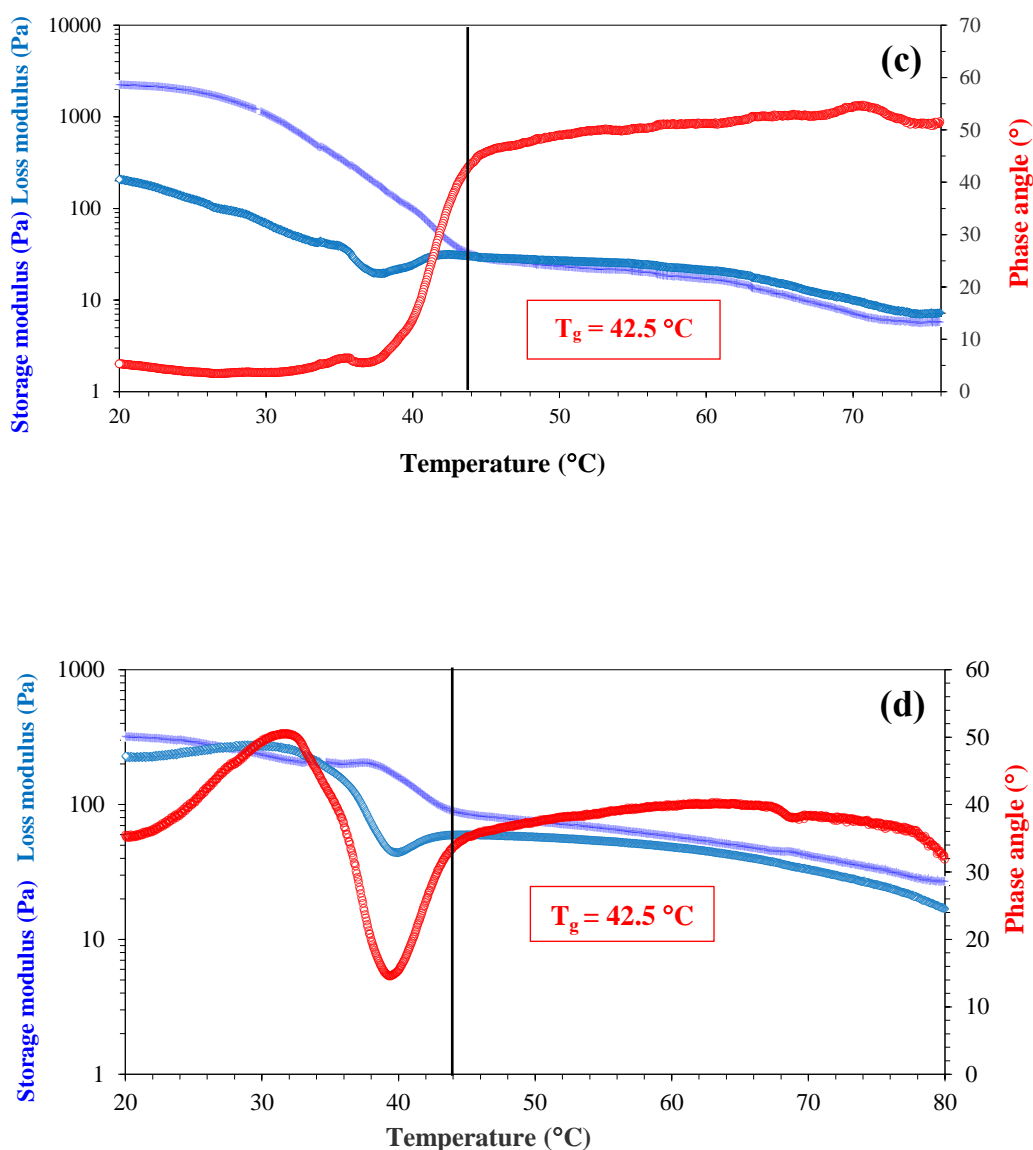


Fig. 4.1 G' , G'' , and Phase angle (δ) of gelcasting mixtures with respect to temperature for K0(a), K4(b), K8(c), and K12(d).

Fig. 4.1 showed the results of the viscoelastic properties of mixtures with different kaolin- Al_2O_3 compositions, there was no change in storage modulus (G') and loss modulus (G'') during the reduction of temperature from 80-43 °C because the mixtures were still in a solution state. But when the temperature dropped below 43 °C, it found that the values increased rapidly. The increasing volumes indicated a transition from solution to gel state [92], being the range of gelling temperature (T_g) of ~42-42.5 °C. as shown in Fig. 4.1a-d.

Since kaolin was added to the Al_2O_3 slurry, (G') and (G'') values showed the initial viscoelastic behavior of the phase angle (δ) at 60° , 52° , and 32° for K4, K8, and K12 respectively (Fig. 4.1b-d). When compared with K0 (Fig. 4.1a) the initial phase angle of 45° indicates that when kaolin was not added to the Al_2O_3 slurry, a double helix formation of agar molecules occurred. However, when the kaolin was added to the gelcasting mixtures, the role of agar in binding and holding the Al_2O_3 particles decreased [93] and the agglomeration of the kaolin structure occurred. This result was mainly due to the surface chemistry between the edge of the kaolin particles and the molecules of agar in the mixtures [Bezerril et al., 2006, Cunha et al., 2006] [94-95], indicating that a region contact between negatively charged clay particles [Avadiar et al., 2015 and Eugene et al., 2017], [96] and negatively charged agar molecules in accordance with the study of Lahrech et al., 2005.[92]

Therefore, the results of the rheological behavior of the addition of kaolin at 0, 4, 8, and 12 wt% confirmed the gelling temperatures. It was found that the temperature ranges from ~ 42 - 60°C can be used to form Al_2O_3 membrane tube samples (K0, K4, K8 and K12) by gelcasting method.

4.2 Dynamic viscosity

The effect of temperature on the Al_2O_3 slurry viscosity for all the samples was examined in the temperature range of 80 to 20°C using different kaolin concentrations of 0, 4, 8, and 12 wt% as shown in Fig. 4.2. From the curve showing the transition between gelling temperature and viscosity to examine the temperature that can be used to form a sample of Al_2O_3 membrane tubes.

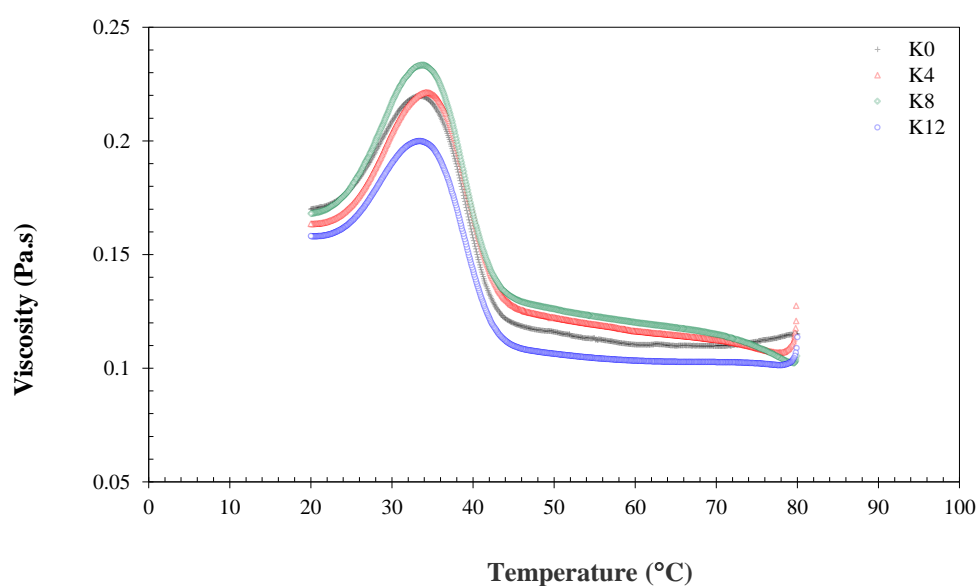
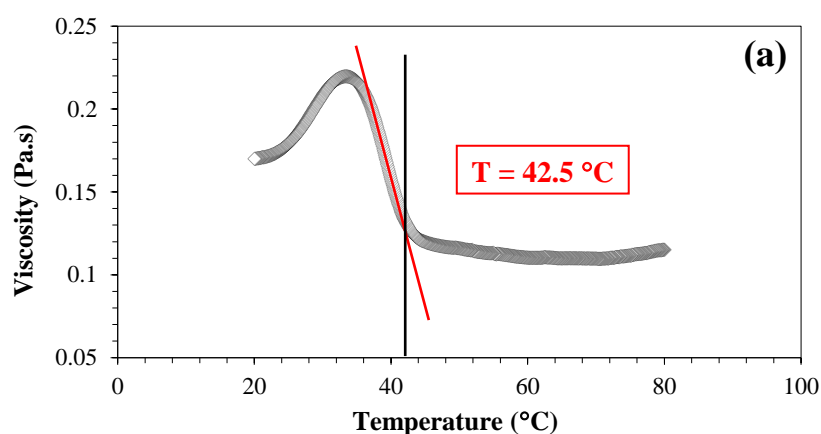


Fig. 4.2 The viscosity of all the gelcasting mixtures with respect to temperature ramp at a range 80 to 20°C .

Fig. 4.3 showed the results of all Al_2O_3 slurries that the viscosity started to change at 0.1 Pa.s and ended at 0.24 Pa.s. It can be seen that the K0, K4 and K8 (Fig. 4.3a-c) samples had similar viscosity values of more than 0.2 Pa.s compared to the sample K12, (Fig. 4.3d) which was less than 0.2 Pa.s. It is most likely that the higher the kaolin concentration, the gradual increase in the viscosity. Since the K12 sample which was more than adequate added a kaolin concentration of 12 wt% in the gelcasting mixtures, the distance between the kaolin particles was reduced making kaolin particles agglomeration or sedimentation of particles. Moreover, it is widely known that kaolinite particles have a platelet shape and relatively rapid precipitation behavior. Therefore, sample K12 might be difficult to pour into the mold due to its highest viscosity. The result in making them more difficult to form, it was likely the occurrence of more agglomeration of kaolin particles compared to the other samples. [97-98] Which makes them unsuitable for the formation of Al_2O_3 membrane tubes. In addition, temperature also has a corresponding influence on viscosity. It can be seen that increasing kaolin concentration resulted in an increase in viscosity as expected. The transition of the state from solution to gel began to occur at a temperature range of 42.5-20 °C. However, this study of temperature and viscosity cannot be attributed to membrane forming. But in this study, the temperature range from 60-42.5 °C, showed the rheological properties confirming the forming and flow temperature of slurry in terms of appropriate viscosity is important and can be attributed to the forming of alumina membrane tube samples which corresponds to Fig. 4.1. Consistent with similar rheological and viscous behavior can be observed from the work of (Hupadillah et al., 2018; Kingsbury & Li, 2009). [73]



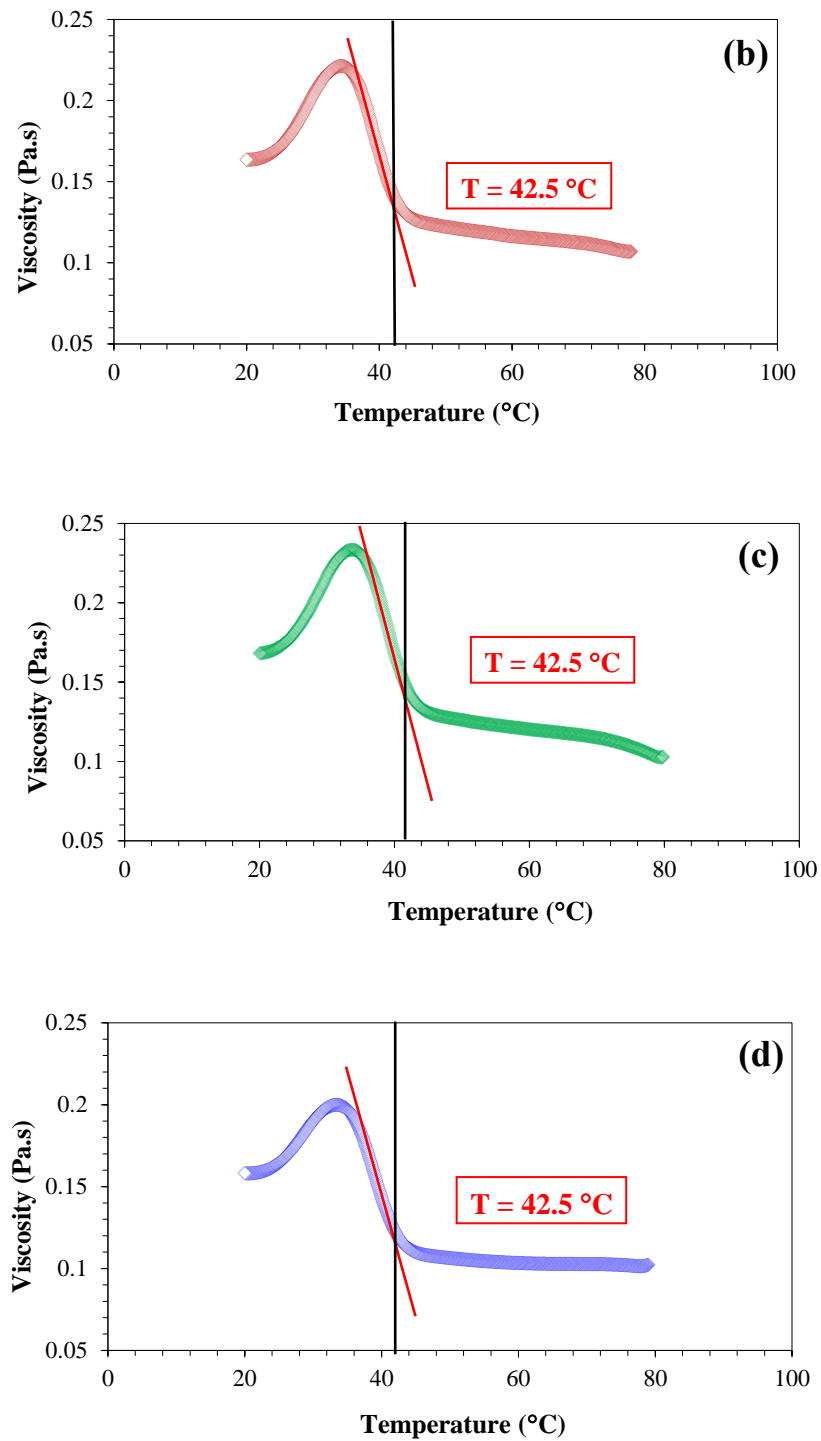


Fig. 4.3 The viscosity of an Al_2O_3 slurry at various kaolin contents varied with temperature in the range of 20 to 80 °C: Kaolin is added in at 0, 4, 8, and 12 wt% in the figures (a)-(d).

4.3 Phase analyses of porous ceramic membrane supports

Based on the XRD pattern of raw kaolin after sintering at 1350 °C as shown in Fig. 4.4, the structure of kaolin was transformed after sintering process from room temperature (25 °C) to 1350 °C. [99] The resulting in the structure of kaolin has a phase change after sintering, the kaolinite phase was not found in the graph, but mullite quartz and cristobalite phases were found. In the phase analysis according to kaolin particles, the original phase could not be identified because kaolinite reacted with Al_2O_3 to form mullite phase ($3\text{Al}_2\text{O}_3 \cdot 2\text{SiO}_2$), which mullite or aluminosilicate, it is one of the most important materials for porous ceramic membranes. It has been recognized in research [100-101] and can also induce porosity in the membrane structure. However, from the research [53,58], studying the raw kaolin group when calcined at 925 °C, kaolinite, ellilite and quartz group were found as the main minerals in raw kaolin. When sintered at temperatures over 925 °C, these ores disappear due to the formation of new phases during the sintering process, this corresponds to Fig. 4.6 showed the schematic diagram shows the mechanism of porosity from the use of kaolin particles to become the mullite phase. The mechanism of pores formation can be explained by the reaction of varying mullite formation with precursors of Al_2O_3 and kaolinite in kaolin particles. It can be seen that the increased pores are caused by the reaction of kaolinite with Al_2O_3 to eventually form mullite phase. ($3\text{Al}_2\text{O}_3 \cdot 2\text{SiO}_2$) Kaolinite is the precursor aluminosilicate formation of mullite, from chemically synthesized precursors usually occurs in the temperature range of 850-1350 °C. Since kaolin particle agglutination is an important factor in determining the reaction mechanism as well as the temperature of mullite formation and sintering is also another factor. From the results of the discussion, when the kaolin concentration is increased as a result, kaolin particles inhibit the sintering of alumina, making the substrate more agglomerate and the higher sintering temperature resulted in a change in pore shape and size. [102]

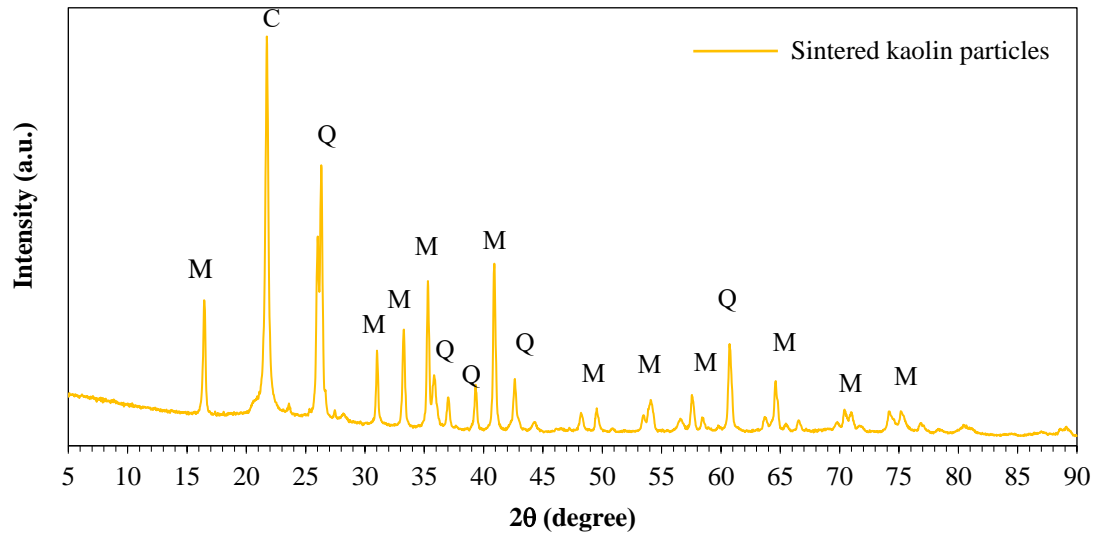


Fig. 4.4 X-ray diffraction of raw kaolin after sintering at 1350 °C for 1 h; (M: mullite), (Q: quartz), and (C: Cristobalite).

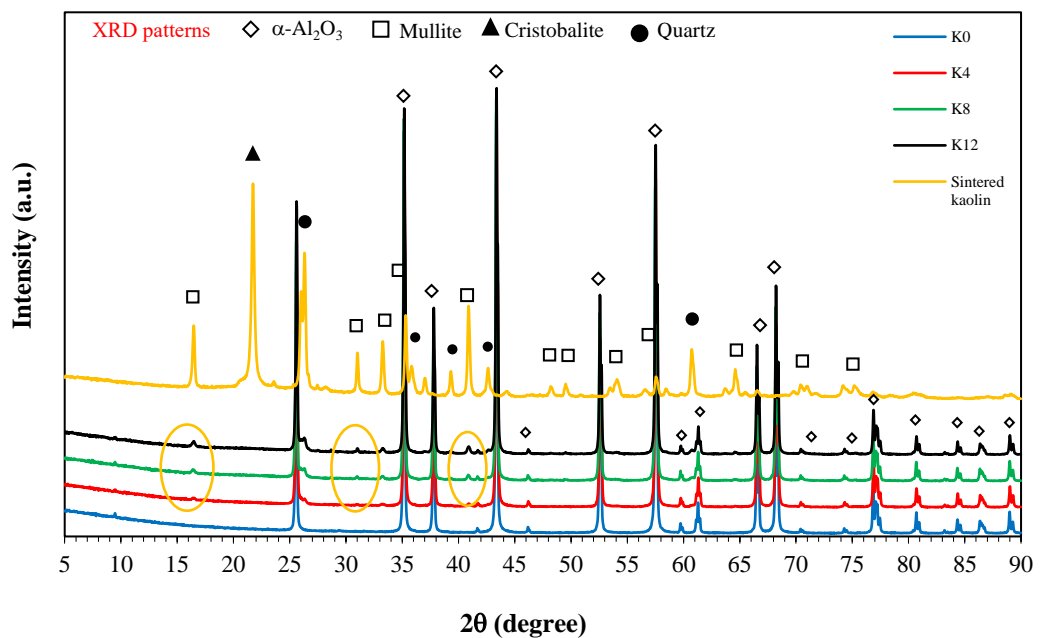


Fig. 4.5 XRD patterns of the raw kaolin and the gelcasting samples after sintering.

Fig. 4.5 showed XRD patterns of the sintered kaolin and the kaolin modified Al_2O_3 tubes. All patterns showed the peaks of $\alpha\text{-Al}_2\text{O}_3$ phase (ICDD card No.00-010-0173). K0 showed the $\alpha\text{-Al}_2\text{O}_3$ peaks only. It was obvious that the peaks of mullite were higher when the amounts of kaolin increased. It was found that the formation of a new phase occurred, i.e., mullite ($3\text{Al}_2\text{O}_3 \cdot 2\text{SiO}_2$), ICDD card no. 00-015-0776, cristobalite (ICDD card no. 01-082-0512) and quartz (ICDD card no. 01-083-0539), compared with the blue line without kaolin addition. Thus, the mullite peaks were apparent when different amounts of kaolin were added. The mullite was able to withstand high temperature up to 1350 °C, thus the mullite phase was observed in this work [103-104].

The XRD patterns of all the kaolin modified Al_2O_3 membrane supports. It was obvious that all the supports contained the phase of $\alpha\text{-Al}_2\text{O}_3$. However, when the amounts of kaolin increased from 0 to 12 wt%, the peaks identified as mullite appeared higher and higher. The increasing peaks of mullite, cristobalite, and quartz were parallel with the result from Fig. 4.4 indicating the mullite phase after sintering at 1350 °C is a major crystalline phase. The results of phase analyses suggested that the kaolin addition to Al_2O_3 gelcasting mixtures might affect the final microstructure and strength of sintered membrane supports [51,105].

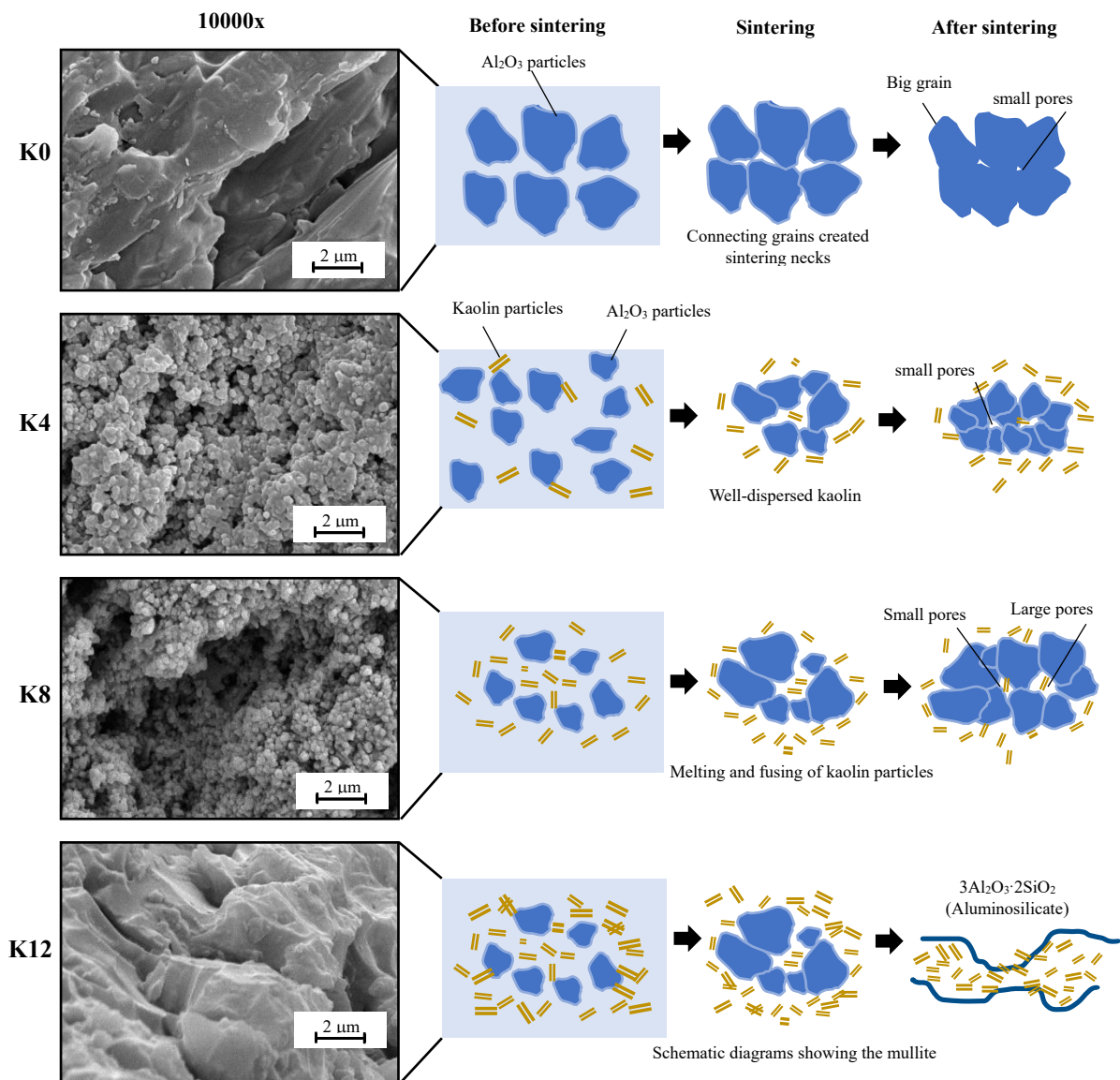


Fig. 4.6 The schematic diagrams showing the mechanism of pore formation from using the kaolin particles together with Al_2O_3 -agar gelcasting mixtures after sintering at $1350\text{ }^\circ\text{C}$ at 10000x magnification.

4.4 Microstructure of tubular Al₂O₃ membrane

Fig. 4.7 showed the SEM images at the surface of all sintered Al₂O₃ membrane tubes, with different amounts of kaolin from 0 to 12 wt%. The SEM images indicated that some of the sintering caused grain growth and partially interconnected pores. [106-107] This combination of particles created closed pores and open pores.

Considering the effect of adding kaolin to the gelcasting mixture shown in sample K4(5000x), small and shallow pores were present. While K8(5000x) showed larger and deeper pores due to the shrinkage of the kaolin particles at high temperatures [108] and the bonding between the kaolin particles.

When adding more kaolin excessively as shown in K12 the surface characteristics of the kaolin became different a different created during the sintering process. [109] The addition of kaolin in excess results in kaolin melting, changing the new structure of the kaolinite group formed by the kaolinite group to react with Al₂O₃ during the sintering process to form a new phase, which is mullite or aluminosilicate, this can be further explained in Figure 4.6 showing the mechanism of pore from kaolin particles. However, increasing kaolin content contributed to higher porosity. [110] Therefore, according to Hedfi et al. [111] kaolin is the preferred raw material for the fabrication of porous ceramic membrane products. But should be added in the suitable amount. If the addition was too much, it might adversely affect the forming process, strength, and membrane permeation performance.

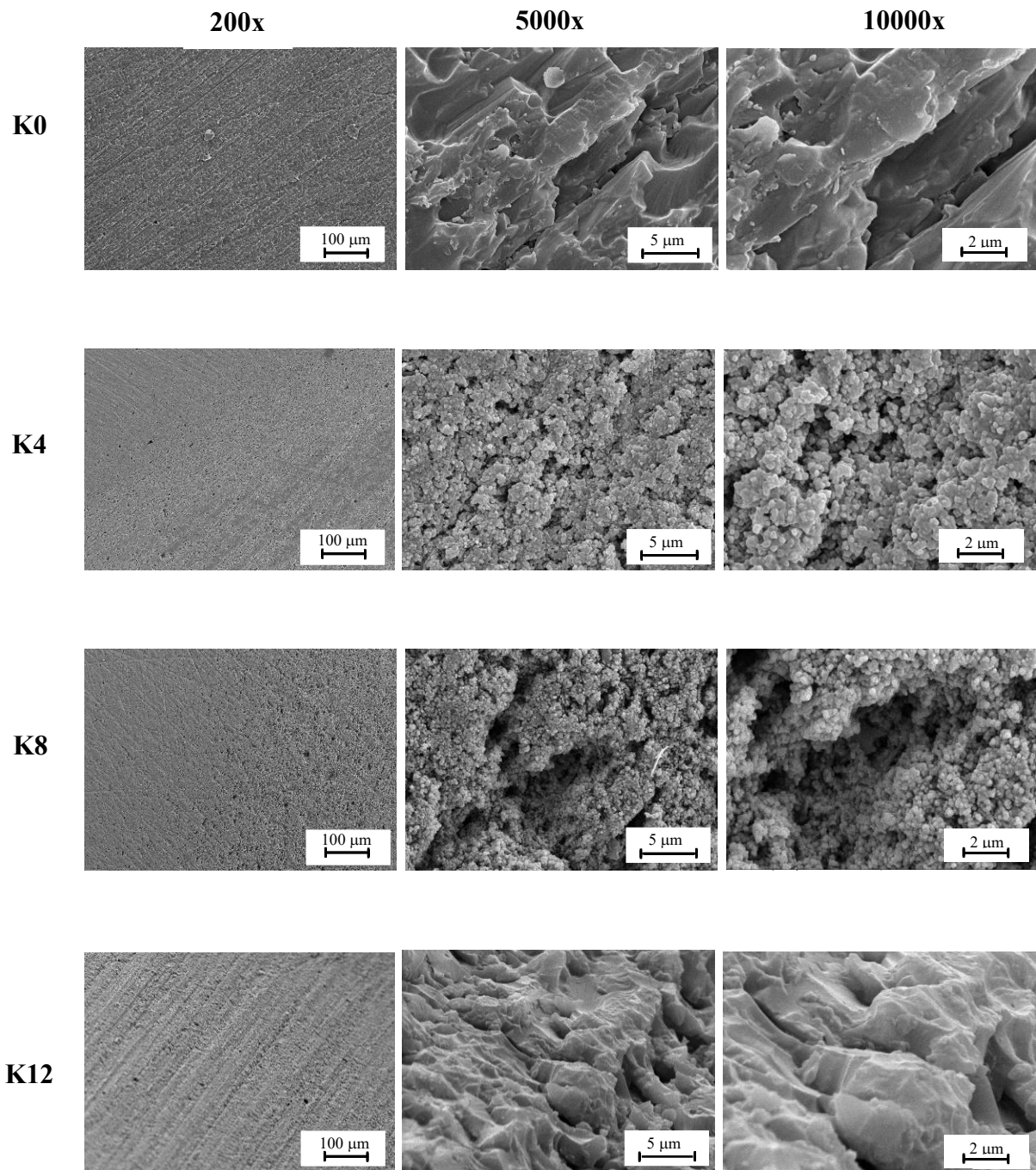


Fig. 4.7 SEM images of tubular Al_2O_3 membrane adding kaolin at 0, 4, 8, and 12 wt% for K0, K4, K8, and K12, respectively after sintering at 1350 °C at different magnification.

4.5 Pore size distribution of tubular Al₂O₃ membrane

Table 4.1 Average pore size from mercury intrusion porosimeter.

Samples	Mercury intrusion porosimetry
	Average pore size (nm)
K0	153
K4	143
K8	151
K12	142

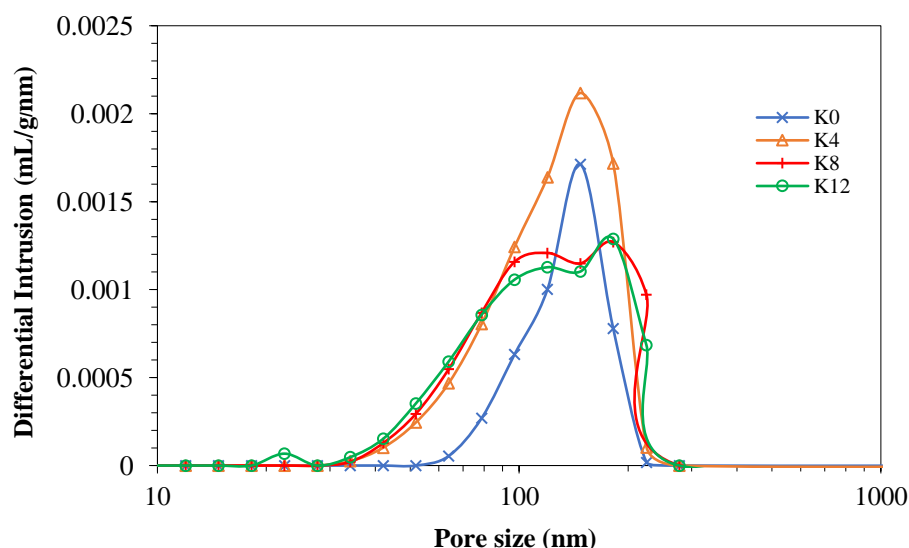
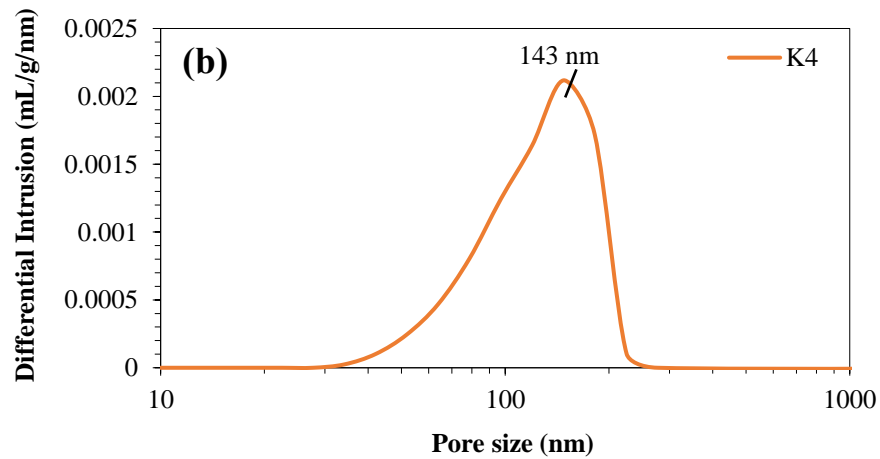
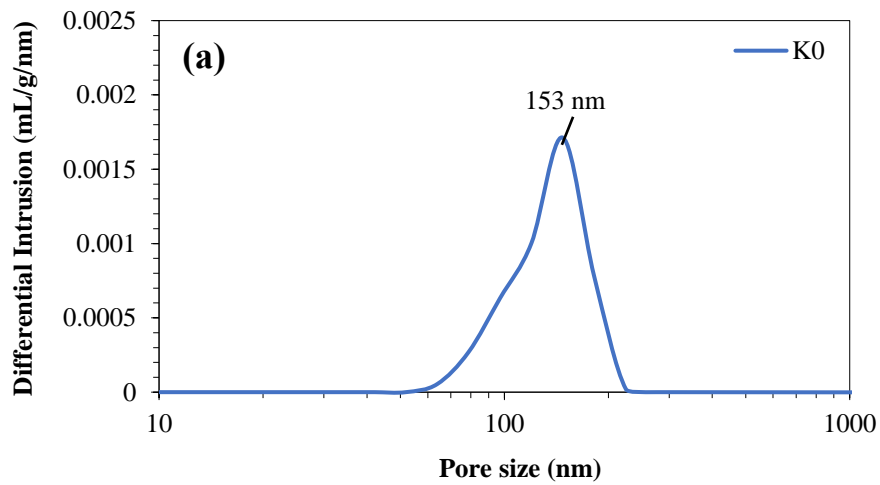


Fig. 4.8 Pore size distribution of all the tubular Al₂O₃ membrane support.

The pore size distribution of all the sintered Al₂O₃ membrane support tubes, with different amounts of kaolin from 0 to 12 wt%, as shown in Fig. 4.8. It was obvious that for all the membrane supports, the pore size distribution range of 0.03-0.2 μm (30-200 nm), this varies depending on the added kaolin. From the pore size distribution results of the Al₂O₃ membrane support tubes as shown in Table 4.1. In this study a function of the particle size effect from the addition of kaolin. It can be seen from MIP analysis for samples K0, K4, K8, and K12, the average pore size value is 153, 143, 151, and 142 nm, restively. When the increasing kaolin content makes pores smaller because of the distribution of higher kaolin particles in the Al₂O₃ membrane between 30 and 200 nm. but for the K8 sample the due to the slightest defect caused by air bubbles trapped in the gelcasting mixture during the process. This gives a maximum average pore size of 0.151 μm (151 nm). For the samples K0 represent the pore size distribution with the pore size region at about 0.153 μm

(153 nm). The pore size is smaller pore distribution inside the Al_2O_3 tubes without kaolin doping exhibited a narrow pore size distribution between 50 and 200 nm (Fig. 4.9a). Therefore, the small pore size is formed due to the presence of gaps between the sintered Al_2O_3 (TM-5D particle size of 0.2 μm) and kaolin particles. However, when the amounts of kaolin increased from 0 to 12 wt%, the large pore size between 30 and 200 nm value is shifted 143, 151, to 142 nm show in samples K4, K8, and K12, (Fig. 4.9b-d), it has small pore size compared to sample K0.



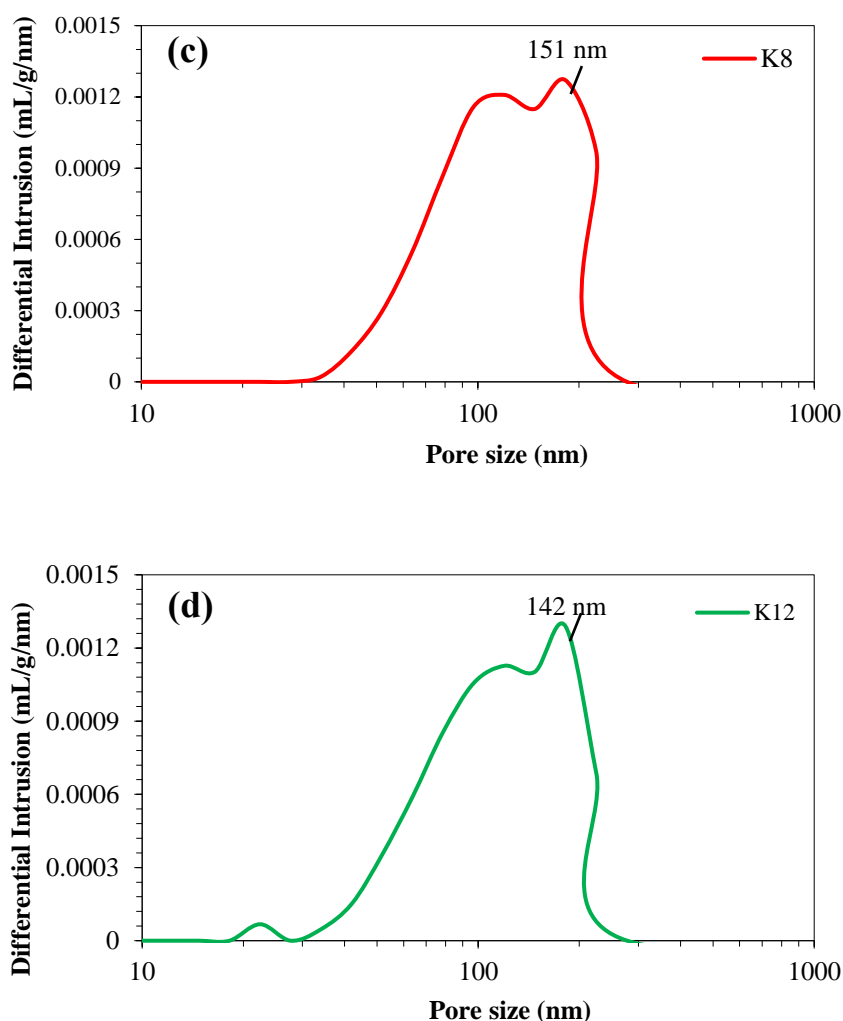


Fig. 4.9 Average pore size of all tubular Al_2O_3 membrane by different adding kaolin at 0 to 12 wt% for K0, K4, K8, and K12, (a-d) after sintering at 1350 °C.

The results of all samples K0, K4, K8, and K12 which are sintered at 1350 °C, it was obvious that for all the membrane supports, the pore size distribution range of 0.03-0.2 μm . It can be confirmed that kaolin can form pores in the membrane support. The results of the pore size distribution measurement indicated that the average pore sizes were within the range of an ultrafiltration (UF) membrane. In addition, it is caused by the formation of the neck structure of mullite particles in kaolin, which is a common phenomenon in high temperature sintering processes depending on the sintering temperature of 1350 °C. This step reduces the number of pores, eventually the membrane undergoes a densification process and finally creates a porous structure. Observe the SEM image of sample K12, this is also consistent with its low mechanical strength and high permeability performance. As a result, more options are available for selecting samples for the production of support membranes.

4.6 Density of Al₂O₃ membrane tubes

The porosity and bulk density of all Al₂O₃ membrane tubes formed by the gelcasting method were shown in Fig. 4.10. When the kaolin particles increased, the porosity of the Al₂O₃ membrane increased from 34 to 46% consistent with the results of Zyryanov and Karakchiev [112], on the other hand, the bulk density of the Al₂O₃ membrane decreased from 2.4 to 2.0 g/cm³, corresponding with SEM images shown in Fig. 4.7. It was found that the increase in porosity and the different distribution of sintered kaolin phases. Therefore, the increasing amount of kaolin was responsible for porosity and the larger pore sizes. Furthermore, the non-uniform distribution might result in a decrease in density, which might affect the strength of the membrane.

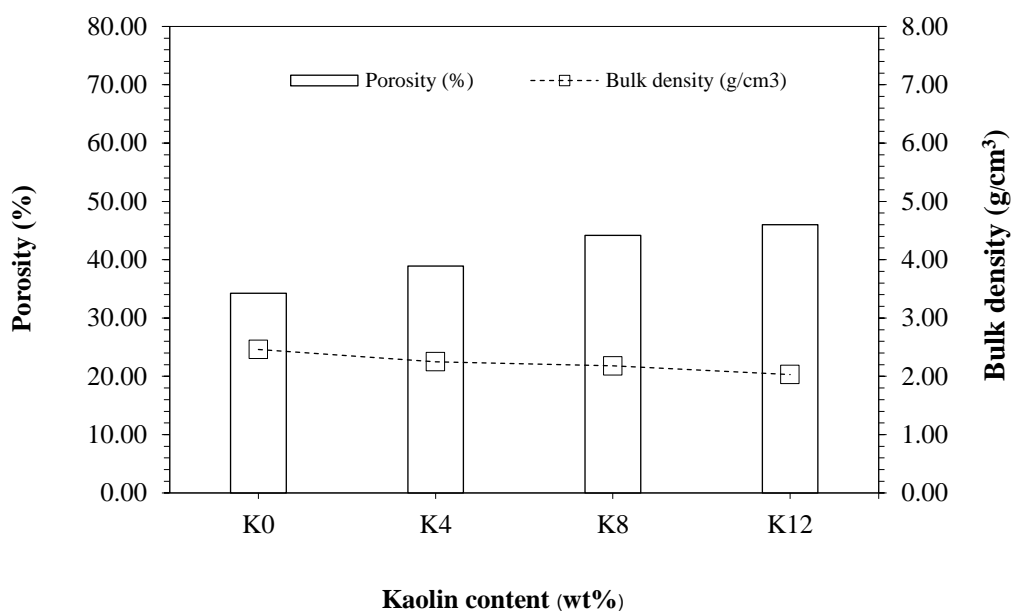


Fig. 4.10 Porosity and bulk density of all the tubular Al₂O₃ membrane.

4.7 Mechanical properties of tubular Al₂O₃ membrane

Table 4.2 The average strength of Al₂O₃ tubes membrane both before and after sintering.

Samples	Flexural strength (MPa)	
	Green strength	Sintered strength
K0	90.84 ± 21.04	4264.70 ± 1,214.57
K4	80.43 ± 21.97	1292.38 ± 573.35
K8	63.48 ± 18.75	1083.58 ± 157.79
K12	55.45 ± 16.48	629.14 ± 339.46

Fig. 4.11 presented the bending strength of all the Al_2O_3 membrane tubes before and after sintering at $1350\text{ }^\circ\text{C}$ using the three-point bending technique. As a result of the addition of kaolin, the strength of the green and sintered samples decreased rapidly. The strength of sample K0 values before and after sintering were 90.84 and 4264.70 MPa. When the kaolin was added for K4, K8, and K12 their flexural strength values continued to decrease. From table 4.2. It confirmed that adding a greater amount of kaolin particles resulted in the decrease in the green strength. This is due to its direct relationship with the dispersion behavior of stacked kaolin [81,113], thus resulting in a high porosity. Thus, it implied that the mechanical properties of the tubular Al_2O_3 membrane were in agreement with the resulting physical properties.

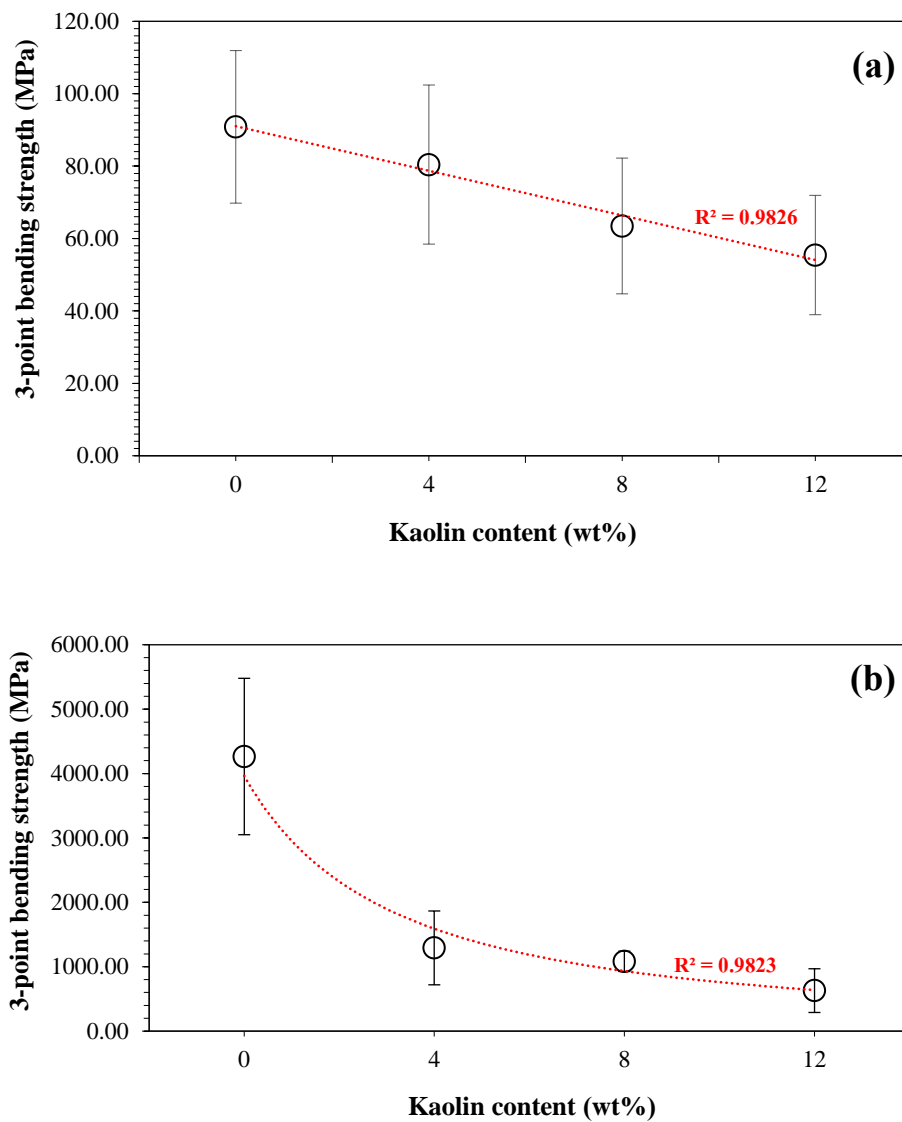


Fig. 4.11 Three-point bending test of tubular Al_2O_3 membrane: (a) before and (b) after sintering at $1350\text{ }^\circ\text{C}$ for adding the kaolin particles from 0 to 12 wt%.

4.8 Permeation test of tubular Al₂O₃ membrane support

Table 4.3 Porosity, bulk density, pore sizes, flexural strength, pure water of all tubular Al₂O₃ membrane support form gelcasting method of after sintering at 1350 °C.

Samples	Porosity (%)	Bulk density (g/cm ³)	Flexural strength (MPa)	Pure water flux (L/m ² ·h)
K0	34	2.5	4,265	40
K4	39	2.3	1,292	73
K8	44	2.2	1,084	1,280
K12	46	2.0	629	12,987

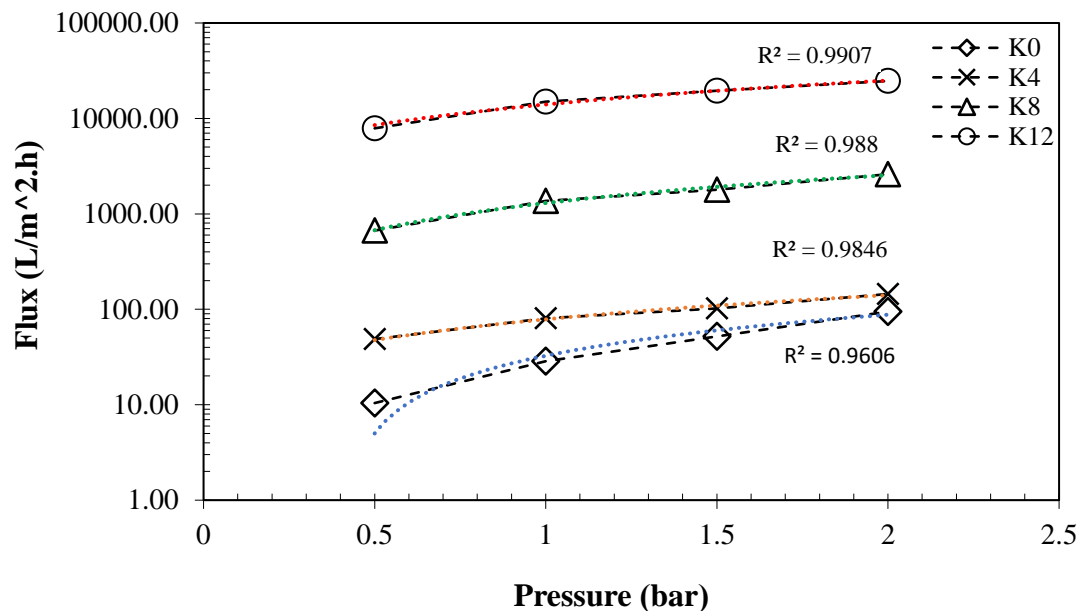


Fig. 4.12 Pure water flux with applied pressure (0-2 bar) for all sintered Al₂O₃ membrane support tubes.

Fig. 4.12 showed the pure water flux as a function of applied pressure for all Al₂O₃ membrane tubes. It was obvious that increasing the applied pressure increased the pure water flux at a linear rate following Darcy's law. The pure water flux values were 40, 73, 1,280, and 12,987 L/m²·h for samples K0, K4, K8, and K12, respectively. The pure water flux values for the kaolin modification (K4, K8, and K12) were greater than those of unmodified membranes. The results depended on the porosity, pore network and pore size.

The results indicated that the pore sizes were within a narrow range for K0 and a wider range for K4, K8, and K12 the sample K12 ability to improve clean water flow by a maximum of 3 times in comparison to the sample without the addition of kaolin. Due to the tortuosity of the flow path that occurs within the porous membrane. [114-115] As a result, the trend of winding direction change depends on the intrinsic shrinkage behavior of porous structured lattice membrane. Thus, tortuosity is defined as the ratio of the lengths of the preferential tortuous fluid pathways and the porous media [116-117] was another crucial factor when adding more and more kaolin. All membrane tubes were within the desired pore size ranges and had great potential for use in ultrafiltration processes. Moreover, the membrane prepared from kaolin formed by gelcasting method had high permeability. As a result, the green and sintered structure played an important role in the final performance of the membrane as observed in the permeation test of crossflow filtration.

However, the permeation test indicates the permeability flux of the solution that passes through the membrane pores. In this work, samples K8 can be used as excellent membranes, with the potential to produce further membrane support. It depends on factors such as kaolin content, forming temperature, pore size, mechanical strength, and water permeability performance. Finally, the increase or decrease of the flux. This will result in the membrane filtration properties or efficiency changing depending on factors such as pressure, viscosity, temperature, and feed concentration including pores in the membrane surface, and also affect the long-term service life of the membrane.

CHAPTER 5

5. CONCLUSIONS

In the study of the influence of adding kaolin for the fabrication of Al_2O_3 membrane tubes by the gelcasting method, conclusions can be examined of the whole work up as follows:

In this research, the membrane tubes were successfully fabricated by gelcasting method, and the results were used to analyze the chemical, physical, mechanical and permeability performance tests from various techniques. The effect of adding different kaolin particles ranging from 0-12 wt% was investigated. It was found that the analysis of the rheological behavior and viscosity of the gelcasting mixtures affected the transition from solution to the gel state in the temperature range of ~42-60 °C. All the membrane support tubes consist mainly of mullite phases, cristobalite and quartz as minor phases, which was caused by the microstructure phase change of the kaolin addition. It can be that the wider pore distribution when kaolin is added is a non-uniform distribution. The void was consolidated with a pore size distribution in the range of 0.03-0.2 μm . Moreover, the membrane tubes are under control within the porosity ratio. and the bulk density was 34-46% and 2.0 to 2.4 g/cm^3 . The flexural strength obtained per specimen, green strength is between 55 and 90 MPa. In addition, the flexural strength was doubled when the after strength was between 629 and 4264 MPa under the specified conditions of sintering at 1350 °C and water permeability were 40, 73, 1,280, and 12,987 $\text{L}/\text{m}^2\cdot\text{h}$, respectively. According to the experimental results membrane support tube samples K0, K4, K8, and K12 can be subsequently used for fabrication of asymmetric support membranes depending on their properties.

Therefore, preliminary studies show that Narathiwat Kaolin supports this work. The potential to manufacture membrane support tubes and control the pore size adjustment to achieve a narrow range of the support layer. Work is underway to deposit ultrafiltration (UF) membranes as well as low-cost and environmentally friendly contributions produced from kaolin. It is a useful parameter and increases the efficiency of product fabrication more suitable for this research. This may expand the scope of use further to be used as an effective support membrane for further study and development of asymmetric membranes in industry.

REFERENCES

- [1] Bipul D, Bandana C, and Pranab B. 2017. Separation of oil from oily wastewater using low cost ceramic membrane. *Korean Journal of Chemical Engineering* 34 (1): 2559-2569.
- [2] Mohsen A, Mojtaba M, Mahdi N, Meysam G, and Toraj Mohammadi. 2021. Performance study of mullite and mullite–alumina ceramic MF membranes for oily wastewaters treatment. *Desalination* 2010 (259): 169-178.
- [3] Fabien S, Anthony B, Van Lam N, Michail T, Philippe V, Corneliu B, Yuji I, Umit D, Philippe M and Samuel B. 2016. Silicon carbide-based membranes with high soot particle filtration efficiency, durability and catalytic activity for CO/HC oxidation and soot combustion. *Journal of membrane Science*. 501 (1): 79-92.
- [4] Donelson R, Paul G, Ciacchi F, and Badwal S. 2014. Permeation and strength characteristics of macroporous supports for gas separation produced by co-sintering mixtures of α -alumina and kaolin. *Journal of membrane Science*. 463 (1): 126-133.
- [5] Catherine C. 2006. 2012. *Membrane Processes in Biotechnology and Pharmaceuticals*. USA.
- [6] Jeong Y, Hermanowicz S and Park C. 2017. Treatment of food waste recycling wastewater using anaerobic ceramic membrane bioreactor for biogas production in mainstream treatment process of domestic wastewater, *Water Res.* 123 (2): 86-95.
- [7] Wei Z, Hou J and Zhu Z. 2016. High-aluminum fly ash recycling for fabrication of cost-effective ceramic membrane supports. *Journal of Alloys and Compounds*. 2016 (683): 474-480.
- [8] Li L, Chen M, Dong Y, Dong X, Cerneaux S, Hampshire S, Cao J, Zhu L, Zhu Z and Liu J. 2016. A low-cost alumina-mullite composite hollow fiber ceramic membrane fabricated via phase-inversion and sintering method. *Journal of the European Ceramic Society*. 2016 (36): 2057-2066.
- [9] Aras A. 2004. *The Change of Phase Composition in Kaolinite and Illite-Rich Clay-Base*. USA: Ceramic Bodies. Applied Clay Science, pp. 257-269.
- [10] Haydn H. 1980. *Murray major kaolin processing developments* Netherlands: Elsevier Scientific Publishing Company, 263-274.
- [11] Millán A, Moreno R and Nieto M. 2002. Thermogelling polysaccharides for aqueous gelcasting-part I: a comparative study of gelling additives. *Journal of the European Ceramic Society*. 2002 (22): 2209-2215.
- [12] Sposito G, Skipper N.T, Sutton R, Park S, Soper A, and Greathouse J. 1999. *Surface geochemistry of the clay minerals*. USA: Proc. Natl. Acad. Sci. USA 96 (7): 3358-3364.
- [13] Mulder M. 1996. *Basic Principles of Membrane Technology*. USA: Springer.
- [14] Baker R. 2012. *Membrane Technology and Applications*. USA: Wiley.

- [15] Bechhold H. 1907. *Kolloidstudien mit der Filtrationsmethode*. Chem: Z. Physik.
- [16] Loeb S and Sourirajan S. 1963. *Sea Water Demineralization by Means of an Osmotic Membrane*. American Chemical Society: Saline Water Conversion-II.
- [17] *RO, UF, MF, World Markets, Membrane Technology*. McIlvaine Company. 2005. pp. 4.
- [18] Finnigan T and Skudder P. 1966. *Using ceramic microfiltration for the filtration of beer and recovery of extract*.
- [19] Scott K. 1995. *Microfiltration, Handbook of Industrial Membranes*. Amsterdam: Elsevier Science, pp. 373-429.
- [20] Mulder M. 1996. *Basic Principles of Membrane Technology*, Springer.
- [21] Baker R.W. 2012. *Membrane Technology and Applications*. Wiley
- [22] Li K. 2007. *Ceramic Membranes for Separation and Reaction*. Wiley.
- [23] Cao J, Dong X, Li L, Dong Y and Hampshire S. Recycling of waste fly ash for production of porous mullite ceramic membrane supports with increased porosity. *Journal of the European Ceramic Society*. 2014 (34): 3181-94.
- [24] Zhiwen Z, Zhaoling W, Wenping S, Jie H, Baohui H and Yingchao D. 2016. Cost-effective utilization of mineral-based raw materials for preparation of porous mullite ceramic membranes via in-situ reaction method. *Applied Clay Science*. 120 (1): 135-141.
- [25] Orbray Co., Ltd. 2023. Porous Ceramics.
<https://orbray.com/en/product/jewel/material/porous-ceramics.html>.
- [26] Yang GCC, Tsai C. Effects of starch addition on characteristics of tubular porous ceramic membrane substrates. *Desalination* 2008; 233:129-36.
- [27] Topates G, Petasch U, Adler J, Kara F, Mandal H. Production and permeability of porous Si₃N₄ ceramics produced by starch addition. *J Asian Ceram Soc* 2013; 1:257-61.
- [28] Bose S, Das C. Preparation and characterization of low-cost tubular ceramic support membranes using saw dust as a pore-former. *Mater Lett* 2013; 110:152-5.
- [29] Chevalier E, Chulia D, Pouget C and Viana M. 2008. Fabrication of porous substrates: a review of processes using pore forming agents in the biomaterial field. *Journal of Pharmaceutical Sciences*. 97 (1): 1135.
- [30] Zeng T, Dong X, Chen S and Yang H. 2007. Processing and piezoelectric properties of porous PZT ceramics. *Ceramics International*. 33 (395): 9.
- [31] Vijayan S, Narasimman R and Prabhakaran K. 2013. A urea crystal templating method for the preparation of porous alumina ceramics with the aligned pores. *Journal of the European Ceramic Society*. 2013 (33): 1929-34.
- [32] Slosarczyk A, Stobierska E and Paszkiewicz Z. 1999. Porous hydroxyapatite ceramics. *Journal of Materials Science Letters*. 1999 (18): 1163-5.
- [33] Larbo A. 1996. *Ceramic processing techniques of support systems for membranes synthesis*. Fundamentals of Inorganic Membrane Science and Technology.

- [34] David C, Arivazhagan M and Ibrahim M. 2015. Spent wash decolourization using nano Al_2O_3 /kaolin photocatalyst: Taguchi and ANN approach, *Journal of Saudi Chemical Society*. 2015 (19): 537-548.
- [35] Jamo H and Abdu S. 2014. Structural analysis and surface morphology kaolin. *Science World Journal*. 9(3): 29-30.
- [36] Kennedy B. 1990. Society for Mining, Exploration, Surface Mining, Second Edition, Society for Mining, Metallurgy, and Exploration 1990.
- [46] Kennedy B. 1990. Society for Mining, Exploration, Surface Mining, Second Edition, Society for Mining, Metallurgy, and Exploration 1990.
- [37] Katherine S. 2003. *Handbook of thermal analysis and calorimetry Applications to Inorganic and Miscellaneous Materials*. Chapter 6 Thermal analysis of clays, page 261-306.
- [38] Satoh S. 1921. A study of the heating and cooling curves of Japanese kaolinite. *Journal of the American Ceramic Society*. 1921 (4): 182-194.
- [39] Chakraborty A.K. 2013. *Phase Transformation of Kaolinite Clay*. India: Springer.
- [40] Richerson D. 2005. *Modern ceramic engineering: properties, processing, and use in design*. CRC press.
- [41] Kameda J, Saruwatari K, Beaufort D and Kogure T. 2008. Textures and polytypes in vermiform kaolins diagenetically formed in a sandstone reservoir: a FIB-TEM investigation. *European Journal of Mineralogy*. 20 (2008): 199-204.
- [42] Jamo H and Abdu S. 2014. Structural analysis and surface morphology of Kaolin. *Science World Journal*. 9 (3): 33-37.
- [43] Fig. 2.9 Scanning electron micrograph of a low defect kaolinite. [47]
- [44] Zakin, R. (2011). *Ceramics-Mastering the Craft*. Krause Publications.
- [45] Hendricks S. 1939. The Crystal Structure of Nacrite $\text{Al}_2\text{O}_3 \cdot 2\text{SiO}_2 \cdot 2\text{H}_2\text{O}$ and the Polymorphism of the Kaolin Minerals. *Zeitschrift für Kristallographie-Crystalline Materials*. 100(1), 509-518.
- [46] Jikan S, Badarulzaman S, Yahaya N and Adamu A. 2017. Delamination of Kaolinite by Intercalation of Urea Using Milling. *Materials Science Forum*. 888 (1): 136–140.
- [47] Sherbini K, Elzahany, Wahba, Drweesh S and Youssef N. 2017. Evaluation of some intercalation methods of dimethylsulphoxide onto HCl-treated and untreated Egyptian kaolinite. *Applied Clay Science*. 137(1): 33-42.
- [48] Frost R and Kristof J. 2004. Raman and Infrared Spectroscopic Studies of Kaolinite Surfaces Modified by Intercalation, in: W. Fernando, S. Kestur Gundappa (Eds.). *Interface Science and Technology*. 184-215.
R.L. Frost, J. Kristof, Raman and Infrared Spectroscopic Studies of Kaolinite Surfaces Modified by Intercalation, in: W. Fernando, S. Kestur Gundappa (Eds.) *Interface Science and Technology*, Elsevier 2004, pp. 184-215.
- [49] Matsushima S, Kennedy G, Akella C and Haygarth J. 1967. A study of equilibrium relations in the systems Al_2O_3 - SiO_2 - H_2O and Al_2O_3 - H_2O . *American Journal of Science*. 265 (1): 28-44.

- [50] Yung-Feng C, Wang M and Min-Hsiung H. 2004. Phase Transformation and Growth of Mullite in Kaolin Ceramics. *Journal of the European Ceramic Society*. 24 (8): 2389-2397.
- [51] Harabi A, Boudaira B, Bouzerara F, Foughali L, Zenikheri F, Guechi A, Ghouil B and Condom S. 2015. Porous ceramic supports for membranes prepared from kaolin (DD3) and calcite mixtures. *Acta Physical Polonica A*. 127 (4): 1164-1166.
- [52] Apinon N, and Sitthisak P. 2006. The Rheological Behavior of Kaolin Suspensions. *Chiang Mai Journal Science*. 33 (3): 271-281.
- [53] Hubadillah S, Othman M, Harun Z, Ismail A, Iwamoto Y, Honda S, Rahman M, Jaafar J, Gani P and Mohd Sokri M. 2016. Effect of fabrication parameters on physical properties of metakaolin-based ceramic hollow fiber membrane (CHFM). *Ceramics International*. 42 (14): 15547-15558.
- [54] Shehu Yahaya et al.,2017 Shehu Y, Suzi S, Nur A, and Ajiya D. 2017. Chemical Composition and Particle Size Analysis of Kaolin. *Path of Science*. 3 (10): 2413-9009.
- [55] Sonia B, Sana G, Jamel B, Andre De and Semia B. 2017. Development and characterization of porous membranes based on kaolin/chitosan composite. *Applied Clay Science*. 143 (1): 1-9.
- [56] Sushma C, Chandan D and Ramagopal U. 2020. feasibility of Low-Cost Kaolin-Based Ceramic Membranes for Organic Lageraria siceraria Juice Production. *Food and Bioprocess Technology*. 13 (1): 1009-1023.
- [57] Sahraoui T, Belhouchet H, Heraiz M, Brihi N and Guermat A. 2016. The effects of mechanical activation on the sintering of mullite produced from kaolin and aluminum powder. *Ceramics International*. 42 (2016): 12185-12193.
- [58] Brindley G and Nakahira M. 1953. The Kaolinite-Mullite Reaction Series: I, II and III. *Journal of the American Ceramic Society*. 42 (1959): 311-324.
- [59] Sahraoui T, Belhouchet H, Heraiz M, Brihi N and Guermat A. 2016. The effects of mechanical activation on the sintering of mullite produced from kaolin and aluminum powder. *Ceramics International*. 42 (2016): 12185-12193.
- [60] Abbasi M and Mowla D. 2014. Analysis of membrane pore-blocking models applied to the MF of real oily wastewaters treatment using mullite and mullite-alumina ceramic membranes. *Desalination and water treatment*. 52 (2014): 2481-2493.
- [61] Lima P, Angélica R and Neves R. 2017. Dissolution kinetics of Amazonian metakaolin in hydrochloric acid. *Clay Minerals*. 52 (1): 75-82.
- [62] Kotal M, and Bhowmick A. 2015. Polymer nanocomposites from modified clays: Recent advances and challenges. *Progress in Polymer Science*. 51: 127-187.
- [63] Liu P, Farzana R, Rajarao R and Sahajwalla V. 2017. Lightweight expanded aggregates from the mixture of waste automotive plastics and clay. *Construction and Building Materials*. 145 (1): 283-291.

- [64] Sengupta P, Saikia P and Borthakur P. 2008. SEM-EDX characterization of an iron-rich kaolinite clay. *Journal of Scientific & Industrial Research*. 67 (1): 812-818.
- [65] Nazir M, Mohamad M, Mohapatra L, Gilani M, Raza M, and Majeed K. 2016. Characteristic Properties of Nano clays and Characterization of Nanoparticulate and Nanocomposites. *Engineering Materials*. 35-55.
- [66] Tang W, Song L, Zhang S, Li H, Sun J, and Gu X. 2016. Preparation of thiourea-intercalated kaolinite and its influence on thermostability and flammability of polypropylene composite. *Journal of Materials Science*. 52 (1): 208-217.
- [67] Sempeho S, Kim H, Mubofu E, Pogrebnoi A, Shao G and Hilonga A. 2015. Dynamics of Kaolinite-Urea Nanocomposites via Coupled DMSO-Hydroxyaluminum Oligomeric Intermediates. *Indian Journal of Materials Science* 2015 (1): 1-10.
- [68] Sujeong L, Youn Joong K, and Hi-Soo M. 1999. Phase Transformation Sequence from Kaolinite to Mullite Investigated by an Energy-Filtering Transmission Electron Microscope. *Journal of the American Ceramic Society*. 82 (10): 2841-2848.
- [69] Brindley G. W. and Nakahira M. 1959. The Kaolinite–Mullite Reaction Series: III, The High-Temperature Phases. *Journal American Ceramic Society*. 42 (7): 319-24.
- [70] Franco F, Cecila J.A, Pérez-Maqueda L.A, Pérez-Rodríguez J.L and Gomes C. 2007. Particle-size reduction of dickite by ultrasound treatments: Effect on the structure, shape and particle-size distribution. *Applied Clay Science*. 2007 (35): 119-127.
- [71] Segura-Monroy S, Uribe-Vallejo A, Ramirez-Godoy A and Restrepo-Diaz H. 2015. Effect of Kaolin Application on Growth, Water Use Efficiency, and Leaf Epidermis Characteristics of *Physallis peruviana* Seedlings under Two Irrigation Regimes. *Journal of Agricultural Science and Technology*. 17 (6): 1585-1596
- [72] Li X, Liu Q, Cheng H, Zhang S and Frost R. 2015. Mechanism of kaolinite sheets curling via the intercalation and delamination process. *Journal of Colloid and Interface Science*. 444 (1): 74-80.
- [73] Jilavenkatesa A, Dapkunas S, and Lum L. 2001. Particle Size Characterization. Retrieved from http://ws680.nist.gov/publication/get_pdf.cfm?pub_id=850451
- [74] Toraman O and Uçurum M. 2017. Investigation of grinding-aid effect on the fineness, particle size distribution, surface area and color properties of calcite powder in dry vertical stirred mill. *Chemistry Research Journal*. 2 (3): 56-65.
- [75] Pertti A. 1996. *Mechanical and physical properties of engineering alumina ceramics*. Finland: Technical Research Centre
- [76] Yi-Fan L, Qin-Qin X, Pei C, Meng-Yuan Z, Xin-Yao W and Jian-Zhong Y. 2018. Effects of operating parameters and ionic liquid properties on fabrication of supported ionic liquid membranes based on mesoporous γ - Al_2O_3 supports. *Journal of Membrane Science*. 545 (2018): 176-184.

- [77] Chemical and Physical Properties of Agar in Cooking. [homepage on internet]. No date. <https://www.scienceofcooking.com>
- [78] Why does melted agarose in solution appear fully transparent but become opaque when polymerized [homepage on internet]. No data. <https://physics.stackexchange.com>
- [79] Jinlong Y, Juanli Y, Yonh H. 2011. Recent developments in gelcasting of ceramics. *Journal of the European Ceramic Society*. 31 (2011): 2569-2591.
- [80] Vasiliki, Elena M, Nikolaos V, Pavlos P, Antonios G and Vassilis. 2015. Application of gel-casting method in ceramics shaping. *LCMT*. 2015(10): 1-2.
- [81] Van Olphen H. 1963. An Introduction to Clay Colloid Chemistry. *Interscience New York*. pp. 9-12.
- [82] Dorlot J.M, Bailon J.P and Masounave J. 1986. *Des Mat&iaux Ecole Polytechnique* de. Canada.
- [83] Sanjay K. 2015. *Clay Materials for Environmental Remediation*. India: Springer.
- [84] Ramnaree K. 2020. Fabrication of low cost alumina tube through agar gelcasting for membrane microfiltration. *Journal Applied Membrane Science & Technology*. 2020 (24): 47-57.
- [85] Abdallah H, Amin S, Abo Almaged H and Abadir M. 2018. Fabrication of ceramic membranes from nano rosette structure high alumina roller kiln waste powder for desalination application. *Ceramics International*. 44 (7): 8612-8622.
- [86] Sheikhi M, Arzani M, Mahdavi H and Mohammadi T. 2019. Kaolinitic clay-based ceramic microfiltration membrane for oily wastewater treatment: Assessment of coagulant addition. *Ceramics International*. 2019 (45) :17826-17836.
- [87] Omatete O, Janney M and Nunn S. 1997. Gelcasting: From laboratory development toward industrial production. *Journal of the European Ceramic Society*. 17 (2-3): 407-413.
- [88] Wang X, Xie Y, Peng C, Wang R, Zhang D and Feng Y. 2019. Porous alumina ceramic via gelcasting based on 2-hydroxyethyl methacrylate dissolved in tert-butyl alcohol. *Transactions of Nonferrous Metals Society of China*. 29 (8): 1714-1720.
- [89] Guo X, Zhou Z, Ma G, Wang S, Zhao S and Zhang Q. 2012. Effect of forming process on the integrity of pore gradient Al₂O₃ ceramic foams by gelcasting. *Ceramics International*. 38 (1): 713-719.
- [90] ASTM C1866-08. This standard is copyrighted by ASTM International, Standard Test Method for Flexural Strength of Advanced Ceramics at Ambient Temperature Cylindrical Rod Strength, West Conshohocken: ASTM International;(2009) 1-21. or through the ASTM website (www.astm.org).
- [91] ASTM C373-88. Standard Test Method for Water Absorption, Bulk Density, Apparent Porosity, and Apparent Specific Gravity of Fired Whiteware Products, West Conshohocken: *ASTM International*. (2006); or through the ASTM website (www.astm.org).

- [92] Eugene H and Anteneh M. 2017. *Study on rheological properties of kaolin and bentonite slurry solution*. Australis.
- [93] Sonia B, Sana G, Jamel B, Andre D and Semia M. 2017. Development and characterization of porous membrane on kaolin/chitosan composite. *Applied Clay Science*. 143 (2017): 1-9.
- [94] Bezerril L, Vasconcelos C, Dantas T, Pereira M, and Fonseca J. 2006. Rheology of chitosan-kaolin dispersions. *Colloids and Surfaces A: Physicochemical and Engineering*. 287 (1-3): 24-28.
- [95] Cunha F, Torem M, and Abreu J. 2006. On the fundamentals of kaolin rheology applied to the paper industry. *Minerals Engineering*. 19 (14): 1462-1464.
- [96] Avadiar L, Yee-Kwong L, and Andy F. 2015. Physicochemical behaviors of kaolin slurries with and without cations Contributions of alumina and silica sheets. *Colloids and Surfaces A: Physicochemical and Engineering*. 468(2017): 103-113.
- [97] Lagaly G. 1989. Principles of flow of kaolin and bentonite dispersions. *Applied Clay Science*. 4 (2): 105-123.
- [98] Kasperski K, Charles T, and Loren G. 1986. Viscosities of dilute aqueous suspensions of montmorillonite and kaolinite clays. *Canadian Journal of Chemistry*. 64 (9): 1919-1924.
- [99] Emami S.M, Ramezani A, Nemat S. 2017. Sintering behavior of waste serpentine from abdasht chromite mines and kaolin blends. *Ceramics International*. S0272-8842 (2017): 31751-0.
- [100] Abbasi M, and Mowla D. 2014. Analysis of membrane pore-blocking models applied to the MF of real oily wastewaters treatment using mullite and mullite–alumina ceramic membranes. *Desalination and water treatment*. 52 (2014): 2481-2493.
- [101] Yung-Feng C, Moo-Chin W, and Min-Hsiung H. 2004. Phase transformation and growth of mullite in kaolin ceramics. *Journal of the European Ceramic Society*. 24 (2004): 2389-2397.
- [102] Romit R, Dipankar D, and Prasanta K. 2022. A review of advanced mullite ceramics. *Engineered Science*. 18 (2022): 20-30.
- [103] Sahraoui T, Belhouchet H, Heraiz M, Brihi N, and Guermat A. 2016. The effects of mechanical activation on the sintering of mullite produced from kaolin and aluminum powder. *Ceramics International*. 42 (2016): 12185-12193.
- [104] Bouzerara F, Harabi A, Achour S, and Larbot A. 2006. Porous ceramic supports for membranes prepared from kaolin and dolomite mixtures. *Journal of the European Ceramic Society*. 26 (2006): 1663-1671.
- [105] Hubadillah S, Dzarfan Othman M, Harun Z, Ismail A, Iwamoto Y, Honda S, Rahman M, Jaafar J, Gani P, and Mohd Sokri M. 2016. Effect of fabrication parameters on physical properties of metakaolin-based ceramic hollow fiber membrane (CHFM). *Ceramics International*. 42 (14): 15547-15558.
- [106] Hanley H.J.M. 1966. Thermal transpiration measurements on a porous ceramic. *Transactions of the Faraday Society*. 62 (1966): 2395-2402.

- [107] Li L, Chen M, Dong Y, Dong X, Cerneaux S, Hampshire S, Cao J, Zhu L, Zhu Z, and Liu J. 2016. A low-cost alumina-mullite composite hollow fiber ceramic membrane fabricated via phase-inversion and sintering method. *Journal of the European Ceramic Society*. 36 (2016): 2057-2066.
- [108] Zyryanov V.V, and Karakchiev L.G. 2007. Porous supports conducting ceramic membranes. *Inorganic Materials*. 44 (2007): 429-437.
- [109] Tschegg C, Ntaflos T, Hein I. 2009. Thermally triggered two-stage reaction of carbonates and clay during ceramic firing-A case study on bronze age cypriot ceramics. *Applied Clay Science* 43. pp. 69-78.
- [110] Van W and Besmertnuk E. 1950. The action of phosphates on kaolin suspensions. *Journal of Physical and Colloid Chemistry*. 54 (1950): 89-106.
- [111] Hedfi I, Hamdi N, Srasra E, and Rodríguez M. 2014. The preparation of micro-porous membrane from a Tunisian kaolin. *Applied Clay Science*. 101 (2014): 574-578.
- [112] Zyryanov V.V, and Karakchiev L.G. 2007. Porous supports conducting ceramic membranes. *Inorganic Materials*. 44 (2007): 429-437.
- [113] Van W, and Besmertnuk E. 1950. The action of phosphates on kaolin suspensions. *Journal of Physical and Colloid Chemistry*. 54 (1950): 89-106.
- [114] Clennell M.B. 1997. Tortuosity: a guide through the maze. *Geological Society London Special Publications*. 122 (1): 299-344.
- [115] Ghanbarian B, Hunt A.G, Ewing R.P, and Sahimi M. 2013. Tortuosity in porous media: a critical review. *Soil Science Society of America Journal*. 77 (5): 1461-1477.
- [116] Jinlong F, Hywel T, and Chenfeng L. 2021. Tortuosity of porous media: Image analysis and physical simulation. *Earth-Science Reviews*. 212: 103439.
- [117] Yoshinori W, and Yoshito N. 2001. Two-dimensional random walk program for the calculation of the tortuosity of porous media. *Journal of Groundwater Hydrology*. 43 (1): 13-22.

APPENDICES

Appendix A: The paper was published



Effect of clay addition to Al₂O₃-agar mixture on pore size and distribution of tubular Al₂O₃ membrane support fabricated by agar gelcasting

Nantawadee Udomsri^{a,c}, Methee Promsawat^a, Suksawat Sirijarukul^{b,c}, Kowit Lertwittayanon^{a,c,*}

^a Division of Physical Science, Materials Science Program, Faculty of Science, Prince of Songkla University, 90112, Thailand

^b Division of Physical Science, Physics Program, Faculty of Science, Prince of Songkla University, 90112, Thailand

^c Center of Excellent in Membrane Science and Technology (CoE-MST), Prince of Songkla University, 90112, Thailand

ARTICLE INFO

Article history:
Available online xxxxx

Keywords:
Agar
Gelcasting
Al₂O₃ membrane
Kaolin
Bentonite
Phase separation

ABSTRACT

The addition of clay particles—kaolin or bentonite—into the mixture of Al₂O₃ slurry and agar solution was examined for creating pores with controllable size in tubular Al₂O₃ membrane. The mixtures were prepared and then molded out of glass tubes using the method of agar gelcasting. The green, gelcast Al₂O₃ tubes were sintered at 1350 °C for 1 h for membrane application. The effect of clay addition from 0 to 2 wt% into the mixture on pore size and structure of Al₂O₃ tubes was observed with SEM. The addition of bentonite provided less uniform pore size and distribution than that of kaolin. Additionally, the step of ball milling the clay particles to make complete dispersion prior to adding to the mixtures was needed to create more uniform pore size and distribution. The ball milling time of 60 min was the optimum condition for preparing Al₂O₃ membrane support.

Copyright © 2022 Elsevier Ltd. All rights reserved.
Selection and peer-review under responsibility of the scientific committee of the Joint International Conference on Applied Physics and Materials Applications & Applied Magnetism and Ferroelectrics.

1. Introduction

Ceramic membrane support is a first layer fabricated for producing an asymmetric ceramic membrane [1]. The support layer not only requires high mechanical strength to withstand operating condition at high pressure but also optimum pore size and surface roughness for reducing the resistance to permeate flow and providing suitably the subsequent layer-coating properties, respectively [2]. The support layer commonly has relatively large pore size, compared with the subsequent coating layer—intermediate and selective layer—thereby needing large ceramic particles [3]. It meant that the large pore size is created from the voids among the sintered large particles [4]. Therefore, the support layer must be sintered at high temperature resulting in high cost [5].

In order to reduce the cost of high-sintering temperature, lower-sintering temperature using small ceramic particle is a possible alternative. However, the pore size of support layer is also

smaller from the voids among the sintered small ceramic particles. Consequently, a strategy to create large pore size while still using the small ceramic particles should be judiciously considered. There are many efforts to add pore forming agent or polymer microspheres into the ceramic slurry to increase porosity in porous ceramics [6–10]. However, the shape of pore created after the decomposition of polymer microspheres is spherical and the interconnectivity of spherical pores—cell window—needs to be present. Additionally, the trade-off between porosity and mechanical strength for the pore-forming microspheres is more difficult when it is considered in fabricating the ceramic support layer requiring thinness.

In addition to the introduction of pore forming agent, direct foaming method is one of the strategies typically chosen for preparing the porous ceramics [11–13]. This method relies on the hydrophobization of ceramic particle surfaces incorporating with gas phase resulting from mechanical frothing, injection of a gas stream, gas-releasing chemical reactions or solvent evaporation [14]. It is found that this method has been suitable for preparing macro porous ceramics with closed and/or open pores. However, the macro pores are benefited for the use as a filter. Therefore,

* Corresponding author at: Division of Physical Science, Materials Science Program, Faculty of Science, Prince of Songkla University, 90112, Thailand.
E-mail address: kowit.l@psu.ac.th (K. Lertwittayanon).

<https://doi.org/10.1016/j.matpr.2022.06.043>

2214-7853/Copyright © 2022 Elsevier Ltd. All rights reserved.

Selection and peer-review under responsibility of the scientific committee of the Joint International Conference on Applied Physics and Materials Applications & Applied Magnetism and Ferroelectrics.

Please cite this article as: N. Udomsri, M. Promsawat, S. Sirijarukul et al., Effect of clay addition to Al₂O₃-agar mixture on pore size and distribution of tubular Al₂O₃ membrane support fabricated by agar gelcasting, Materials Today: Proceedings, <https://doi.org/10.1016/j.matpr.2022.06.043>

the pore size from the direct foaming method is far too large for using as the membrane support. It should be noted that there is effort to combine the direct foaming method and the microsphere pore former to produce ceramic foams with highly open channel [15].

In this work, we propose a new alternative to create membrane pore network relying on the mechanism of phase separation. The separation of phases between clay particles and agar molecules might offer optimum pore structure and size for preparing the membrane support. On the basis of the charges on clay particles [16] and the functional groups of agar molecules [17], it is likely to create an interaction of repulsive force between negative charges on clay surface and negative ions $-\text{SO}_3^-$ and OH^- in agar molecules. As a consequence, the separate clusters between agar and clay occur leading to pore formation due to shrinkage and decomposition during drying and sintering, respectively.

According to the elemental aspect of repulsive interaction between the agar molecules and clay particles, it is adopted for preparing tubular Al_2O_3 membrane support by agar gelcasting. Since the amount of clay has an important effect on the size and distribution of pores and the Al_2O_3 structure and properties, the clay type—kaolin and bentonite—and their amounts between 0 and 2 wt% are examined. The particular small amounts of clays are used to prevent an adverse effect on the Al_2O_3 structure and properties. The SEM images show more homogeneous microstructure of the kaolin-modified Al_2O_3 membrane support, compared with bentonite-modified one. Subsequently, the kaolin powder is ball milled separately from the Al_2O_3 slurry to make the kaolin particles well dispersed prior to mixing with the Al_2O_3 slurry. It is indicated that 60-min ball milling offers the most homogeneous microstructure and well distributed pores. It is deduced that the well-dispersed kaolin addition leads to the kaolin-agar phase separation homogeneously and thereby the pore interconnection corresponding to the requirement of membrane support.

2. Experimental

2.1. Raw materials

$\alpha\text{-Al}_2\text{O}_3$ with average particle size of 0.167 μm (TMDAR, Taimei Co., Ltd., Japan) was used for preparing tubular Al_2O_3 membrane support at low sintering temperature. Ranong kaolin (local supplier, Thailand) and bentonite (Minmat Co. Ltd., Thailand) were employed as pore former due to the phase separation between the agar molecules and the clay particles. Ammonium salt of polyacrylic acid (Dispex AA 4040, BASF) was used as a dispersant. MgO nanopowder (Alfa Aesar) was used as sintering aid. Acetone (99.8% purity) functioned as a liquid drying agent. Agar powder from Chile was used for gelling agent. Reverse osmosis (R/O) water used for preparing all the gelcasting mixtures.

2.2. Preparation of gelcasting mixture

Al_2O_3 slurry with 75 wt% solid loading was prepared by ball milling in HDPE bottle for 2 h to make thoroughly dispersion of Al_2O_3 powder. The clay powders—kaolin and bentonite—was varied at 0, 0.1, 0.2, 0.3, 0.4, 0.5, 1, 1.5 and 2 wt%. The dispersant was used at 1 wt% of solid loading. The MgO powder was employed at 0.03 wt% of solid loading. After ball milling, the Al_2O_3 slurry was kept warm at 70 °C in a water bath. Agar solution was subsequently prepared by heating the agar powder in RO water until a clear yellow solution was obtained. The agar solution was prepared at the concentration of 2 wt%. The warm Al_2O_3 slurry was mechanically mixed with the prepared agar solution for 3 min. The mixture

of Al_2O_3 slurry and agar solution contained the true agar at 0.6 wt% solid loading.

Moreover, the comparison of mixing routes between the ball milling of kaolin together with the Al_2O_3 slurry and the separation of ball milling of kaolin—kaolin slip—from that of the Al_2O_3 slurry was compared. The alumina beads were used for dispersion of kaolin particles in HDPE bottle. The kaolin slip with 50 wt% solid loading was ball milled for 5, 30 and 60 min. The dispersant was used at 1 wt% of the solid loading. The other raw materials, i.e. MgO, kaolin and agar, and their amounts were used the same as the above explanation, except for kaolin used at 0.5, 1, 1.5 and 2 wt%. The ball-milled kaolin slip was added into the Al_2O_3 slurry and then mixed by magnetic stirring at 750 rpm for 30 min. The stirred Al_2O_3 slurry was kept warm at 70 °C in an ultrasonic bath. Subsequently, the hot agar solution was mechanically mixed with the warm Al_2O_3 slurry for 3 min and simultaneously kept warming at 70 °C. The mixture of the agar solution and the Al_2O_3 slurry was gelcast in the subsequent step.

2.3. Fabrication of tubular Al_2O_3 membrane support

The prepared mixture was first molded by pouring into a set of warm glass tubes. The fabrication process was detailed in [18]. A brief explanation was given as the following. The mixture subsequently transformed into gel phase with tubular shape. The gelled tube was removed from the glass-tube mold and then immersed in acetone for 50 h. Thereafter, the acetone-rich gelled tube was removed from the immersing container and thereby the gelled tube dried rapidly due to the evaporation of acetone. Finally, the dried tube was sintered at 1300 °C for 1 h.

2.4. Characterization

The microstructure of all the Al_2O_3 membrane support was observed with SEM (SEM-JSM5800LV, JEOL) at 20 kV. The sintered Al_2O_3 membrane support was cut with cutting machine and SiC cut-off wheel. The cut sample was dried and then coated with gold using a sputtering technique for 2 times of each 60 s. The phase analysis was performed with XRD (Panalytical, Empyrean model, Netherlands) using $\text{Cu K}\alpha$ radiation in the range of 2θ between 5 and 90°. The porosity and bulk density of sintered Al_2O_3 membrane supports were determined from Archimedes method following ASTM C378-88. 3-point bending strength of the Al_2O_3 membrane supports was carried out according to ASTM C1684-08. The measurement of the three-point bending strength values were performed with a tensile tester (Universal testing machine 50 kN) provided with a load cell for 500 N and maintaining a support span of 85 mm at a stroke rate of 0.5 mm/min. The tubular membrane sample was fixed on the sample holder, which has 100 mm distance. The bending strength was calculated from the following equation:

$$\sigma_F = (8FLD) / (\pi(D^4 - d_i^4))$$

where, F is the measured force at which fracture takes place; L , D and d_i are the length (100 mm), the outside diameter and the inner side diameter of the tube, respectively. Five samples were tested to get an average strength.

3. Results and discussion

In order to confirm the microstructure of bentonite-modified Al_2O_3 membrane support in terms of the pore size and pore size distribution, SEM was used for the observation. Fig. 1(a)–(i) showed the SEM images of the sintered Al_2O_3 membrane support containing the different amounts of bentonite from 0 to 2 wt%.

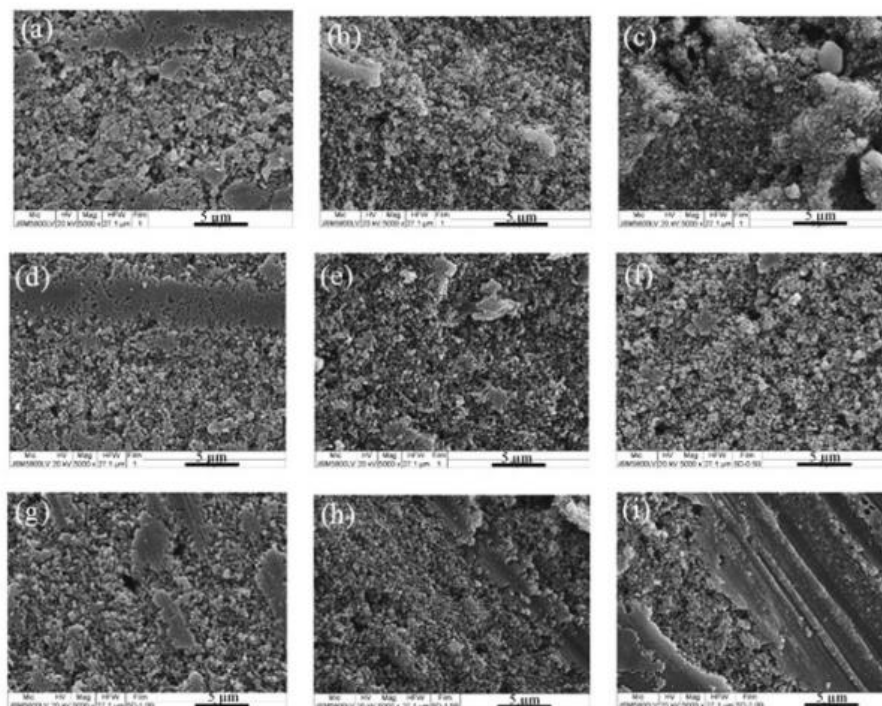


Fig. 1. Al_2O_3 membrane supports prepared by simultaneously ball milling of bentonite and Al_2O_3 powder, containing the different amounts of bentonite at (a) 0, (b) 0.1, (c) 0.2, (d) 0.3, (e) 0.4, (f) 0.5, (g) 1.0, (h) 1.5, and (i) 2 wt%.

The microstructure of Al_2O_3 membrane support unmodified by bentonite as shown in Fig. 1(a) indicated some part of sintering resulting in grain growth. Moreover, there was some pores of which was not interconnected. The formed shallow pores resulted partly from the Al_2O_3 sintering responsible for shrinkage and thereby the small pore formation. The sintered parts showed neck and pores within the Al_2O_3 grains indicating that they were not sintered fully. Furthermore, small and deep pores in a little amount appeared which might be originated from air bubbles remaining in the gelcasting mixture. Considering the effect of increasing bentonite in the gelcast mixtures as shown in Fig. 1(b) to (i), there were more sintered parts and a tendency to form their own layers, especially for 1–2 wt% bentonite. The formed layers were attributed to the sintering between the Al_2O_3 and bentonite particles. Their sintering resulted in the large area of prominent layers, especially for 2 wt% bentonite. Therefore, adding the bentonite at ≥ 1 wt% was responsible for the large clusters of bentonite. The existed large clusters inferred that the ball milling together of the Al_2O_3 and bentonite particles was not efficient enough to make the bentonite powder dispersed well.

Fig. 2 displayed the SEM images of the sintered Al_2O_3 membrane supports containing the different amounts of kaolin from 0.5 to 2 wt%. The microstructure of kaolin modified Al_2O_3 membrane supports showed the existence of large clusters of sintered kaolin. The morphology of sintered kaolin clusters was the same

as that of sintered bentonite clusters. It revealed that the kaolin particles were not well dispersed as well as the bentonite particles.

According to the problem of clay–bentonite and kaolin–agglomeration in ball milling the clay and Al_2O_3 powder at the same time, a separate step of separately ball milling clay should be performed. The clay agglomeration was a common characteristic of clay platelets [19]. Therefore, the optimum ball-milling time brought about the dispersion of clay platelets. The investigation of ball milling time employed only kaolin powder since it was easier for dispersing than bentonite. Moreover, it was well known that the bentonite powder absorbed a lot of water resulting in its swelling [20]. Fig. 3 indicated the SEM images of kaolin modified Al_2O_3 membrane supports prepared from separately ball milling the kaolin slip at different time of 5, 30 and 60 min. Apparently, at the magnification of 10,000x the optimum ball milling time of 60 min showed the most uniform distribution of pores, compared with the other Al_2O_3 membrane supports. At the low magnification of 500x, the 60-min ball milled Al_2O_3 membrane supports had the uniform microstructure with no defects.

Fig. 4 showed XRD patterns of all the Al_2O_3 membrane supports prepared from separately ball milling the kaolin slip at 5, 30 and 60 min. All the patterns showed the peaks of $\alpha\text{-Al}_2\text{O}_3$ (PDF No. 00-010-0173). In addition, there were peaks of muscovite appearing clearly when the ball milling time increased to 60 min. The muscovite peaks occurred from the existence of muscovite phase

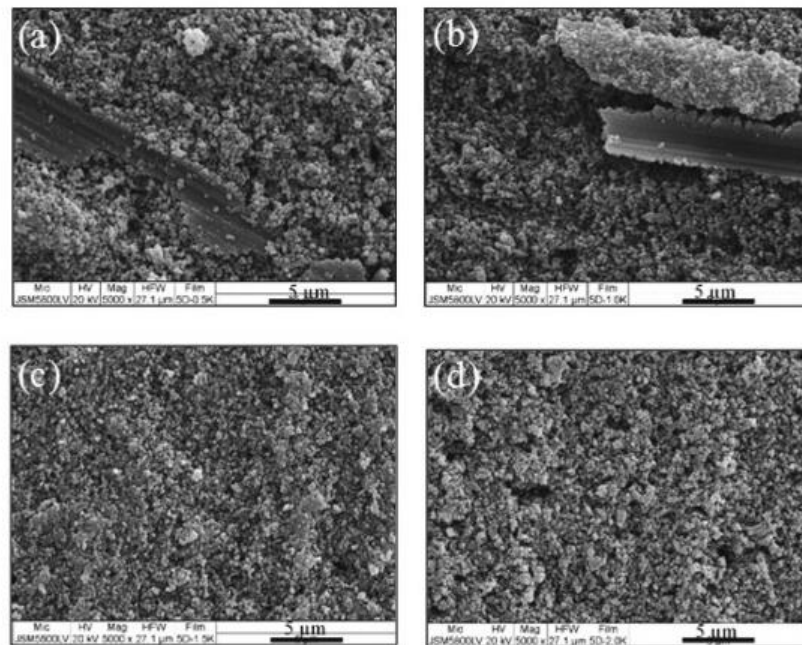


Fig. 2. Al_2O_3 membrane supports prepared by simultaneously ball milling of kaolin and Al_2O_3 powder, containing the different amounts of kaolin at (a) 0.5, (b) 1, (c) 1.5, and (d) 2 wt%.

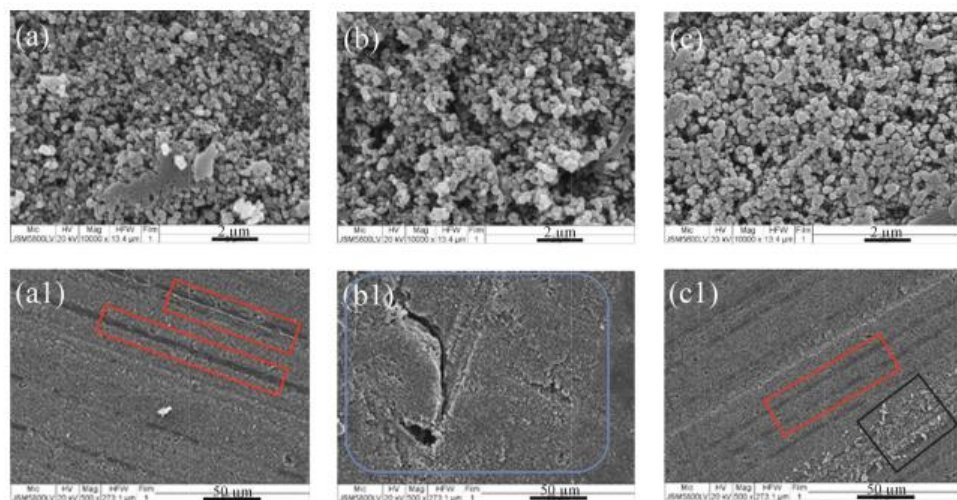


Fig. 3. Al_2O_3 membrane supports prepared by separately ball milling of kaolin slip at 5, 30 and 60 min at the magnification of 10000x (a – c) and 500x (a1 – c1), respectively, before mixing with Al_2O_3 slurry, for which all the membrane supports contained the equal kaolin particles at 1.5 wt%.

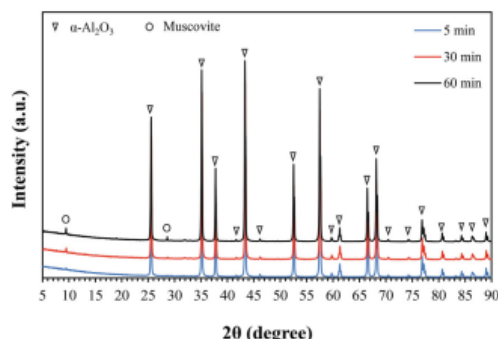


Fig. 4. XRD patterns of Al_2O_3 membrane supports prepared by separately ball milling of kaolin slip at 5, 30 and 60 min.

in Ranong kaolin [21]. The muscovite could withstand high temperature up to 1300 °C; therefore, it showed no phase change of muscovite in this work. It implied that muscovite platelets broken down from the kaolin articles and then stacked up for the duration of ball milling responsible for the peaks with higher intensity at 2θ of 9.638° (d-spacing of 9.694 Å). The large d-spacing corresponded with stacking up the muscovite platelets. It was well known that the identified peaks at 2θ of $< 10^\circ$ leading to the large d-spacing were in agreement with the stacking up of particles with flake shape. In other words, the peaks at 2θ of $> 10^\circ$ were the interatomic distance of crystalline materials. Moreover, from Fig. 3 (a1) and (c1) the red frame showed the kaolin phase separated from Al_2O_3 phase clearly. The phase separation was well observed as shown in Fig. S1 (supplementary information). It was also found that the evolution of muscovite particles stacked up gradually. Fig. 3(a1) showed that the white flake of muscovite dispersed distantly and became dispersed more closely when the ball milling time reached 30 min as shown in the light blue frame in Fig. 3(b1); whereas Fig. 3(c1) displayed the line of decent stacking up of muscovite flake as shown in the black frame as well as Fig. S2. The lines of muscovite flakes were similar to the lines found out by Mokma

[22]. Therefore, the SEM images from Fig. 3 were in line with the XRD results. It was noteworthy that XRD was unable to detect the phase from the sintered kaolin, while the SEM images were fully capable of observing the sintered kaolin.

The porosity and bulk density of all the Al_2O_3 membrane supports prepared from separately ball milling the kaolin slip at 0, 5, 30 and 60 min were shown in Fig. 5. When the ball milling time increased, the porosity of the Al_2O_3 membrane supports increased from 40 to 46%. On the other hand, the bulk density of the Al_2O_3 membrane supports decreased from 2.4 to 2.25 g/cm^3 when the ball milling time increased. Consequently, the increase in the ball milling time led to the volume expansion of the Al_2O_3 gelcasting mixtures and thereby that of Al_2O_3 membrane supports after sintering. The volume expansion might be attributed to the stacking up of muscovite platelets.

Fig. 6 demonstrated the 3-point bending strength for all the Al_2O_3 membrane supports prepared from separately ball milling the kaolin slip at 0, 5, 30 and 60 min. It pointed out that the bending strength tended to decrease slightly when the ball milling time increased from 0 to 60 min. The decreasing bending strength was closely related to the stacking up of muscovite flakes and thereby the increasing porosity.

Therefore, the microstructure of all the Al_2O_3 membrane supports prepared from separately ball milling the kaolin slip at different time confirmed that the more the ball milling time, the more the porosity of the Al_2O_3 membrane supports.

4. Conclusion

The tubular Al_2O_3 membrane supports were fabricated by agar gelcasting using the small Al_2O_3 particle size to reduce the sintering temperature and then their cost. The two types of clay, i.e., bentonite and kaolin, were used for creating pores with suitable size for functioning as the membrane supports. The ball milling of clay and Al_2O_3 powder at the same time in preparing the Al_2O_3 slurry resulted in the issue of clay agglomeration responsible for the existence of large clay clusters in the Al_2O_3 membrane supports. The clay clusters brought about non-uniform microstructure of Al_2O_3 membrane supports. However, the ball milling of clay (kaolin) and Al_2O_3 powder in the separate steps led to the higher porosity

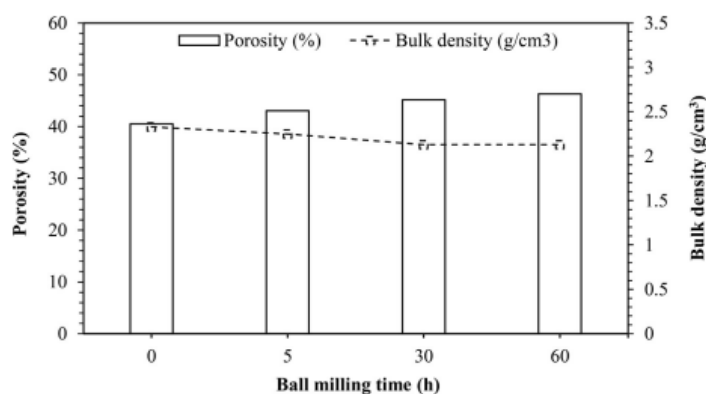


Fig. 5. Porosity and bulk density of Al_2O_3 membrane supports prepared by separately ball milling of kaolin slip at 0, 5, 30 and 60 min.

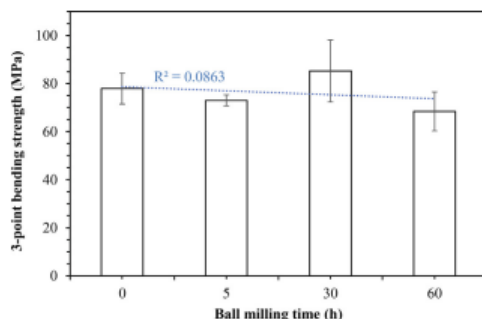


Fig. 6. 3-point bending strength of Al_2O_3 membrane supports prepared by separately ball milling of kaolin slip at 0, 5, 30 and 60 min.

of 46% and bending strength of 70 MPa for 60-min ball milling time. The separate kaolin milling for 60 min was optimum for preparing the Al_2O_3 membrane supports.

CRedit authorship contribution statement

Nantawadee Udomsri: Investigation. **Methee Promsawat:** Conceptualization. **Suksawat Sirjarukul:** Conceptualization. **Kowit Lertwittayanon:** Writing – review & editing, Supervision, Conceptualization.

Declaration of Competing Interest

The authors declare that they have no known competing financial interests or personal relationships that could have appeared to influence the work reported in this paper.

Acknowledgements

The authors would like to thank Center of Excellent in Membrane Science and Technology (CoE-MST) for the research scholarship. This research was supported by National Science, Research and Innovation Fund (NSRF) and Prince of Songkla University (Grant No. SCI6305091a).

Appendix A. Supplementary material

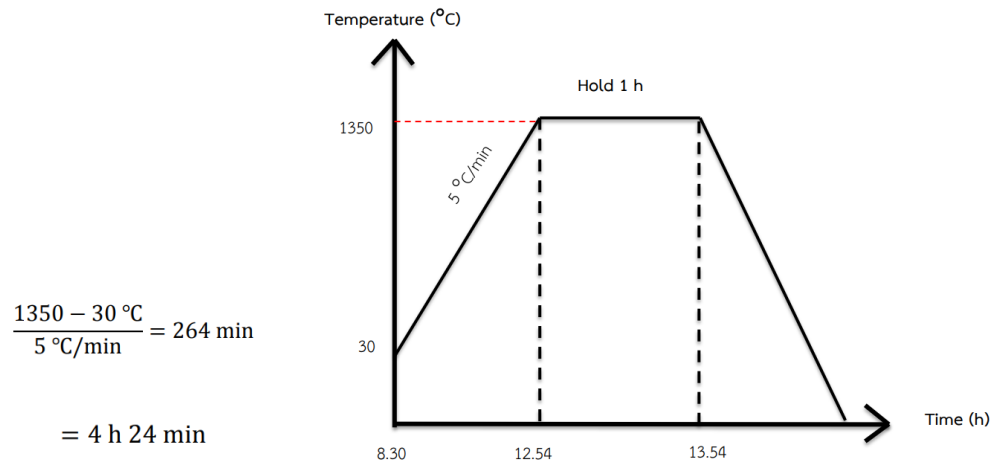
Supplementary data to this article can be found online at <https://doi.org/10.1016/j.matpr.2022.06.043>.

References

- [1] K. Li. Ceramic Membranes for Separation and Reaction, John Wiley & Sons Ltd, 2007.
- [2] B.C. Bonekamp, in: Fundamentals of Inorganic Membrane Science and Technology, Elsevier, 1996, pp. 141–225.
- [3] A. Larbot, in: Fundamentals of Inorganic Membrane Science and Technology, Elsevier, 1996, pp. 119–139.
- [4] D. Liang, J. Huang, H. Zhang, H. Fu, Y. Zhang, H. Chen, Influencing factors on the performance of tubular ceramic membrane supports prepared by extrusion, Cer. Int. 47 (2021) 10464–10477.
- [5] S. Lakshmi Sandhya Rani, K.R. Vinoth, Insights on applications of low-cost ceramic membranes in wastewater treatment: A mini-review, CSCE. 4 (2021) 100149–100159.
- [6] M. Qiu, X. Chen, Y. Fan, W. Xing, in: Comprehensive Membrane Science and Engineering, second ed., Elsevier, 2017, pp. 270–297.
- [7] N. Ahmed, F.Q. Mir, Preparation and characterization of ceramic membrane using waste almond shells as pore forming agent, Mater. Today: Proc. 47 (2021) 1485–1489.
- [8] L.A. Xavier, T.V. Oliveira de, W. Klitzke, A.B. Mariano, D. Eiras, R.B. Vieira, Influence of thermally modified clays and inexpensive pore-generating and strength improving agents on the properties of porous ceramic membrane, Appl. Clay Sci. 168 (2019) 260–268.
- [9] D. Liang, J. Huang, Y. Zhang, Z. Zhang, H. Chen, H. Zhang, Influence of dextrin content and sintering temperature on the properties of coal fly ash-based tubular ceramic membrane for flue gas moisture recovery, J. Eur. Ceram. Soc. 41 (2021) 5696–5710.
- [10] J. Du, D. Ai, X. Xiao, J. Song, Y. Li, Y. Chen, L. Wang, K. Zhu, Rational design and porosity of porous alumina ceramic membrane for air bearing, Membranes. 11 (2021) 872–883.
- [11] M.F. Zawrah, R.M. Khattab, L.G. Girgis, E.E. El Sherefy, S.E. Abo Sawan, Effect of CTAB as a foaming agent on the properties of alumina ceramic membranes, Cer. Int. 40 (2014) 5299–5305.
- [12] B. Dong, M. Yang, F. Wang, L. Hao, X. Xu, G. Wang, S. Agathopoulos, Novel fabrication processing of porous alumina/mullite membrane supports by combining direct foaming, sol-gel, and tape-casting methods, Mater. Lett. 240 (2019) 140–143.
- [13] F. Wang, S. Hao, B. Dong, N. Ke, N.Z. Khan, L. Hao, L. Yin, X. Xu, S. Agathopoulos, Porous-foam mullite-bonded SiC-ceramic membranes for high-efficiency high-temperature particulate matter capture, J. Alloys Compd. 893 (2022) 162231.
- [14] A. Pokhrel, D.N. Seo, S.T. Lee, L.J. Kim, Processing of Porous Ceramics by Direct Foaming: A review, J. Korean Ceram. Soc. 50 (2013) 93–102.
- [15] Y. Zheng, X. Luo, J. You, Z. Peng, S. Zhang, Ceramic foams with highly open channel structure from direct foaming method in combination with hollow spheres as pore-former, J. Asian Ceram. Soc. 9 (2021) 24–29.
- [16] G. Sposito, N.T. Skipper, R. Sutton, S.-h. Park, A.K. Soper, J.A. Greathouse, Surface geochemistry of the clay minerals, Proc. Natl. Acad. Sci. USA 96 (7) (1999) 3358–3364.
- [17] A.J. Millán, R. Moreno, M.I. Nieto, Thermogelling polysaccharides for aqueous gelcasting-part I: a comparative study of gelling additives, J. Eur. Ceram. Soc. 22 (2002) 2209–2215.
- [18] R. Kaemkit, S. Vichaphund, K. Lertwittayanon, Fabrication of low cost alumina tube through agar gelcasting for membrane microfiltration, AMST. 24 (2020) 47–57.
- [19] M. Dor, Y. Levi-Kalishman, R.J. Day-Stirrat, Y. Mishaal, S. Emmanuel, Assembly of clay mineral platelets, tactoids, and aggregates: Effect of mineral structure and solution salinity, J. Colloid Interface Sci. 566 (2020) 163–170.
- [20] A. Idiart, M. Laviña, B. Cochepin, A. Pasteau, Hydro-chemo-mechanical modelling of long-term evolution of bentonite swelling, Appl. Clay Sci. 195 (2020) 05717–105728.
- [21] L. Uttamasil, An investigation of Ranong clay in Thailand, Georgia Institute of Technology, 1969, Master's thesis.
- [22] D.L. Mokma, J.K. Syers, M.L. Jackson, Cation exchange capacity and weathering of muscovite microflakes, Soil Sci. Soc. Am. J. 34 (1970) 146–151.

Appendix B: Raw data of experimental results

- Graph of sintering temperature



Calculation method

- Preparation of Al₂O₃ slurry

It has a solid loading of 75:25, prepared in 75 g.

Note: instead of X = weight of Al₂O₃ Slurry in g. e.g., to prepare 100 g of solids loading

- 75 g of powder Al₂O₃ 75 g and RO water 25 g

$$\text{Solid loading} = \frac{X \cdot 75}{100}$$

$$\text{Solid loading} = X \text{ (g)}$$

- Preparation of kaolin slip (50:50)

Note: instead of X = weight of kaolin in g. e.g., to prepare 100 g of solids loading

$$\text{Solid loading} = \frac{X \cdot 50}{100}$$

- 50 g of powder kaolin 25 g and RO water 25 g

- Al₂O₃ slurry by ball mill for 2 h.

Total solution	Water (%)	Solid (%)	Water
100	25	75	$\frac{Water(\%)}{100} \times Total\ solution$
Solid	TM-5D %wt of solid *concentration	kaolin %wt of Solid *concentration	kaolin slip (ball mill 2nd) for 45 min. *concentration
$\frac{Solid(\%)}{100} \times Total\ solution$	100	0	50
TM-5D	kaolin (%)	water (%) in kaolin slip	
$\frac{TM - 5D\ \%wt\ of\ solid}{100} \times Solid$	$\frac{kaolin\ \%wt\ of\ Solid}{100} \times Solid$	$\frac{kaolin\ (\%)}{kaolin\ slip\ (ball\ mill\ 2nd)} \times (100 - Skaolin\ slip\ (ball\ mill\ 2nd))$	
water ball (ball mill 1st)	Slurry (ball mill 1st)	% Displex AA (ball mill 1st)	ball mill 1st
<i>wate – water (%) in kaolin slip</i>	<i>TM – 5D – water ball (ball mill 1st)</i>	1	$\frac{\% Displex\ AA\ (ball\ mill\ 1st)}{100} \times TM - 5D$
MgO (%) *concentration	MgO		
0.03	$\frac{MgO\ (\%)}{100} \times TM - 5D$		

Note: All calculations are done using the program Excel for more accuracy.

- Kaolin by ball mill for 45 min.

slurry TM-5D	solid loading TM-5D	Required amount of kaolin	Required amount of water
70	52.5	$\frac{\text{solid loading } TM - 5D}{TM - 5D} \times \text{kaolin } (\%)$	$\frac{\text{solid loading } TM - 5D}{TM - 5D} \times \text{water } (\%) \text{ in kaolin slip}$
		Solution	Prepare the kaolin solution.
		<i>Required amount of kaolin + Required amount of water</i>	30
		Amount of kaolin weighed	Amount of water weighed
		$\frac{\text{kaolin slip (ball mill 2nd)}}{100} \times \text{Prepare the kaolin solution.}$	$\frac{(100 - \text{kaolin slip (ball mill 2nd)})}{100} \times \text{Prepare the kaolin solution.}$
Agar Concentration	Amount of agar weighed		
0.6	$\frac{\text{Agar Concentration}}{100} \times \text{solid loading } TM - 5D + \text{Required amount of kaolin}$		
Agar in solution *concentration	Mix the water into the agar		
2	$\frac{98}{\text{Agar in solution}} \times \text{Amount of agar weighed}$		
% Displex AA (ball mill 2nd)	(ball mill 2nd)		
2	$\frac{\% \text{ Displex AA (ball mill 2nd)}}{100} \times \text{Amount of kaolin weighed}$		

- Density of Al₂O₃ membrane tubes

Samples	W ₁ (g)	W ₂ (g)	W ₃ (g)	V	V _{op}	%P _A	%A _w	ρ _B	ρ _A
A	8.87	6.62	10.57	3.95	1.7	43.04	19.17	2.25	3.94
B	6.7	5.02	8.31	3.29	1.61	48.94	24.03	2.04	3.99
C	7.54	5.62	9.1	3.48	1.56	44.83	20.69	2.17	3.93
D	7.22	5.36	8.75	3.39	1.53	45.13	21.19	2.13	3.88
E	6.25	4.58	7.57	2.99	1.32	44.15	21.12	2.09	3.74
F	7.77	5.81	9.46	3.65	1.69	46.30	21.75	2.13	3.96
G	6.16	4.59	7.23	2.64	1.07	40.53	17.37	2.33	3.92

Samples	W ₁ (g)	W ₂ (g)	W ₃ (g)	V	V _{op}	%P _A	%A _w	ρ _B	ρ _A
0 wt%	10.79	7.91	12.29	4.38	1.5	34.25	13.90	2.46	3.75
4 wt%	4.86	3.54	5.7	2.16	0.84	38.89	17.28	2.25	3.68
8 wt%	5.04	3.75	6.06	2.31	1.02	44.16	20.24	2.18	3.91
12 wt%	5.84	4.29	7.16	2.87	1.32	45.99	22.60	2.03	3.77

Samples	%P _A	ρ _B
K0	34.25	2.46
K4	38.89	2.25
K8	44.16	2.18
K12	45.99	2.03

Mechanical properties

- Green strength

Specimen	D	di	Max load (N)	Maximum stress (MPa)	Flex modulus (MPa)	Ext/Max Flex load (mm)	Flex strain/ Max flex load (mm/mm)
0wt% / M2	13.46	9.59	8.59	0.76	456.54	-0.33	0.0036
0wt% / M6	13.12	9.43	14.05	1.35	674.71	-0.49	0.0054
0wt% / M7	13.27	9.66	8.73	0.81	780.58	-0.28	0.003
0wt% / M9	13.13	9.57	15.48	1.48	503.91	-0.48	0.0053
0wt% / M11	13.15	9.32	11.67	1.11	592.4	-0.36	0.0039

L(mm)	D ⁴ (mm)	d _i ⁴ (mm)	3.14	8	8*F*L*D	D ⁴ -d _i ⁴	σ _F (MPa)
100	32823.14865	8458.131418	3.14	8	4916022.72	76506.1541	64.26
100	29630.25166	7907.63784	3.14	8	7081756.16	68209.00741	103.82
100	31008.70943	8707.801203	3.14	8	8286637.28	70024.85183	118.34
100	29720.69113	8387.793908	3.14	8	5293070.64	66985.29728	79.02
100	29902.19101	7545.076534	3.14	8	6232048.00	70201.33944	88.77
							$\bar{X} = 90.84$
							SD=21.07

- Sintered strength

Specimen	D	di	Max load (N)	Maximum stress (MPa)	Flex modulus (MPa)	Ext/Max Flex load (mm)	Flex strain/ Max flex load (mm/mm)
4wt% / N2	12.9	9.78	110.78	11.17	6716.81	-0.41	0.0044
4wt% / N4	13.33	9.84	105.21	9.61	4528.78	-0.63	0.007
4wt% / N6	13.21	9.86	106.52	10.00	5528.78	-0.86	0.0094
4wt% / N8	13.07	9.29	196.21	19.02	10166.33	-0.48	0.0052
4wt% / N10	12.64	9.61	189.39	20.3	11267.54	-0.44	0.0046

L(mm)	D ⁴ (mm)	d _i ⁴ (mm)	3.14	8	8*F*L*D	D ⁴ -d _i ⁴	σ _F (MPa)
100	27692.2881	9148.616423	3.14	8	69317479.2	58227.12907	1190.47
100	31573.34518	9375.196815	3.14	8	48294909.92	69702.18588	692.88
100	30451.68092	9451.650624	3.14	8	58428147.04	65940.09512	886.08
100	29181.14646	7448.397677	3.14	8	106299146.5	68240.83118	1557.71
100	25526.32508	8528.910374	3.14	8	113937364.5	53371.88219	2134.78
							\bar{X} =1292.38
							SD=573.35

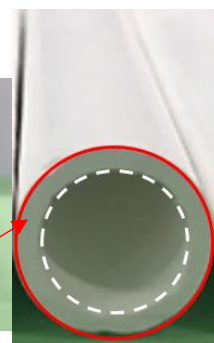
Green strength

Specimen	Bending strength (MPa)	SD
0 wt%	90.84	21.07
4 wt%	80.43	21.97
8 wt%	63.48	18.75
12 wt%	55.45	16.48

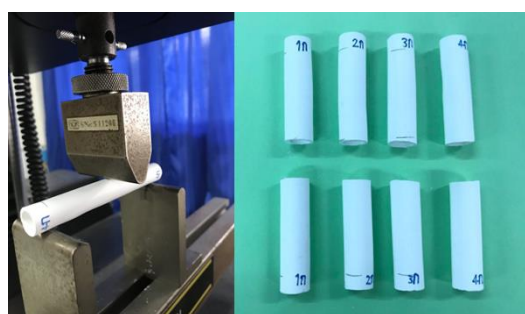
Sintered strength

Specimen	Bending strength (MPa)	SD
0 wt%	4264.70	1214.57
4 wt%	1292.38	573.35
8 wt%	1083.58	157.79
12 wt%	629.14	339.46

Fabrication of tubular



Three-point bending test



Permeation test



- Permeation test

M	ชื่อชิ้นงาน สูตร 1 Alumina+Kaolin 0 wt%				ขนาดความยาวชิ้นงาน 62 mm A=40mm				*เปลี่ยน ml เป็น L				A ต่ ม		A จ้ง		Flux (L/m ² .h)				Conclusion	
	Time (min)	ค่าวม	Pressure (bar)		ค่าวม	Pressure (bar)		ค่าวม	Pressure (bar)	ค่าวม	Pressure (bar)	ค่าวม	Pressure (bar)	Time(h)			0.5	1	1.5	2	Pressure (bar)	Flux (L/m ² .h)
	0	0.5	1	1.5	2	0	0	0	0	0	0	0	0	0.04	0	0.0016	0.00	0.00	0.00	0.00	0.5	10.41
	5	5.75	12.57	29.35	59.74	1.76	5.08	9.21	16.99	0.00176	0.00508	0.00921	0.01699		0.083333	0.0016	13.20	38.10	69.08	127.43	1	28.50
	10	9.27	22.74	47.99	93.12	3.52	10.17	18.64	33.38	0.00352	0.01017	0.01864	0.03338		0.166667	0.0016	13.20	38.14	69.90	125.18	1.5	52.13
	15	11.85	27.79	57.16	109.92	6.1	15.22	27.81	50.18	0.0061	0.01522	0.02781	0.05018		0.0016	0.0016	15.25	38.05	69.53	125.45	2	94.51
																Average	10.41	28.57	52.13	94.51		
N	ชื่อชิ้นงาน สูตร 2 Alumina+Kaolin 4 wt%				ขนาดความยาวชิ้นงาน 79 mm A=59mm				*เปลี่ยน ml เป็น L				A ต่ ม		A จ้ง		Flux (L/m ² .h)				Conclusion	
	Time (min)	ค่าวม	Pressure (bar)		ค่าวม	Pressure (bar)		ค่าวม	Pressure (bar)	ค่าวม	Pressure (bar)	ค่าวม	Pressure (bar)	Time(h)			0.5	1	1.5	2	Pressure (bar)	Flux (L/m ² .h)
	0	16.66	83.54	181.29	332.96	0	0	0	0	0	0	0	0	0.059	0	0.003481	0.00	0.00	0.00	0.00	0.5	48.75
	5	35.61	114.9	221.66	389.97	18.95	31.36	40.37	57.01	0.01895	0.03136	0.04037	0.05701		0.083333	0.003481	65.33	108.11	139.17	196.53	1	80.45
	10	54.48	146.31	259.82	445.02	37.82	62.77	78.53	112.06	0.03782	0.06277	0.07853	0.11206		0.166667	0.003481	65.19	108.19	135.36	193.15	1.5	102.30
	15	72.77	175.34	298.48	497.7	56.11	91.8	117.19	164.74	0.05611	0.0918	0.11719	0.16474		0.003481	0.003481	64.48	105.49	134.66	189.30	2	144.75
																Average	48.75	80.45	102.30	144.75		
O	ชื่อชิ้นงาน สูตร 3 Alumina+Kaolin 8 wt%				ขนาดความยาวชิ้นงาน 57 mm A=39mm				*เปลี่ยน ml เป็น L				A ต่ ม		A จ้ง		Flux (L/m ² .h)				Conclusion	
	Time (min)	ค่าวม	Pressure (bar)		ค่าวม	Pressure (bar)		ค่าวม	Pressure (bar)	ค่าวม	Pressure (bar)	ค่าวม	Pressure (bar)	Time(h)			0.5	1	1.5	2	Pressure (bar)	Flux (L/m ² .h)
	0	78.51	524.64	1322.45	1417.86	0	0	0	0	0	0	0	0	0.039	0	0.001521	0.00	0.00	0.00	0.00	0.5	668.35
	5	191.54	756.96	1622.59	1857.64	113.03	232.32	300.14	439.78	0.11303	0.23232	0.30014	0.43978		0.083333	0.001521	891.76	1832.90	2367.97	3469.66	1	1365.97
	10	301.68	983.67	1931.76	2297.42	223.17	459.03	609.31	879.56	0.22317	0.45903	0.60931	0.87956		0.166667	0.001521	880.36	1810.77	2403.59	3469.66	1.5	1796.28
	15	421.23	1216.78	2240.21	2737.2	342.72	692.14	917.76	1319.34	0.34272	0.69214	0.91776	1.31934		0.001521	0.001521	901.30	1820.22	2413.57	3469.66	2	2602.25
																Average	668.35	1365.97	1796.28	2602.25		
P	ชื่อชิ้นงาน สูตร 4 Alumina+Kaolin 12 wt%				ขนาดความยาวชิ้นงาน 49 mm A=30mm				*เปลี่ยน ml เป็น L				A ต่ ม		A จ้ง		Flux (L/m ² .h)				Conclusion	
	Time (min)	ค่าวม	Pressure (bar)		ค่าวม	Pressure (bar)		ค่าวม	Pressure (bar)	ค่าวม	Pressure (bar)	ค่าวม	Pressure (bar)	Time(h)			0.5	1	1.5	2	Pressure (bar)	Flux (L/m ² .h)
	0	109.54	1054.73	2010.25	2955.08	0	0	0	0	0	0	0	0	0.03	0	0.0009	0.00	0.00	0.00	0.00	0.5	7877.78
	5	1033.23	2972.23	3529.7	5422.1	923.69	1917.5	1519.45	2467.02	0.92369	1.9175	1.51945	2.46702		0.083333	0.0009	12315.87	25566.67	20259.33	32893.60	1	14954.60
	10	1557.75	3564.15	6567.12	7889.62	1448.21	2509.42	4556.87	4934.54	1.44821	2.50942	4.55687	4.93454		0.166667	0.0009	9654.73	16729.47	30379.13	32896.93	1.5	19443.21
	15	2256.16	4997.24	8115.48	10356.21	2146.62	3942.51	6105.23	7401.13	2.14662	3.94251	6.10523	7.40113		0.0009	0.0009	9540.53	17522.27	27134.36	32893.91	2	24671.11
																Average	7877.78	14954.60	19443.21	24671.11		

VITEA

Name Miss Nantawadee Udomsri

Student ID 6310220038

Education Attainment

Degree	Name of Institution	Year of Graduation
Bachelor of Science (B.S.) (Materials Science)	Prince of Songkla University	2019
Master of Science (M.S.) (Materials Science)	Prince of Songkla University	2022

Scholarship Awards during Enrolment

Center of Excellence in Membrane Science and Technology (CoE-MST), Prince of Songkla University

List of Publication and Proceeding

Nantawadee U, Methee P, Suksawat S and Kowit L. 2022. Effect of clay addition to Al₂O₃-agar mixture on pore size and distribution of tubular Al₂O₃ membrane support fabricated by agar gelcasting. *Materials Today: Proceeding*. 65 (4): 2426-2431

